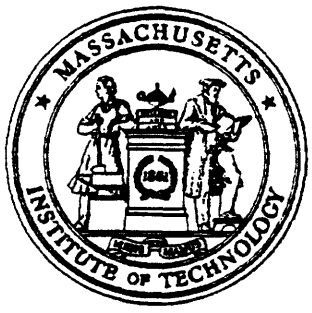

Moving-Object Reconstruction from Camera-Blurred Sequences Using Interframe and Interregion Constraints

RLE Technical Report No. 542

April 1989

Stephen Charles Hsu

Research Laboratory of Electronics
Massachusetts Institute of Technology
Cambridge, MA 02139 USA

Moving-Object Reconstruction from Camera-Blurred Sequences
Using Interframe and Interregion Constraints

by

Stephen Charles Hsu

Submitted to the
Department of Electrical Engineering and Computer Science
on August 19, 1988 in partial fulfillment of the requirements for the Degree of
Doctor of Philosophy in Electrical Engineering

Abstract. This investigation is concerned with reconstructing the original images of a scene's overlapping moving surfaces, given a sequence of frames blurred by camera integration. Conventional image formation models do not account for the blurred transition zone at the interface between images of occluding surfaces moving with different velocities, and unique reconstruction of a surface is impossible using only intraframe, intraregion data. Specifically, the component of the input signal that is periodic with wavelength equal to the blur distance (exclusive of any DC level) is unrecoverable, and its absence leaves a visible artifact in the deblurred image when the blur is not minute compared to the size of the surface. Most existing approaches to resolving ambiguity rely on a priori information about the signal to be recovered. The approach proposed here exploits constraints from multiple frames and multiple overlapping surfaces to achieve more complete restoration. Once it is assumed that the positions of all surfaces and boundaries are known throughout time, restoration is a linear measurement-inversion problem: in this respect the treatment is routine. The novel aspect of this work is a coherent theory of the determinacy of reconstruction as a function of surface and boundary velocities, making use of the correct model of transition zones. Feasibility of the approach is studied by examining its performance with noise, sampling, and errors in system identification.

Three prototype reconstruction problems are examined, primarily for a simple one-dimensional model of blurred image formation and reconstruction. (1) Intraregion reconstruction processes observations in the interior of a blurred region, avoiding transition zones. (2) Transition zone compensation augments the intraregion problem with data from a blurred boundary, assuming that prior knowledge of the contribution of one side to the zone allows it to be subtracted off at the outset. (3) Interregion reconstruction also uses data from the blurred boundary, replacing prior knowledge of one side with the requirement that the boundary move in lockstep with one side. Each reconstruction problem is analyzed by finding the nullspace of the linear transformation that maps input surface images to a set of blurred observations in one or more frames. The predictions of unrecoverable components are confirmed by computing the expected MSE of a linear least-squares reconstruction given random process input signals and by visually inspecting a restored test picture.

It is found that the new methods can produce deblurred images of better quality than the conventional intraframe, intraregion approach. Due to the existence of unfavorable combinations of velocities, however, the constraints are not guaranteed to determine the original input signal uniquely. Furthermore, observation noise and boundary position estimation errors may weaken the advantage of transition zone compensation and interregion reconstruction over the conventional approach.

Thesis Supervisor: Dr. William F. Schreiber

Title: Professor of Electrical Engineering

Contents

List of Figures

Acknowledgments

It gives me pleasure to dedicate this thesis to a very dear Professor of Mathematics, my father, who has instilled a degree of technical proficiency in mathematical reasoning as well as an appreciation for its aesthetic value. Mom and Dad, thanks for twenty-eight years of love and encouragement, in good times and bad.

I am grateful to my advisor Dr. William Schreiber for encouraging me to pursue this research, and to readers Dr. Jae Lim and Dr. David Staelin for new viewpoints. Thanks to Avideh and Julien for innumerable technical discussions, along with doses of reality.

This work was supported by the AT&T Foundation through a Bell Laboratories Ph.D. Scholarship. Research facilities were provided by the Advanced Television Research Program at the Media Laboratory.

Chapter 0

Introduction

Many advances in the main areas of electronic picture processing—image coding, image enhancement, and image restoration—can be attributed to a growing use of scene analysis and image understanding techniques in problems formerly approached by signal processing alone. The image models employed have progressed from purely intensity-based representations to those containing increasing levels of scene semantics. More to the point, use of the optical flow field of a time-varying image makes various image processing procedures more efficient and less detrimental to the picture quality. Interframe image coding, noise reduction, and spatial or temporal sampling rate conversion are the applications of motion compensation previously investigated. On the other hand, the area of image deconvolution has not yet been touched by dynamic scene analysis.

The ultimate goal of this research is to reconstruct the original images of a scene's overlapping moving surfaces, given a sequence of frames blurred by camera integration. The individual deblurred images may be used directly for object recognition and inspection tasks, or may be combined through animation to synthesize the image sequence that would be recorded by an ideal non-integrating camera, at any desired frame rate. Sharp images are welcomed in scientific, industrial, biomedical, security, and entertainment applications.

The primary concern of this thesis is the problem of motion-blurred image restoration subsequent to analysis of the scene configuration. Conventional image formation models do not account for the blurred transition zone at the interface between images of occluding surfaces moving with different velocities, and unique reconstruction of a surface is impossible using only intraframe, intraregion data. Specifically, the component of the input signal

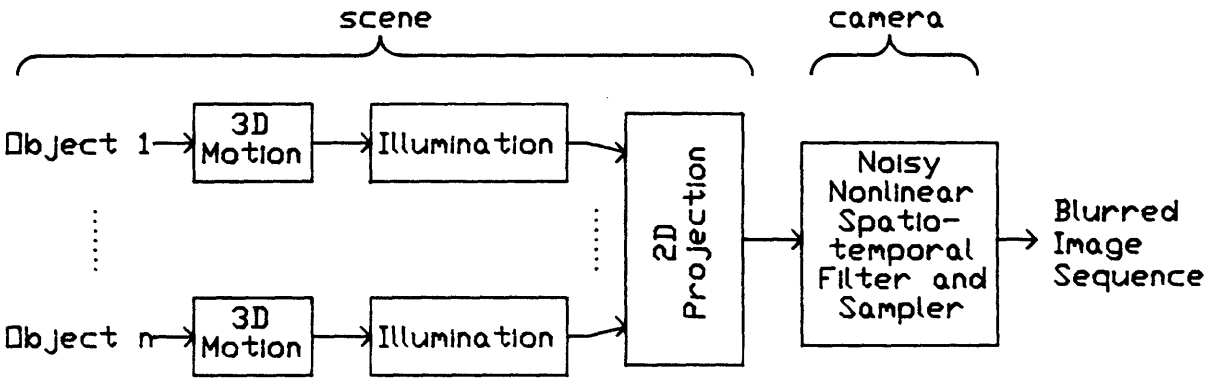

Figure 0.1: General model of image formation

that is periodic with wavelength equal to the blur distance (exclusive of any DC level) is unrecoverable, and its absence leaves a visible artifact in the deblurred image when the blur is not minute compared to the size of the surface. Most existing approaches to resolving ambiguity rely on a priori information about the signal to be recovered. The approach proposed here exploits constraints from multiple frames and multiple overlapping surfaces to achieve more complete restoration. Once it is assumed that the positions of all surfaces and boundaries are known throughout time, restoration is a linear measurement-inversion problem: in this respect the treatment is routine. The novel aspect of this work is a coherent theory of the determinacy of reconstruction as a function of surface and boundary velocities, making use of the correct model of transition zones. Feasibility of the approach is studied by examining its performance with noise, sampling, and errors in system identification.

0.1 Model of Image Formation

A fairly general model of image formation is shown in Figure 0.1. Three-dimensional objects moving through space are illuminated, and a two-dimensional scene is formed by perspective projection. A sequence of blurred images is then recorded by the camera, a noisy nonlinear spatio-temporal filter and sampler. This research, however, considers only the much simpler model of Figure 0.2. Flat, rigid, opaque surfaces bearing time-invariant brightness patterns undergo time-varying shifts. As represented by a switch, one surface is visible at every

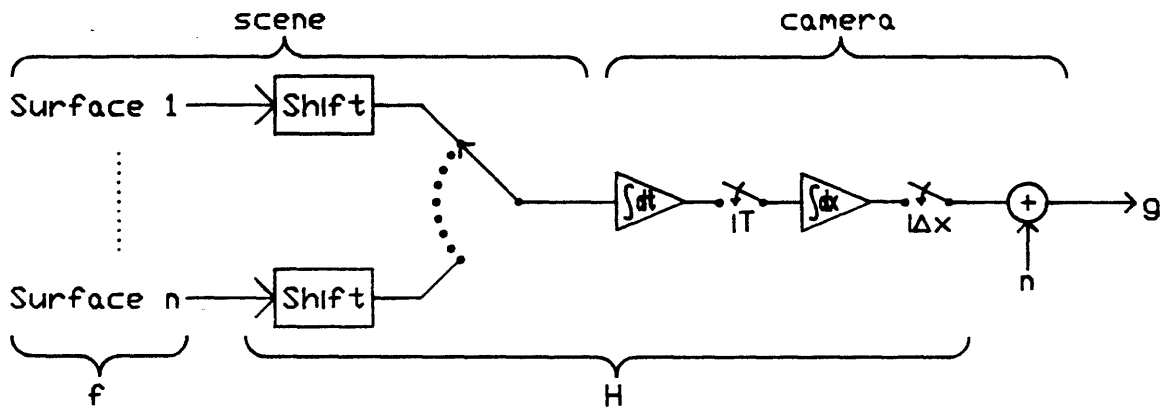

Figure 0.2: Simple model of image formation used in this research

location according to the arrangement of surfaces in depth. A permissible scene is shown in Figure 0.3. A noisy linear camera contains a temporal integrator and sampler, and a spatial filter and sampler. In this model, image reconstruction is the problem of estimating the union of input surface patterns, symbolized by **f**, given the union of output frames, **g**. The entire chain of processes in the scene and camera is denoted by **H**, a linear transformation specified by the shifts and switch positions.

The simple model is restrictive in some aspects but flexible in others. The translatory motion assumption forbids scenes containing deformable objects, rotation, or translation in depth. Violation does not ipso facto preclude reconstruction, since the system **H** is always defined. The assumption certainly facilitates the task of scene analysis, but the most important reason for it is mathematical tractability, so that the system can be analyzed in closed form. On the other hand, since boundaries are not assumed to move in lockstep with a surface, objects are permitted to undergo erosion or dilation at edges. The model allows for such changes in shape because each input surface can be thought of as extending to infinity in all directions, using the switch to define the part actually visible.

A further simplifying assumption will be maintained in all but one chapter of this thesis: surfaces may only translate horizontally. In this event, points on different rows do not interact during the process of forming blurred frames. A convenient simplification, therefore, is to process each line of the image sequence separately. While it may be suboptimal to ignore interline dependencies, it is easier to study image formation, scene analysis, and

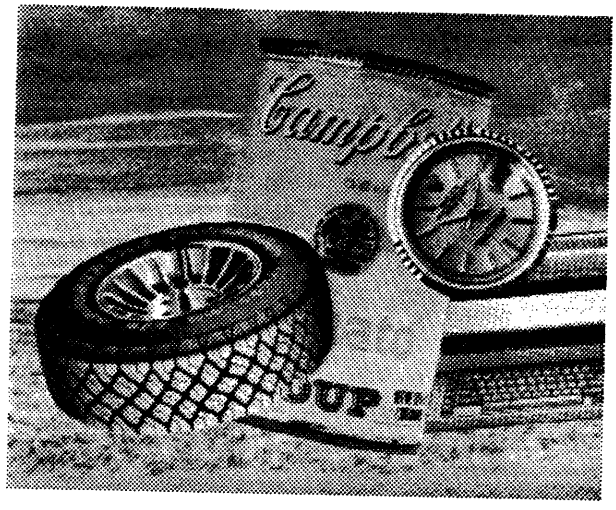

Figure 0.3: Snapshot of scene permissible under the simple model

image reconstruction for a time-varying image with only one spatial dimension.

0.2 Outline of the Thesis

Following this introduction, the thesis consists of six chapters and concluding remarks. The first four chapters deal with the uniqueness of reconstruction from a theoretical standpoint, while the last two chapters consider practical issues. Accordingly, perfect knowledge of the system **H** and noiseless, spatially continuous data are assumed in the beginning.

Chapter 1 examines the motivations for this research, namely, the underdeterminacy of image deconvolution when only one frame and one surface is processed at a time. The input signal components that are completely annihilated by the blurring system are deemed unobservable modes. Signal modeling approaches to resolving ambiguity are reviewed.

Chapter 2 develops the principal results of this thesis, for one-dimensional blur and reconstruction. Three scenarios are examined—intraregion reconstruction, reconstruction after transition zone compensation, and uncompensated interregion reconstruction—using one or more frames of data. The structure of the nullspace of **H** is found to vary systematically with the velocities of boundaries and surfaces adjacent in space or time. This effort yields necessary and sufficient conditions on velocity quotients for unique reconstruc-

tion. Some predictions are surprising; for example, rational and irrational quotients impart different properties to **H**.

Chapters 3 and 4 partially extend the foregoing results to observations with arbitrary camera integration time and to linear motion in two dimensions, respectively. These chapters are not essential to the sequel and may be skipped without loss of continuity.

Chapter 5 takes up the issues of noisy and discretized data, using linear least squares estimation to measure performance characteristics and produce test pictures. Experiments confirm the predicted structure of the nullspace and demonstrate that the new approach of this thesis can be an improvement over the conventional intraframe, intraregion restoration, even with less than perfect data. Noise and finite bandwidth are found to bridge the gap between physical reality and the theoretical curiosities of previous chapters.

Chapter 6 barely scratches the surface on another practical issue, the sensitivity of reconstruction to errors in identifying the system **H**. Specifically, the artifacts induced by errors in boundary position and blur estimates are displayed. An accurate method of local boundary estimation based on minimizing the linear least squares cost function is established.

When the simple image formation model is valid, this thesis shows that reconstruction via interframe and interregion constraints has three principal limitations: first, certain velocity combinations will create unobservable modes that no number of frames can recover; second, high SNR is needed for the interregion constraints to be reliable; third, robust segmentation is a prerequisite. Much work is still required before fully automatic, real-time image sequence restoration can be carried out. Nevertheless, the subject of this thesis is another excellent illustration of the manifold benefits of dynamic scene analysis in image processing.

Chapter 1

Underdeterminacy of Conventional Restoration

This chapter introduces the restoration problem for one-dimensional signals, demonstrating that a single motion-blurred frame does not contain enough information to uniquely reconstruct the input. It is found that a priori signal models do not reliably resolve this ambiguity. These limitations suggest that in order to restore even one object in a blurred image sequence, it is necessary to exploit couplings between multiple objects and frames—the focus of this thesis investigation.

1.1 Motion Blur and Deconvolution

Two elementary explanations of underdeterminacy and its consequences will be presented. First, the conventional frequency-domain formulation of the image restoration problem assumes support on the infinite interval and shift-invariant blur. This explanation is indirect because physical observations have finite spatial extent. Second, a signal-domain formulation provides a boundary condition interpretation.

When the surface displacement during the exposure of one frame is b, the point spread function is a rectangular pulse of length b. The frequency response is the sinc function

$$H(\omega) = \frac{\sin b\omega/2}{b\omega/2},$$

with transmission zeros at $\omega = \frac{2\pi}{b}, \frac{4\pi}{b}, \ldots$ (Figure 1.1). Image restoration is, roughly speaking, the problem of finding $F(\omega)$ given $G(\omega) = H(\omega)F(\omega)$. The obvious solution is inverse

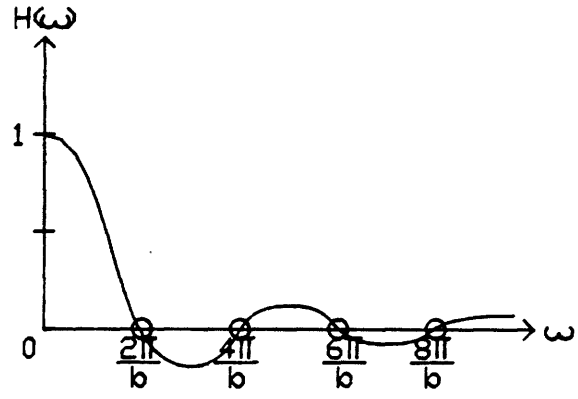

Figure 1.1: Frequency response of motion blur

filtering, i.e., $\hat{F}(\omega) = \frac{1}{H(\omega)}G(\omega)$. However, restoration is an underdetermined problem because Fourier components of the input signal at the zero frequencies are nulled out by the blur, and their amplitudes cannot be determined from the blurred signal alone. In other words:

The component of the input signal that is periodic with wavelength b (exclusive of any DC level) is unobservable.

On the infinite interval, the unobservable component contains 0% of the signal energy as long as $F(\omega)$ is bounded at the zeros, since the latter occupy a vanishingly small fraction of the spectrum. Hence, failure to recover this component is usually inconsequential. If the observation is windowed to a finite interval, though, the periodic component is still unobservable, but now its share of the total energy in a finite segment of the input signal can be a positive fraction.

In the absence of additional a priori or a posteriori information, the resulting ambiguity in certain components of the image may have undesirable visible consequences. A trivial way to deal with ambiguity is the pseudoinverse method of image restoration, which sets the unobservable component to zero but recovers all other components perfectly (in the absence of noise). For example, the input signal segment in Figure 1.2a is decomposed into its periodic and nonperiodic components, with respect to horizontal motion blur of one-eighth the input signal width. A noiseless blurred image restored by the pseudoinverse method would look like Figure 1.2d. The characteristic artifact of motion blur restoration

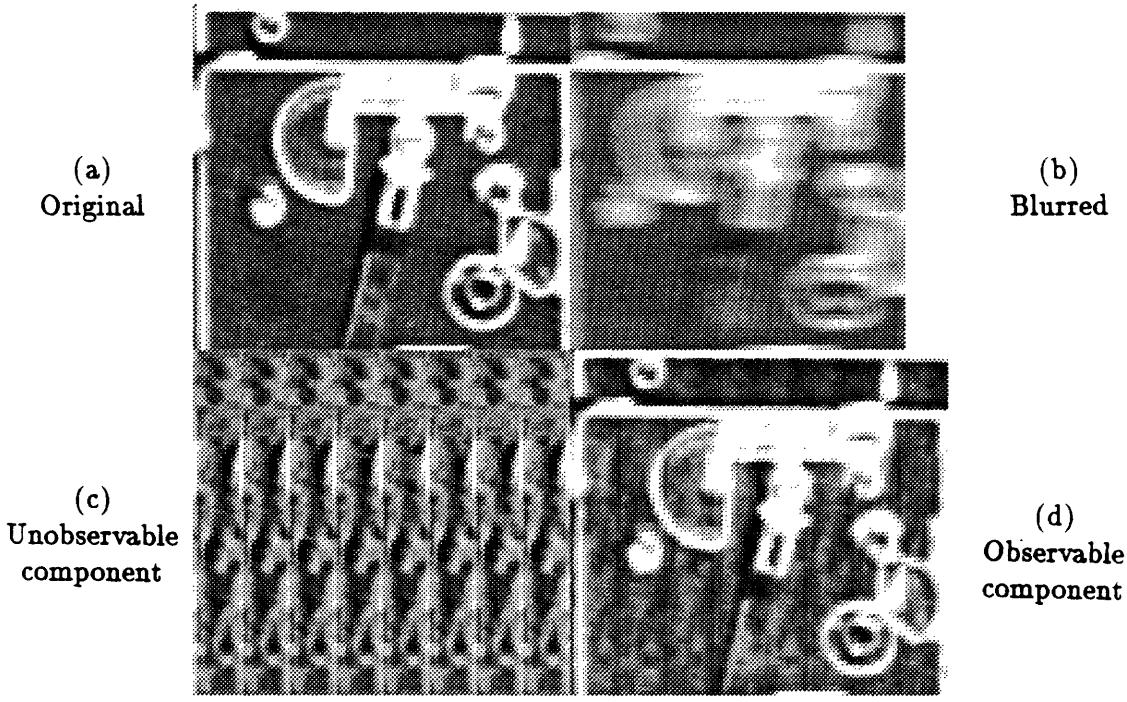

Figure 1.2: Orthogonal decomposition of an image:
(a) original;
(b) motion-blurred image;
(c) periodic component with respect to this blur (reproduced with DC shift and dynamic range expanded by 2.8);
(d) non-periodic component recovered by pseudoinverse.

is a "ghost"-like periodic replication of prominent image features. In fact, all parts of the surface contribute with equal weight to the unobservable component. Although an artifact is usually thought of as an added perturbation, this artifact is really caused by absence of an internal component of the desired signal.

The power in this unobservable component is 4% of the variance of the original image. Since this percentage seems surprisingly large, its order of magnitude can be checked by the following argument. A segment of length L from a signal of bandwidth π has L independent dimensions or degrees of freedom, while the subspace of signals with DC-free periods of length b has $b-1$ degrees of freedom. Therefore, for a spectrally white image the fraction of unobservable energy is $(b-1)/L$, or 11% for the above example. Since the image is really low-pass, the actual unobservable energy is less.

For purposes of this investigation, the simple Fourier transform description of degradation and restoration is deficient. Some reasons for abandoning the frequency domain are the following:

1. The Fourier transform is defined as an integral on $(-\infty, \infty)$. Unless prior considerations (e.g., finite support input signal) dictate that the blurred image is zero outside the observation interval, the Fourier transform of the output signal, $G(\omega)$, is not completely specified by a finite-length observation.

   Moreover, it does not help to represent the impulse response and finite-length signals by Fourier series, because the observed image segment is not generated by circular convolution.

2. The frequency response $H(\omega)$ does not readily explain the nonzero energy in the unobservable component of reconstruction from a finite, noise-free observation of a blurred image.

3. The concept of frequency response is restricted to shift-invariant convolutions and cannot describe the blurred image formed by overlapping surfaces moving at different speeds.

4. The Fourier representation does not show how side information gathered in the signal domain can overcome underdeterminacy.

Accordingly, the theory of reconstruction from multiple frames and multiple surfaces will be expressed in terms of linear transformations in the signal domain.

A signal-domain description of motion-blur restoration is straightforward and provides another explanation of underdeterminacy in conventional restoration. This discussion assumes that the observed signal segment, of finite or infinite length, is produced by shift-invariant motion blur; a segment that lies entirely inside a uniformly translating region satisfies this requirement. A signal $f(x)$ filtered by impulse response $h(x)$ can be recovered exactly from blurred signal $g(x)$ by applying any inverse filter whose impulse response $k(x)$ satisfies

$$h(x) \star k(x) = \int_{-\infty}^{\infty} h(x-u)k(u)\,du = \delta(x).$$

Any convolutional inverse for $h(x)$ must be IIR (infinite impulse response), for the convolution of two finite support signals can only have longer support than either input and thus could not be $\delta(x)$. Both one-sided (causal, anticausal) and two-sided inverse filters exist for deconvolution of motion blur, but the following causal filter is the most revealing:

$$k_{\text{causal}}(x) = b\sum_{r=0}^{\infty} \delta^{(1)}(x - rb),$$

where b is the amount of blur and $\delta^{(1)}$ is the doublet $\frac{d}{dx}\delta(x)$.

$f(x) = k_{\text{causal}}(x) \star g(x)$ is recursively computable by

$$f(x) = f(x-b) + b\frac{d}{dx}g(x), \tag{1.1}$$

provided that suitable boundary conditions on $f(x)$ are given—for instance, if $f(x)$ is known on some interval of length b [Slepian67, Woods85, Ku86]. In general, however, such knowledge is unavailable and so the periodic component is unconstrained. One could try to guess $\hat{f}(x)$ on an interval of length b, but any error $\hat{f}(x) - f(x)$ will be propagated periodically. Often this error is correlated with the true signal, giving rise to ghost artifacts of period b.

Yet another explanation of underdeterminacy is that any finite observation interval in the blurred signal depends on an input signal interval longer by the amount b. The corresponding system of linear equations has more unknowns than equations, so to speak. Therefore, the observation cannot uniquely specify the original signal.

In summary, a signal $f(x)$ to be recovered from a finite segment of a motion-blurred recording can be expressed as the sum of its observable and unobservable components:

$$f(x) = f_{\text{obs}}(x) + f_{\text{unobs}}(x).$$

Until $f_{\text{unobs}}(x)$ is pinned down, there exists a whole space of reconstructions that are consistent with the data.

1.2 Resolving Underdeterminacy by Signal Modeling

There are basically two complementary strategies leading to estimation of the unobservable periodic component: utilizing a signal model or expanding the observation domain. The former exploits a priori expectations concerning the unknown signal but ignores the possibility of using observations in spatial or temporal proximity to the initial domain; the latter exploits interframe and interregion relationships but largely ignores signal properties. Neither strategy alone reliably reconstructs the unobservable component, so both should be considered in any practical system for restoring motion-blurred image sequences. Signal modeling approaches, to be surveyed in this section, fail if the model is inappropriate for the specific image to be restored. Constraints from an expanded observation set are insufficient for unique reconstruction if unfavorable surface and boundary velocity relationships hold, as demonstrated in the rest of this thesis.

A signal model disambiguates $f_{\text{unobs}}(x)$ by favoring some choices of $f(x)$ in the space of consistent reconstructions. The preference is expressed through a cost functional $J(f)$. Many different models have appeared in the signal reconstruction literature, but the best choice depends on the kind of signal to be recovered—e.g., continuous-tone imagery, bilevel patterns, power spectra, probability density functions—as well as the specific observation model, such as shift-invariant convolution or tomographic projections. Therefore, not all of the following approaches are suitable for restoring natural images degraded by uniform motion blur.

1.2.1 Deterministic Models

Deterministic properties of the unknown signal can sometimes narrow the set of acceptable reconstructions. These are often expressed as inequality or equality constraints on functions of individual samples or groups of samples. Possibilities are constraints on total energy, support, and minimum/maximum value. For example, a range constraint can be expressed by

$$J(f) = \int [f(x)]_A^B \, dx, \quad [s]_A^B = \begin{cases} C|s - B|, & \text{if } s > B; \\ 0, & \text{if } A \le s \le B; \\ C|s - A|, & \text{if } s < A. \end{cases} \tag{1.2}$$

Neither energy nor support makes sense for the kind of signals considered in this research, but even dynamic range is practically useless because most samples of $f_{\text{obs}}(x)$ should be far

away from the clipping levels and would satisfy the constraint for many choices of $f_{\text{unobs}}(x)$.

1.2.2 Statistical Models

Many approaches seek to maximize the likelihood of $f(x)$ or some other quantity based on an underlying statistical model for the unknown signal. Since simple models can hardly begin to describe natural scenes, it may be best to think of cost functionals $J(f)$ as merely recipes for selecting $f(x)$, disregarding any probabilistic connotations.

1. The statistics most commonly available (or assumed) about $f(x)$ are first and second moments, $\bar{f}(x) = \mathrm{E}\{f(x)\}$ and $R_f(x,y) = \mathrm{E}\{(f(x) - \bar{f}(x))(f(y) - \bar{f}(y))\}$. These lead to inner-product functionals such as covariance-weighted energy,

$$J(f) = \int\int (f(x) - \bar{f}(x)) R_f^{-1}(x,y)(f(y) - \bar{f}(y))\, dx\, dy, \tag{1.3}$$

the L_2-norm smoothness metric

$$J(f) = \int \left\| \frac{df}{dx} \right\|^2 dx, \tag{1.4}$$

and minimum energy metric

$$J(f) = \int f^2(x)\, dx. \tag{1.5}$$

Since $f_{\text{obs}}(x)$ and $f_{\text{unobs}}(x)$ are orthogonal, setting $f_{\text{unobs}}(x)$ to zero minimizes energy (pseudoinverse approach).

2. Another way to utilize second moments is autocorrelation matching, which minimizes the discrepancy between the expected autocorrelation and actual autocorrelation of the reconstruction [Sahasrabudhe79]. For stationary processes, the cost functional is something of the form

$$J(f) = \int \left\| R_f(\tau) - \int f(x) f(x+\tau)\, dx \right\|^2 d\tau.$$

3. A number of entropy-like expressions can be developed from likelihood functionals for photon allocation models of image formation, where the probability of a picture cell containing n photons is governed by laws of statistical mechanics [Frieden80]. The principle of maximum degeneracy selects the $f(x)$ whose photon distribution could have occurred in the largest number of ways, leading to expressions like

$$J(f) = -\int f(x) \log f(x)\, dx.$$

4. The final example is to model the derivative of a signal as a sequence of independent Laplacian random variables [Ku86]. The log likelihood takes the form

$$J(f) = \int \left| \frac{df}{dx} \right| dx, \tag{1.6}$$

which can be interpreted as an L_1-norm measure of smoothness.

To use any of these criteria, $J(f_{\text{obs}} + f_{\text{unobs}})$ should be minimized with respect to $f_{\text{unobs}}(x)$. The inner-product cost functionals can be minimized by solving linear equations, while the autocorrelation matching and maximum entropy methods require nonlinear optimization procedures. In principle, the L_1-smoothness metric can be minimized by linear programming; however, there is a simple, nearly optimum approximation that requires only a few median computations [Ku86].

Which method is best able to estimate $f_{\text{unobs}}(x)$? If there is little or no energy at frequencies $\frac{2\pi}{b}, \frac{4\pi}{b}, \ldots$ in some subregion of $f(x)$, then the pseudoinverse can correctly restore that area. The reconstructed subregion can then serve as boundary condition for the rest of the image. For example, the large blank area in the lower left quadrant of Figure 1.2a could be used. The hard part is detection of a suitable subregion of $f(x)$, if one indeed exists, since only $f_{\text{unobs}}(x)$ is known. In the absence of this detection step, the subregion must default to the whole observation interval and periodic artifacts will usually appear.

The other inner-product functionals perform no better than pseudoinverse, apparently because $f_{\text{obs}}(x)$ and $f_{\text{unobs}}(x)$ tend to be nearly orthogonal for reasonable wide-sense stationary processes (§5.1). The author has no direct experience with autocorrelation matching, but it is probably unable to resolve ambiguity since it is insensitive to phase. The success of maximum entropy methods seems to depend strongly on the picture. Surprisingly, the L_1-smoothness criterion often works very well, in contrast to the failure of L_2-smoothness. Therefore, this approach is highly recommended for the signal modeling strategy of unique motion-blur restoration.

1.3 Summary

Conventional image restoration works from one region of a single frame. The presence of zeros in the Fourier transform of a boxcar point spread function suggests that the original signal cannot be completely recovered from a motion-blurred observation. The missing

component is DC-free and periodic, with wavelength equal to the amount of blur. When the blur is more than a minor fraction of the observation interval, loss of this component leaves a visible artifact in the deblurred image. This artifact is not a problem in typical previous studies of image restoration, where a large image is degraded by a relatively small blur. On the other hand, the difficulty arises when deblurring small moving regions in a complex scene.

A more precise framework for dealing with operations on finite-length signals is the signal domain. Reconstruction is underdetermined because a boundary condition requirement—prior knowledge of a section of the original image—is unfulfilled.

Additional information is needed to recover the unobservable signal component. One strategy is to minimize the cost function of a signal model, based on expected deterministic or statistical properties. A number of common cost functionals have been reviewed. However, no matter how well combinations of such techniques work for some pictures, there will be other pictures for which they do poorly. This difficulty, plus the ad hoc nature of statistical image models, is motivation for an entirely deterministic approach that exploits constraints from additional observations.

Chapter 2

One-Dimensional Theory

This chapter addresses the fundamental limits to perfect image restoration from noiseless, spatially continuous data. The principal theme will be characterization of the nullspace of the linear transformation that maps surface images to a sequence of blurred frames. Unique reconstruction is prevented by the existence of nonzero signals in the nullspace, also known as the unobservable subspace, since arbitrary amounts of these signals can be added to the input image with no effect on the blurred data. While the component of an image orthogonal to the nullspace is uniquely specified, the component in the nullspace is completely unconstrained.

A typical scene contains several overlapping surfaces. Instead of trying to solve the global image reconstruction problem, however, it is more fruitful to analyze the reconstruction of a single surface, drawing constraints from at most one adjacent surface and boundary. The unobservable subspaces will be determined for a progression of reconstruction problems of increasing complexity:

1. *Intraregion,* in which data collection is limited to the interior of a blurred region;

2. *Transition zone compensation,* which augments the intraregion problem with data from a blurred boundary, assuming that the contribution of the surface on the other side of the boundary to the zone is known or can be computed;

3. *Interregion,* which replaces knowledge of the adjacent surface image with the requirement that the boundary move in lockstep with that surface.

The reverse interregion problem, where the boundary tracks the surface for which recon-

struction is desired, does not require special attention. Once the adjacent surface is computed by interregion processing, the desired surface can be reconstructed via transition zone compensation.

These results are relevant to the global problem. Under favorable circumstances, all the surfaces in a complex scene can be recovered independently, using local data, or recovered one after the other, using information propagated from previously computed surfaces. Some surfaces could even be overdetermined if all available constraints were exploited; conversely, with unfavorable scene configurations some surfaces might remain underdetermined. All of this depends on the specific scene in question, and general statements cannot be made.

The reconstruction theory will first be formulated for one-dimensional motion blur from a camera integrating light for the entire time between successive frames (this is called 100% duty cycle or 360° shutter angle). In future chapters, the results will be extended to arbitrary duty cycle and two-dimensional linear motion.

2.1 Preview

The main findings of this chapter are summarized with an outline of the reasoning involved.

2.1.1 Intraregion

The nullspace for an intraframe, intraregion domain of observation contains all periodic signals whose periods of wavelength $v_1 T$ contain no DC component, where v_1 is the surface velocity and T is the integration time and frame period. The result is familiar, as the inverse periods are the zeros of the Fourier transform of a rectangular pulse, namely, a sinc function.

Now suppose the same surface is observed in another frame, during which it has velocity $v_2 \neq v_1$. By combining observations from two frames, many of the previous nullvectors are eliminated, leaving only periodic signals with DC-free periods of length $\gcd(v_1 T, v_2 T)$. As later defined in §2.2.2, the greatest common divisor can equal zero, so that, at least in theory, dual-velocity observations have the potential for complete reconstruction of the surface. If the gcd is not zero, nullvectors cannot be eliminated entirely. However, the gcd is never larger, and often much smaller, than both $v_1 T$ and $v_2 T$. Since unobservable modes at shorter wavelengths tend to be less visible, an interframe reconstruction is still preferable

to an intraframe one.

2.1.2 Transition Zone Compensation

A moving occlusion boundary produces a transition zone in each blurred frame, a region where the blurred signal is a mixture of information from two adjacent surfaces. Transition zone compensation is the process of subtracting out the contribution of one surface using prior knowledge, leaving the remaining blurred signal to provide boundary conditions for restoring the unknown surface. Depending on velocity relationships, these additional constraints may or may not suffice for unique reconstruction in one frame of data. The dichotomy arises from two possible shapes for the region of support of the central linear transformation, which is either an acute or obtuse triangle. The acute triangle arises when the unknown surface moves in the same direction as, and faster than, the boundary, and yields a nullspace consisting of selected signals with DC-free periods of length $v_1 T$. Otherwise, the triangle is obtuse and the only nullvector is $\mathbf{0}$. In particular, the situation of a blurred object with rigidly attached boundaries moving in front of a stationary surface leads to a right triangle, which shares the uniqueness property of obtuse triangles.

A second frame is very useful when transition zone compensation in one frame possesses nontrivial nullvectors. Assuming time-invariant velocities, all unobservable modes will be eliminated, except for one pathological case: when the unknown surface moves with twice the velocity of the boundary, all additional frames are redundant and the nullspace is just as for one frame.

2.1.3 Interregion

The final type of reconstruction problem is called interregion because the blurred data it employs depends on signals from two surfaces. However, the assumption of time-invariant velocities and the requirement that the boundary move with the foreground surface nearly reduces this problem to that of transition zone compensation. When pairs of blurred frames are shifted so that their transition zones are in register, and then subtracted, the contribution of the foreground surface completely vanishes. A displaced-frame-difference image is therefore similar to a single blurred frame that had transition zone compensation applied to it.

Since an observation of one frame does not permit frame differencing, the nullspace for

the background surface, moving with velocity v_b, consists of signals with DC-free periods of length v_bT, as before.

Additional frames eliminate some of the foregoing nullvectors. Among those that cannot disappear, however, are the signals that simultaneously have period $(v_e - v_b)T$, where v_e is the boundary velocity, since their displaced frame difference is zero; therefore, the unobservable subspace contains all signals with DC-free periods of length $\gcd(v_bT, (v_e - v_b)T)$. In addition, when the background moves in the same direction as, and faster than, the boundary, the nullspace could also contain a selection of periodic signals with the original wavelength v_bT. The latter nullvectors exist only if fewer than three consecutive frames are observed or if the previously stated pathological case occurs.

To sum up, certain signal components cannot be recovered from an observation domain confined to one region and frame. Some or all of these components can be recovered if the corresponding nullvectors are incompatible with the constraints provided by additional observations. For reference, the nullspaces for all of the reconstruction problems have been tabulated in Figure 2.1, using notation to be explained in the sequel.

Problem Classification	Special Assumptions	Frames	v_b/v_e	$N(\mathbf{H})$	Notes
Intraregion		M		$\Pi_0(\gcd(v_1T,\ldots,v_MT))$	$N(\mathbf{H}) = \{\mathbf{0}\}$ if $\exists i,j$ such that v_i/v_j =irrational
Transition Zone Compensation (one unknown region, one known region)	constant velocities	1	≤ 1	$\{\mathbf{0}\}$	
			> 1	$N(\mathbf{H}\angle)\cap\Pi_0(v_bT)$	
		≥ 2	$\neq 2$	$\{\mathbf{0}\}$	
			$= 2$	{odd functions} $\cap\,\Pi_0(v_bT)$	
Interregion (two unknown regions)	constant velocities, $v_f = v_e$	1		$\Pi_0(v_bT)$	same as intraregion
		2	≤ 1	$\Pi_0(\gcd(v_bT,v_eT))$	$N(\mathbf{H}) = \{\mathbf{0}\}$ if v_b/v_e =irrational
			> 1	$N(\mathbf{H}\angle\Delta)\cap\Pi_0(v_bT)$	$N(\mathbf{H}) \supseteq \Pi_0(\gcd(v_bT,v_eT))$
		≥ 3	$\neq 2$	$\Pi_0(\gcd(v_bT,v_eT))$	$N(\mathbf{H}) = \{\mathbf{0}\}$ if v_b/v_e =irrational
			$= 2$	({odd functions} $\cap\,\Pi_0(v_bT)$) $\oplus\Pi_0(v_bT/2)$	

$$(\mathbf{H}\angle f)(x) = \frac{1}{v_bT}\int_{(1-v_b/v_e)x}^{x} f(u)\,du, \quad x \in [0, v_eT]$$

$$(\Delta f)(x) = f(x + (v_e - v_b)T) - f(x)$$

Figure 2.1: Unobservable subspaces of 1D reconstruction problems, 100% duty cycle: For other notation see text. The results assume that the spatial extent of observations is "large enough."

2.2 Intraregion Reconstruction

The first class of prototype reconstruction problems is intraregion. The results presented in this section are not original; in particular, the underdeterminacy of intraframe, intraregion reconstruction was already explained in Chapter §1. However, the results are developed in a new framework that is also suitable for analyzing the remaining two classes of problems.

2.2.1 Intraframe

Let $f_c(x,\tau)$ be the image function as seen through the lens of the camera, where x and τ are continuous position and time variables. Let T be the duration of each exposure, which is equal to the frame period, and let t be a discrete time variable taking values $0, T, 2T, \ldots$. Suppose that the blurred image sequence $g_c(x,t)$ is observed at $t = 0$ for $x \in [vT, L]$, and that all optical flow lines contributing to this domain come from a single surface moving with constant velocity $v > 0$, i.e.,

$$g_c(x,t) = \frac{1}{T}\int_t^{t+T} f_c(x,\tau)\,d\tau$$

where

$$f_c(x,\tau) = f(x - v\tau).$$

Then

$$g_c(x,0) = \frac{1}{vT}\int_{x-vT}^{x} f(u)\,du \tag{2.1}$$

$$= \int_0^L h(x,u) f(u)\,du \tag{2.2}$$

where the kernel of this integral equation is

$$h(x,u) = \begin{cases} \dfrac{1}{vT}, & \text{if } vT \le x \le L \text{ and } 0 \le x - u \le vT; \\ 0, & \text{otherwise.} \end{cases}$$

The space-time configuration of this dynamic scene and the region of support of $h(x,u)$ are sketched in Figure 2.2.

The input signal $f(x)$ is uniquely specified by the observation if and only if the homogeneous equation

$$g_c(x,0) = 0 \tag{2.3}$$

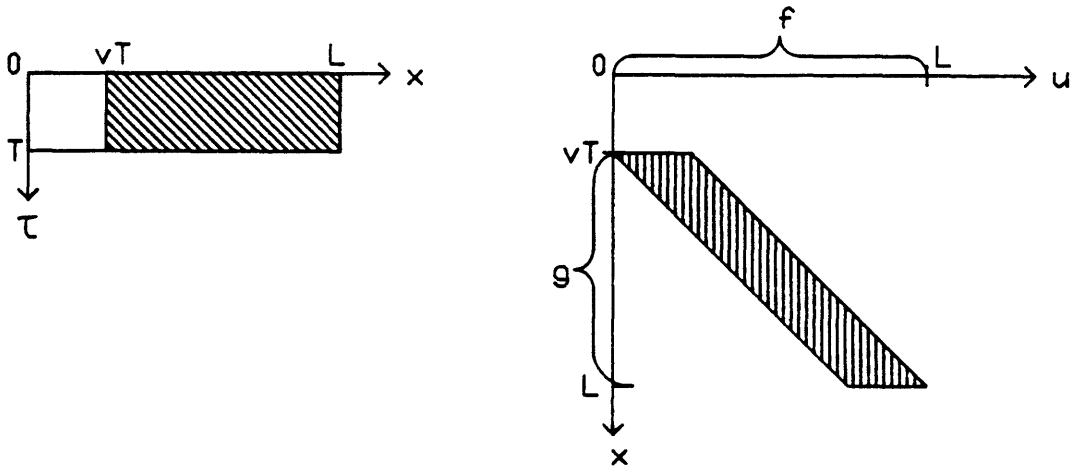

Figure 2.2: Intraframe, intraregion observation domain: (left) observation domain in space-time, with shading to suggest optical flow lines; (right) corresponding integral operator $\mathbf{H}$ with region of support shaded; $\mathbf{f}$ and $\mathbf{g}$ denote supports of input and output signals.

is satisfied by only the trivial solution. In other words, the nullspace of the linear transformation

$$\mathbf{H} : L_2(0, L) \rightarrow L_2(vT, L)$$

defined by (2.1), written $N(\mathbf{H})$, must be the set $\{\mathbf{0}\}$. $L_2(B, A)$ denotes the space of square-integrable functions on the interval (B, A).

Unfortunately, this reconstruction problem is underdetermined and there are nontrivial solutions. If $f(x)$ is a nullvector then $\frac{d}{dx} g_c(x, 0) = 0$, where

$$\frac{d}{dx} g_c(x, 0) = \frac{1}{vT}(f(x) - f(x - vT)),$$

so that any nullvector must be periodic with wavelength vT. As the integral over any period must be zero to satisfy (2.3), the nullspace can be characterized as the set of signals with DC-free periods of length vT. A basis for $N(\mathbf{H})$ is the set of complex exponentials

$$\left\{\phi_k(x) = e^{j\frac{2\pi k}{vT}x}, \quad 0 \leq x \leq L, \quad k = \pm 1, \pm 2, \pm 3, \ldots\right\},$$

whose frequencies are the zeros of the Fourier transform of the point spread function of motion blur.

The results can be summarized as follows.

Definition.

$$\begin{aligned}\Pi(z;S) &= \text{set of signals with period } z \text{ in the interval S} \\ &= \{f \mid f(x) = f(x+z) \text{ whenever } x \in S \text{ and } x+z \in S\}\end{aligned}$$

$\Pi(0;S)$ is deemed to be the set of constant signals.

$$\begin{aligned}\Pi_0(z;S) &= \text{set of signals whose average over every subinterval } [x, x+z] \text{ within } S \text{ is } 0 \\ &= \left\{f \;\middle|\; \int_0^1 f(x+\alpha z)\,d\alpha = 0 \text{ whenever } x \in S \text{ and } x+z \in S\right\}\end{aligned}$$

These are abbreviated to $\Pi(z)$ or $\Pi_0(z)$ when S is understood from context. Under these definitions, f may take arbitrary values outside S (i.e., it doesn't have to be zero).

Theorem 2.2.1. For intraregion reconstruction in one frame, the unobservable modes are

$$\begin{aligned}N(\mathbf{H}) &= \Pi_0(vT;S) \\ &= \Pi(vT;S) \cap \left\{f \;\middle|\; \int_0^1 f(x+\alpha vT)\,d\alpha = 0 \text{ for some } x \in S \text{ such that } x+vT \in S\right\}.\end{aligned}$$

2.2.2 Interframe

Since one frame alone is insufficient for unique intraregion reconstruction, we can consider combining observations from corresponding intervals of additional frames. Corresponding intervals are the parts of each blurred frame affected by, and only by, a given set of optical flow lines, as shown in Figure 2.3. If the velocity were constant for all time, though, the new frames would merely repeat the information present in the first frame. For this reason, assume that the velocity, and hence the amount of motion blur, is different in each frame. However, allow the velocity to change only at the time instants between exposures, in order to preserve the rectangular point spread function in each frame. As first pointed out by [Ghiglia84], unequal blurs cause the zeros of the frequency response to fall on different sets of frequencies. With two or more blurred views of the same signal, therefore, a frequency component of the signal is completely invisible only where zeros happen to coincide (Figure 2.4).

Since the Fourier transform approach is, strictly speaking, not applicable when the observation domains are finite intervals, the same idea is now developed in terms of linear spaces in the signal domain. Suppose that the sequence of frames $g_c(x, iT)$, $i = 1, 2, \ldots, M$

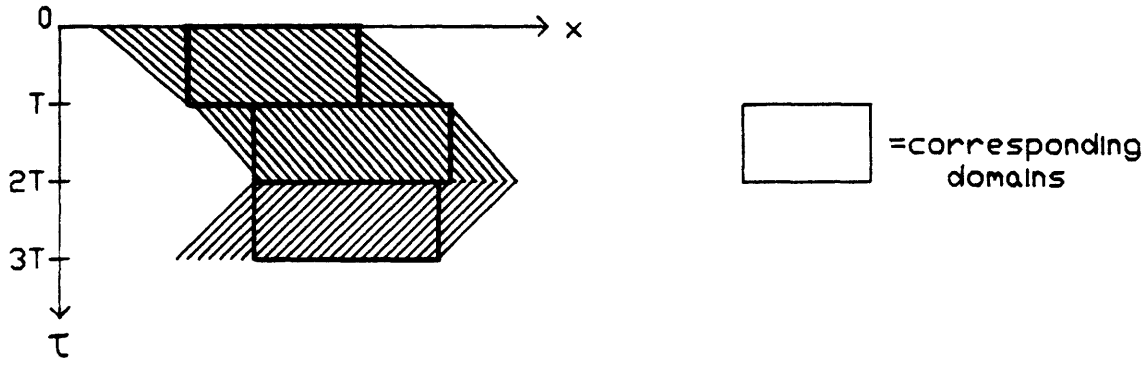

Figure 2.3: Interframe, intraregion observation domains: Corresponding observation domains in space-time, indicated by dark rectangles, are affected by, and only by, a given set of optical flow lines.

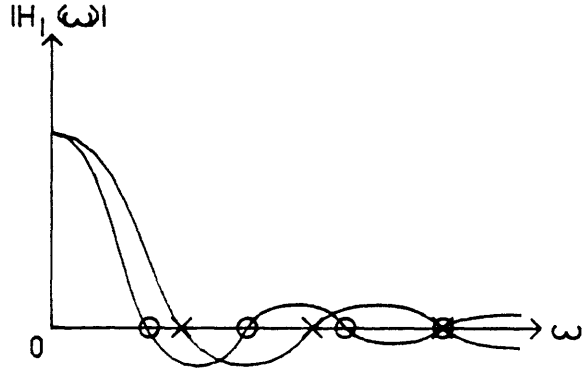

Figure 2.4: Frequency responses of unequal blurs: most zeros do not coincide.

is available, and that the velocity throughout the integration of frame i is v_i. If $f(x)$ is a nullvector for the interframe reconstruction problem, then $g_c(x, iT) = 0$ for all x in the corresponding interval in frame i, for all i. Hence, $f(x) \in \Pi_0(v_iT)$ for all i, that is, the nullvector must belong to the nullspace of each individual frame. Consequently, the unobservable subspace of the interframe problem must be

$$N(\mathbf{H}) = \bigcap_{i=1}^{M} \Pi_0(v_iT).$$

For example, a signal with DC-free periods belongs to the intersection set if its wavelength evenly divides every v_iT. In fact it can be shown that such signals are the only nullvectors as long as the intervals are large enough. Here are the precise statements.

Definition. By analogy with the greatest common divisor of integers, let $\gcd(z_1, \ldots, z_M)$ of a set of real numbers be the largest number for which every z_i is an integer multiple, or 0 if no such number exists.

Properties:

1. The numbers $m_i = z_i / \gcd(z_1, \ldots, z_M)$ are relatively prime integers, if they are defined.

2. $\gcd(z_1, \ldots, z_M) \leq |z_i|$ for all i.

3. The gcd is zero if and only if z_i and z_j are *incommensurate* (z_i/z_j is irrational) for some i, j.

gcd is a violently discontinuous function, as illustrated in Figure 2.5.

Theorem 2.2.2. If the length of each corresponding observation interval in a sequence of frames is at least $\min_i v_iT$ then the unobservable modes for intraregion reconstruction are

$$N(\mathbf{H}) = \Pi_0(\gcd(v_1T, \ldots, v_MT)).$$

Proof. Observing $g_c(x, iT)$ over an interval of length$\geq \min_i v_iT$ insures that the participating optical flow lines emanate from an interval of $f(x)$ whose length is at least $\min_i v_iT + \max_i v_iT$. Therefore, the lemma given in §A.1 is applicable. ∎

From this discussion we see that as few as two frames could be sufficient, in principle, to obtain unique reconstruction.

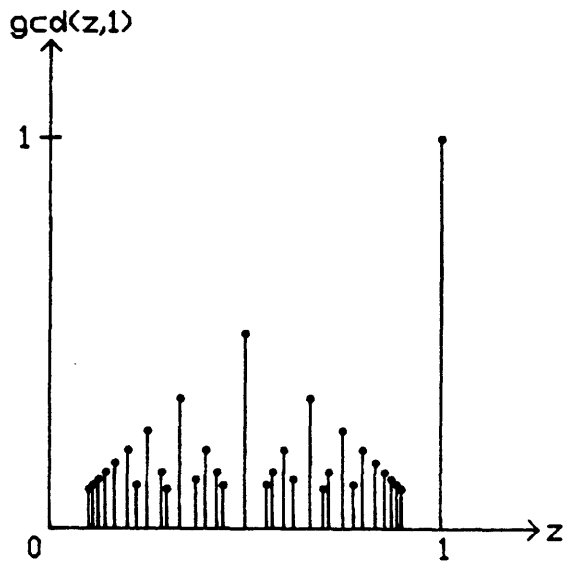

Figure 2.5: Rational samples of the discontinuous function $\gcd(z, 1)$

2.3 Transition Zone Compensation

After intraregion restoration the next level of complexity is to deal with two adjoining surfaces simultaneously, since the transition zone they share will yield additional constraints not accessible when the observation domain is restricted to the interior of a region. This part explores transition zone compensation, in which one surface is already known at full resolution so that it can be subtracted out of $g_c(x,t)$ before attempting to restore the other surface. The source of this prior knowledge does not matter, whether it arises from previous reconstruction calculations or, more simply, from absence of motion. Under favorable circumstances, a compensated transition zone at one end of a blurred region is enough of a boundary condition to uniquely reconstruct the rest of the region.

2.3.1 Definitions

When two surfaces meet, as in Figure 2.6, there are in general three velocities of concern. Throughout this chapter define:

$$
\begin{aligned}
f_f(x) &= \text{“foreground” surface image at } \tau = 0 \\
f_b(x) &= \text{“background” surface image at } \tau = 0 \\
v_f &= \text{“foreground” surface velocity} \\
v_b &= \text{“background” surface velocity} \\
v_e &= \text{edge velocity (in general } \neq v_b \text{ or } v_f).
\end{aligned}
$$

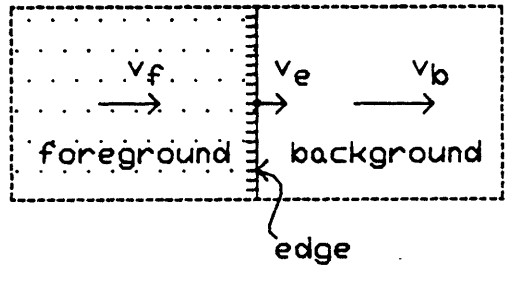

Figure 2.6: Velocities at a boundary

It is required that $v_e \neq 0$, for otherwise there is no transition zone to work with. In general $v_e \neq v_f$ since the foreground object could be dilating or eroding at the edge. Indeed, by assigning $v_e = v_b$ one could model the situation where the so-called background surface is really a solid object, with rigidly attached edges, translating in front of another surface, the so-called foreground. For the time being, "foreground" and "background" are just arbitrary designations.

For argument's sake, choose the coordinate system so that the boundary moves along the path $x = v_e\tau$. Also assume that $v_e > 0$ (reversing time if necessary), i.e., the space covered by the foreground is growing. These two assumptions have no effect on the eventual conclusions, which work even if $v_e < 0$. The foreground surface $f_c(x,\tau) = f_f(x - v_f\tau)$ is exposed where $x < v_e\tau$ and the background surface $f_c(x,\tau) = f_b(x - v_b\tau)$ is exposed where $x > v_e\tau$. The subscript c denotes a Composite time-varying scene or image sequence, made up of background and foreground components.

In the frame integrated from t to $t+T$, the transition zone occupies the interval $x \in [v_e t, v_e(t+T)]$. The integrated image sequence recorded by the camera is

$$g_c(x,t) = \frac{1}{T}\int_t^{t+T} f_c(x,\tau)\,d\tau = g_f(x,t) + g_b(x,t) \tag{2.4}$$

where the foreground surface contribution is

$$g_f(x,t) = \frac{1}{v_f T}\int_{x-v_f(t+T)}^{(1-v_f/v_e)x} f_f(u)\,du, \quad x \in [v_e t, v_e(t+T)] \tag{2.5}$$

and, similarly, the background surface contribution is

$$g_b(x,t) = \frac{1}{v_b T}\int_{(1-v_b/v_e)x}^{x-v_b t} f_b(u)\,du, \quad x \in [v_e t, v_e(t+T)]. \tag{2.6}$$

See Figure 2.7.

The preceding geometry and definitions will be retained throughout this chapter. In the problem of transition zone compensation, though, only the boundary and the unknown surface—which is deemed background—are relevant since the contribution of the known surface to $g_c(x,t)$ is assumed to be removed. Therefore, f_f, g_f, and v_f are presently irrelevant.

2.3.2 Intraframe

The analysis may be limited to reconstruction of the portion of the background surface that contributes to the transition zone. Let I denote the set of position coordinates of this

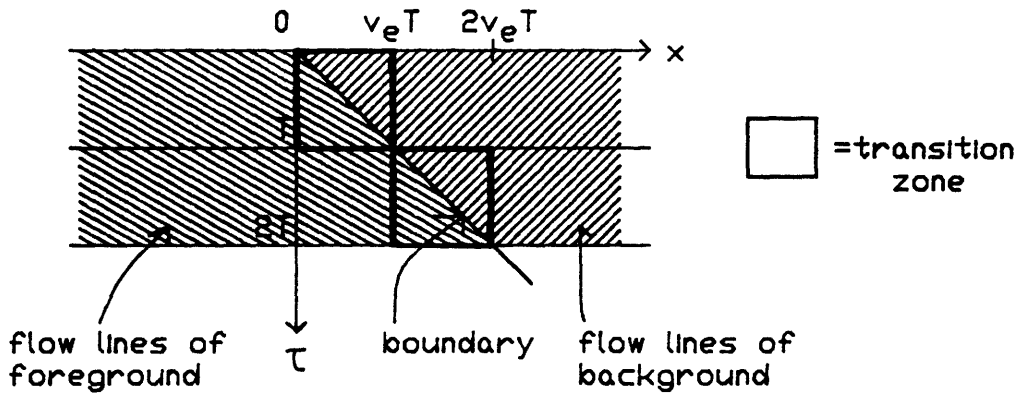

Figure 2.7: Space-time diagram of the image configuration at a boundary, showing transition zones

portion of $f_b(x)$. Although the size of the transition zone itself is determined by v_e, I will always be a closed interval at least as long as v_bT. Recall that knowledge of the background surface on any interval of length v_bT is sufficient as a boundary condition for reconstructing the rest of the surface. Therefore, unique reconstruction is possible if one can solve for $f_b(x)$ in I; conversely, without other sources of constraints, reconstruction is not possible if no part of I can be determined. Accordingly, observability questions can be settled by concentrating on the transition zone of the blurred image and the optical flow lines that enter it.

In the blurred frame at $t = 0$, the transition zone signal after compensation is

$$g_b(x,0) = \frac{1}{v_bT}\int_{(1-v_b/v_e)x}^{x} f_b(u)\,du, \quad x \in [0, v_eT]. \tag{2.7}$$

This integral defines a linear transformation that maps $L_2(I)$ to $L_2(0, v_eT)$, where set I is the interval

$$I = \begin{cases} [0, (v_e - v_b)T], & \text{if } v_b/v_e < 0; \\ [0, v_eT], & \text{if } 0 < v_b/v_e \leq 1; \\ [(v_e - v_b)T, v_eT], & \text{if } v_b/v_e > 1. \end{cases} \tag{2.8}$$

The shape of the region of support, as shown in Figure 2.8, depends on the velocity ratio v_b/v_e. It changes from an obtuse to an acute triangle as v_b/v_e increases past unity, marking a significant change in the nullspace of (2.7). ($v_b/v_e = 1$ gives a right triangle, which behaves like an obtuse triangle and will be combined with the $v_b/v_e < 1$ case.)

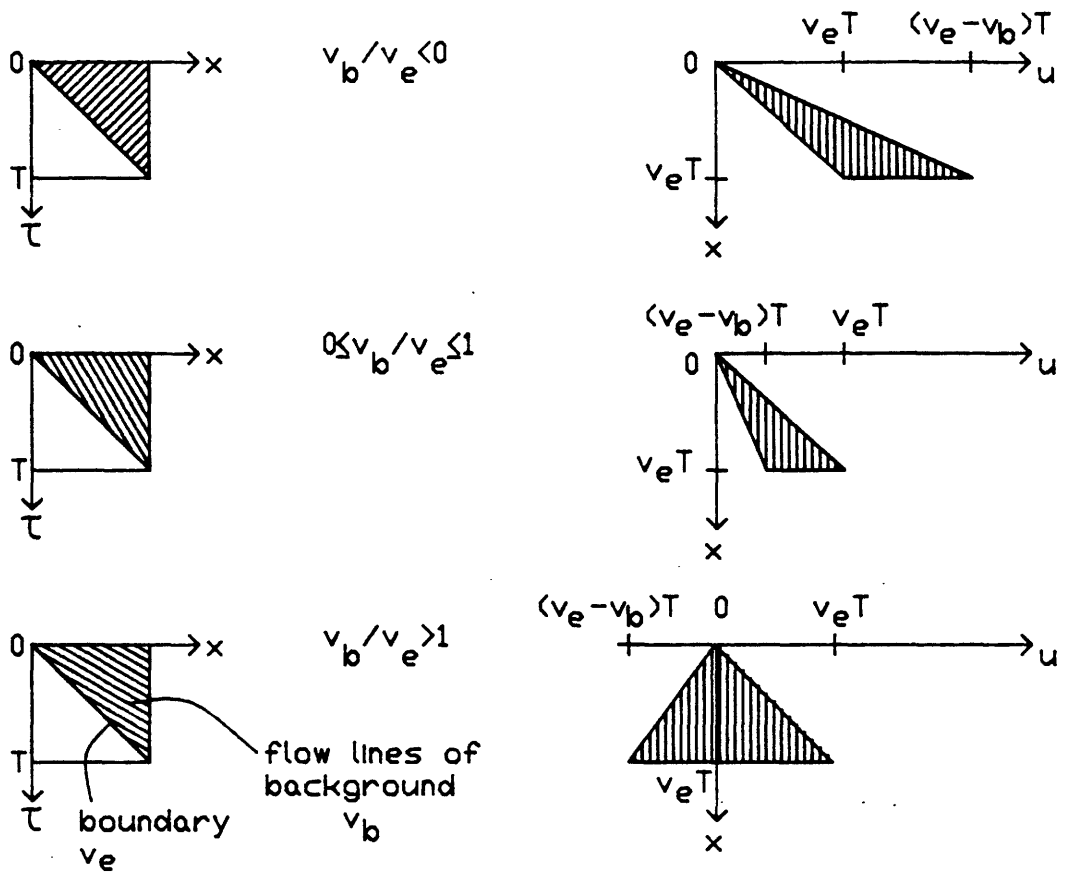

Figure 2.8: Three cases of intraframe transition zone compensation: (left) Space-time diagrams of a compensated transition zone, showing the background contribution to g_c after transition zone compensation; (right) corresponding integral operators. From top to bottom: $v_b/v_e < 0$, $0 \leq v_b/v_e \leq 1$, $v_b/v_e > 1$.

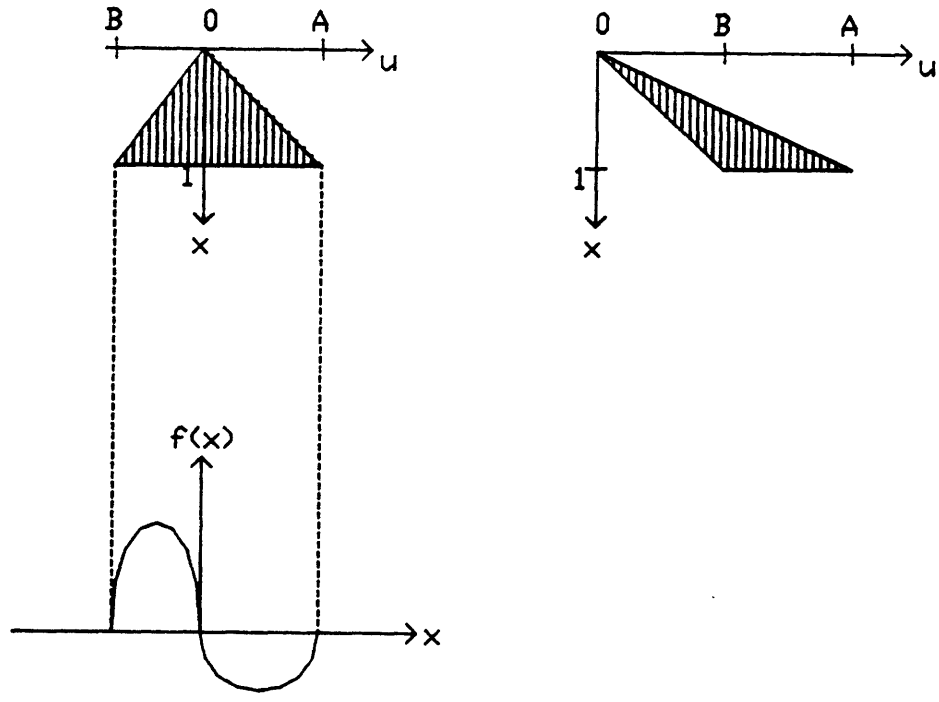

Figure 2.9: Linear transformations $\mathbf{H}_{\angle}$ and $\mathbf{H}_{\llcorner}$, with sample nullvector of $\mathbf{H}_{\angle}$

Using the analogy of finite dimensional matrices, intuition suggests that the linear transformation will be invertible in the obtuse triangle case: a lower triangular matrix with no zeros on the main diagonal is always invertible. Integral equations with lower triangular kernel are called Volterra equations and correspond to causal systems. On the other hand, the acute triangle case appears to be non-invertible: no matter what arbitrary signal is chosen for $f_b(x), x \leq 0$, the Volterra form of the kernel for $x \geq 0$ means that the rest of $f_b(x)$ can be chosen so as to satisfy (2.7). These properties are formalized as follows (Figure 2.9).

Definition.

a) Let $\mathbf{H}_{\angle}$ (read "H-acute") be the linear transformation from $L_2(B, A)$ to $L_2(0, 1)$, where $B < 0 < A$, given by

$$g(x) = \frac{1}{A - B} \int_{Bx}^{Ax} f(u)\, du, \quad x \in [0, 1]. \tag{2.9}$$

The region of support of the kernel is an acute triangle.

b) Let $\mathbf{H}_{\backslash}$ ("H-obtuse") be the linear transformation from $L_2(0, A)$ to $L_2(0, 1)$, where $0 \leq B < A$, given by the same formula. The region of support of the kernel is an obtuse triangle.

Lemma 2.3.2.

a) $N(\mathbf{H}_{\angle}) = \{f \mid Bf(Bx) = Af(Ax), \text{ for } x \in [0, 1]\}$, that is, the graph of any nullvector for negative abscissae is a scaled and inverted replica of the graph for positive abscissae.

b) $N(\mathbf{H}_{\backslash}) = \{\mathbf{0}\}$, i.e., the only solution of $g(x) = 0$ when $0 \leq B < A$ is $f(x) = 0$.

Proof. Let $F(x) = \int_0^x f(u)\, du$, so that $F(Ax) - F(Bx) = (A - B)g(x) = 0, \quad x \in [0, 1]$. If $B < 0 < A$ then it is trivial to devise functions $F(x)$ meeting this condition. Differentiation with respect to x yields the equivalent condition in (a). On the other hand, when $0 \leq B < A$ write the condition as $F(x) = F(Bx/A), \quad x \in [0, A]$. Recursive application of the latter yields $F(x) = F((B/A)^n x) \to F(0) = 0$ as $n \to \infty$, so that $F(x)$ must be the zero function. Therefore the only nullvector is $f(x) = 0$. ∎

Returning to the transition zone compensation problem, one can immediately recognize the linear transformation (2.7) as $\mathbf{H}_{\backslash}$ when $v_b/v_e \leq 1$ and as $\mathbf{H}_{\angle}$ when $v_b/v_e > 1$. Hence,

$$g_b(x, 0) = 0, \quad x \in [0, v_e T]$$

$$\Longrightarrow \quad \begin{cases} f_b(x) = 0, \quad x \in I, & \text{if } v_b/v_e \leq 1; \qquad (2.10) \\ f_b(x) \in N(\mathbf{H}_{\angle}), \quad x \in [(v_e - v_b)T, v_e T], & \text{if } v_b/v_e > 1. \qquad (2.11) \end{cases}$$

In addition, it may be assumed that the blurred frame can be observed in some interval $[v_e T, L]$ outside the transition zone. In order to have $g_b(x, 0) = 0$ for $x > v_e T$, a nullvector $f_b(x)$ must also belong to $\Pi_0(v_b T)$ for $x \geq \min(v_e T, (v_e - v_b)T)$. (2.10) specifies that the

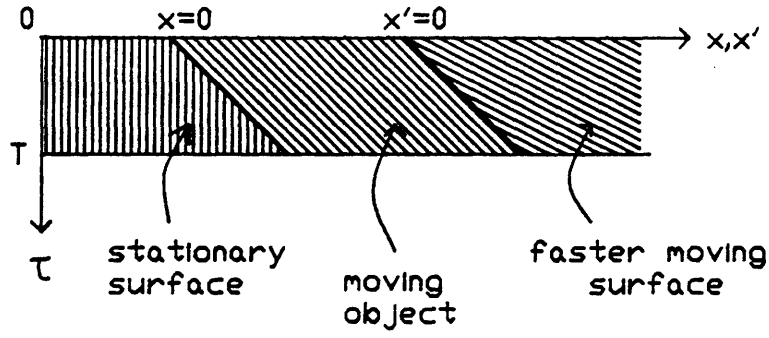

Figure 2.10: Space-time diagram for transition zone compensation example

periodic nullvector is zero over one period and thus everywhere; therefore, the observed data is sufficient to uniquely recover the background surface as long as it does *not* move in the same direction as, and faster than, the boundary. If it does, then nontrivial nullvectors are not ruled out, and the only restriction on the periodic waveform of a nullvector is (2.11). In summary, we have deduced this

Theorem 2.3.2. After transition zone compensation in one frame, the unobservable modes are

$$N(\mathbf{H}) = \begin{cases} \{\mathbf{0}\}, & \text{if } v_b/v_e \leq 1; \\ N(\mathbf{H}_\angle) \cap \Pi_0(v_b T), & \text{if } v_b/v_e > 1. \end{cases}$$

Examples

1. Suppose the left edge of an unknown moving object uncovers a stationary surface, as in Figure 2.10. With $v_b = v_e > v_f = 0$, the moving object can be reconstructed from one blurred frame once the stationary surface contribution $g_f(x,0) = (1-\frac{x}{v_e T})f_f(x), \quad x \in [0, v_e T]$ is subtracted out. Of course, one must look ahead into the following frame in order to observe $f_f(x), \quad x \in [0, v_e T]$. The inherent observability of the stationary surface has propagated to the moving object through the transition zone.

2. Suppose the right edge of the object just reconstructed occludes an unknown surface moving twice as fast. Here one has $v_b > v_e = v_f > 0$; consequently, observability of the slower moving region does not propagate to the faster one. With $v_b/v_e = 2$ the region of support of the linear transformation $\mathbf{H}_\angle$ is an isosceles triangle, so that functions

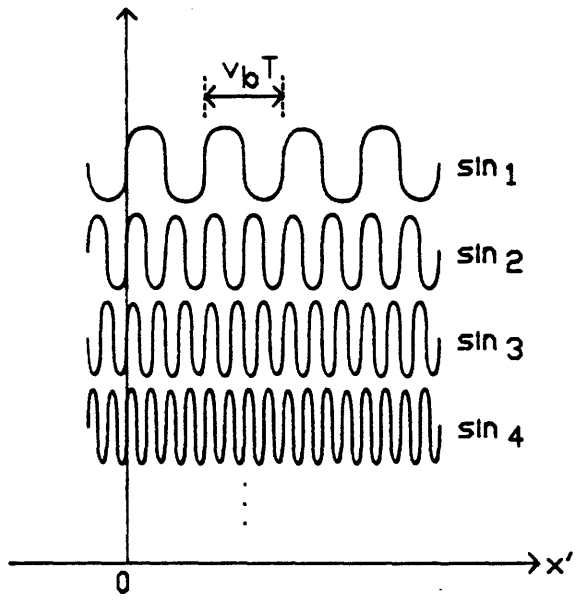

Figure 2.11: Nullvectors of transition zone compensation when $v_b/v_e = 2$

in $N(\mathbf{H}_\angle)$ must have odd symmetry within the interval $x' \in [-v_eT, v_eT]$. Therefore, the nullspace $N(\mathbf{H}_\angle) \cap \Pi_0(v_bT)$ consists of signals with DC-free and odd-symmetric periods of length v_bT and can be denoted by $\{\text{odd functions}\} \cap \Pi_0(v_bT)$. A natural basis for this subspace is the set of sinusoids with periods $v_bT, \frac{v_bT}{2}, \frac{v_bT}{3}, \ldots$ phased to cross zero at $x' = 0$, the intersection of the right boundary with $\tau = 0$ (Figure 2.11).

2.3.3 Interframe

The preceding results can be extended to observations of two or more successive frames, assuming that the surface and boundary velocities remain time-invariant. (The time-varying problem has resisted analysis, but at least the interframe, intraregion results are applicable.) There is no need to treat boundaries at which $v_b/v_e \leq 1$ since intraframe transition zone compensation is enough for unique reconstruction. Accordingly, only the case of $v_b/v_e > 1$ will be reconsidered.

In the blurred frame at $t = T$, the transition zone signal after compensation is

$$g_b(x,T) = \frac{1}{v_bT} \int_{(1-v_b/v_e)x}^{x-v_bT} f_b(u)\,du, \quad x \in [v_eT, 2v_eT]. \tag{2.12}$$

Taken together, the integrals (2.7) and (2.12) depend on $f_b(x)$ in the interval $[2(v_e - v_b)T, v_eT]$. A third constraint on the background signal in that interval can be obtained by observing the blurred frame $g_b(x,T)$ in the interval $[2v_eT, (v_e + v_b)T]$, which lies just outside the transition zone (Figure 2.12). In order for $f_b(x)$ to be a nullvector, (2.7) and (2.12), as well as $g_b(x,T)$, $x \in [2v_eT, (v_e + v_b)T]$, must all be zero. In other words, it is required that $f_b(x)$ satisfy

$$\begin{aligned} f_b(x) &\in N(\mathbf{H}_\swarrow) \\ f_b(x + (v_e - v_b)T) &\in N(\mathbf{H}_\swarrow) \\ f_b(x) &\in \Pi_0(v_bT; [2(v_e - v_b)T, v_eT]). \end{aligned} \tag{2.13}$$

These simultaneous equations are solved in §A.3, whose conclusions are summed up as follows:

1. If $v_b/v_e = 2$, the set of solutions to (2.13) consists of all odd-symmetric signals in $\Pi_0(v_bT)$.

2. If $v_b/v_e \neq 2$, the solution set contains only $\mathbf{0}$.

Therefore, the observed data in two frames is almost always sufficient to recover the background surface. In the pathological case of $v_b/v_e = 2$, all of the nullvectors from intraframe transition zone compensation, as displayed in Figure 2.11, survive as nullvectors in the two-frame problem. Moreover, frames beyond the second are redundant and cannot reduce the unobservable subspace. Since a nullvector $f_b(x)$ must have period v_bT and the relative displacement between the two surfaces after two frames is also v_bT, the data segment $g_b(x, iT)$, $x \in [iv_eT, (i+1)v_eT]$, when $f_b(x)$ is a nullvector, is identical to either (2.7) or (2.12) when i is even or odd, respectively.

To summarize these new findings along with the previously verified observability of the $v_b/v_e < 1$ case, we state the following

Theorem 2.3.3. After transition zone compensation in two or more frames, the unobservable modes are

$$N(\mathbf{H}) = \begin{cases} \{\mathbf{0}\}, & \text{if } v_b/v_e \neq 2; \\ \{\text{odd functions}\} \cap \Pi_0(v_bT), & \text{if } v_b/v_e = 2. \end{cases}$$

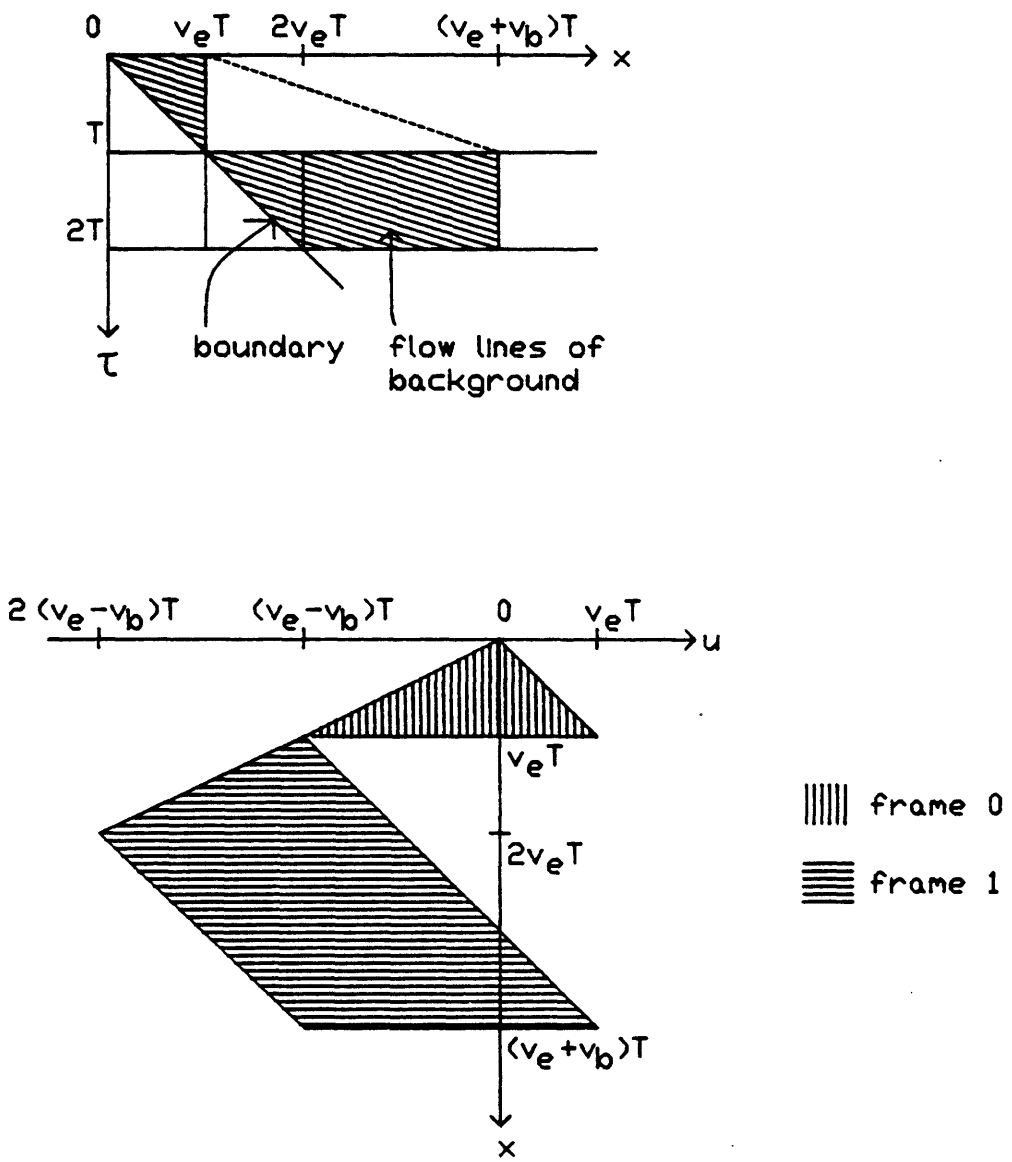

Figure 2.12: Transition zone compensation in two frames: (top) Space-time diagram of relevant observation intervals, showing background contribution to g_c after compensation; (bottom) corresponding integral operators for the observations in both frames.

2.4 Interregion Reconstruction

In order to reconstruct a surface using the idea of transition zone compensation, complete knowledge of an adjoining surface is required. In the absence of such information, though, certain weaker conditions on the foreground surface's contribution to the transition zone could still yield new constraints on the unobservable modes of the background, possibly enough for unique reconstruction.

Specifically, we will assume that the boundary moves in conjunction with the foreground surface, i.e., $v_e = v_f$, and that all velocities are time-invariant. Under these conditions, the contribution of the foreground surface to the transition zone—whose motion tracks the boundary—is identical in each frame of a sequence. Because this property gives a strong constraint on the background surface signal, and because this surface/boundary configuration should occur frequently in actual scenes, this set of assumptions deserves special study and will be called the interregion reconstruction problem. The main idea is that the interregion problem is related to transition zone compensation of the displaced-frame-difference sequence.

2.4.1 Intraframe

Any possibility of interregion reconstruction using one frame alone can be quickly dismissed. In reference to the geometry defined in §2.3.1, recall that the observation of $g_c(x,0)$ for $x \geq v_e T$ gives an intraframe, intraregion reconstruction problem, for which the unobservable subspace of the background surface image is $\Pi_0(v_b T)$. Adding data from the uncompensated transition zone cannot eliminate any nullvectors because the foreground signal is unconstrained. Indeed, given any function $f_b(x)$ that yields $g_c(x,0) = g_b(x,0) = 0$ for all $x \geq v_e T$, choose

$$f_f(x) = \begin{cases} v_f T \dfrac{d}{dx} g_b(x + v_f T, 0), & \text{if } x \in [-v_f T, 0]; \\ f_f(x + v_f T), & \text{otherwise} \end{cases} \tag{2.14}$$

to make $g_c(x,0) = 0$ everywhere else (differentiate (2.5) to obtain this result). Any such pair (f_b, f_f) is a nullvector for the intraframe, interregion reconstruction problem.

2.4.2 Two Frames

Knowledge of M blurred frames is equivalent to knowledge of the first frame and $M-1$ difference frames $\underline{\Delta}\, g_c(x,t)$, where

$$\underline{\Delta}\, g_c(x,t) = g_c(x+v_eT, t+T) - g_c(x,t).$$

However, since the foreground and boundary have the same velocity, $g_f(x,t)$ vanishes and the displaced frame difference $\underline{\Delta}\, g_c(x,t)$ depends only on the background signal, even within transition zones:

$$\underline{\Delta}\, g_c(x,t) = \frac{1}{v_bT}\int_{(1-v_b/v_e)x}^{x-v_bt} \Delta f_b(u)\, du, \quad x \in [v_et, v_e(t+T)], \tag{2.15}$$

where Δ is the operation of linear convolution with $\delta(x+(v_e-v_b)T) - \delta(x)$, so that

$$\Delta f_b(x) = f_b(x+(v_e-v_b)T) - f_b(x). \tag{2.16}$$

The determination of the nullspace for interregion reconstruction given two frames proceeds in the same manner as for transition zone compensation in one frame. From the first frame, $g_c(x,0) = 0$ already restricts nullvectors to $\Pi_0(v_bT)$, and now $g_c(x,T) = 0$ should further narrow the nullspace.

If (2.15) is compared to (2.6), it is evident that $\Delta f_b(x)$ is mapped to $\underline{\Delta}\, g_c(x,0)$ by the linear transformation $\mathbf{H}_{\backslash}$ or $\mathbf{H}_{\angle}$, depending on the velocity ratio v_b/v_e. Thus,

$$\begin{aligned} g_c(x,0) = g_c(x,T) = 0 \quad &\Longrightarrow \quad \underline{\Delta}\, g_c(x,0) = 0 \\ &\Longrightarrow \quad \begin{cases} \Delta f_b(x) = 0, & \text{if } v_b/v_e \le 1; \qquad (2.17) \\ \Delta f_b(x) \in N(\mathbf{H}_{\angle}), & \text{if } v_b/v_e > 1, \qquad (2.18) \end{cases} \end{aligned}$$

using (2.10) and (2.11).

(2.17) translates to $f_b(x) \in \Pi((v_e-v_b)T)$ for $x \ge 0$; therefore, by the lemma given in §A.1, the nullspace is exactly $\Pi_0(v_bT) \cap \Pi((v_e-v_b)T) = \Pi_0(\gcd(v_bT, v_eT))$ as long as the background surface does *not* move in the same direction as, and faster than, the foreground and boundary. This nullspace degenerates to $\{\mathbf{0}\}$ when the velocity ratio is irrational.

If $v_b/v_e > 1$, though, additional nullvectors are not ruled out, the only restriction on the periodic waveform of a nullvector being (2.18). The nullspace can be expressed as $N(\mathbf{H}_{\angle}\Delta) \cap \Pi_0(v_bT)$, which contains $\Pi_0(\gcd(v_bT, v_eT))$ since any function annihilated by Δ is most certainly annihilated by $\mathbf{H}_{\angle}\Delta$. It is not obvious, however, whether this nullspace

has any "interesting" solutions, that is, signals in $\Pi_0(\gcd(v_bT, v_eT))^\perp$ or, more importantly, signals with fundamental period v_bT. Basically the question is whether the simultaneous equations

$$\begin{aligned} f_b(x + (v_e - v_b)T) - f_b(x) &\in N(\mathbf{H}_\angle) \\ f_b(x) &\in \Pi_0(v_bT; [2(v_e - v_b)T, v_eT]) \end{aligned} \tag{2.19}$$

can be fulfilled without having $\Delta f_b(x) = 0$.

One approach for constructing an interesting solution to (2.19) is to start with any element $\phi \in N(\mathbf{H}_\angle) \cap \Pi_0(v_bT)$, which is known to be a non-trivial space; then $\Delta^{-1}\phi$ must be a solution. Δ^{-1} is the operation of deconvolution onto $\Pi_0(\gcd(v_bT, v_eT))^\perp$. The principal difficulty, however, is that $\Delta^{-1}\phi$ might not exist for certain (or all) choices of ϕ. As long as v_b/v_e is rational, §A.2 verifies that (2.19) does indeed possess finite nontrivial solutions, but the answer for irrational v_b/v_e is not presently known. This gap in the theory is not serious, though, since the three-frame problem will be solved completely (see also §5.3.4).

Theorem 2.4.2. For the interregion reconstruction problem using two frames, the unobservable modes are

$$N(\mathbf{H}) = \begin{cases} \Pi_0(\gcd(v_bT, v_eT)), & \text{if } v_b/v_e \leq 1; \\ N(\mathbf{H}_\angle\Delta) \cap \Pi_0(v_bT), & \text{if } v_b/v_e > 1. \end{cases}$$

In fact, $N(\mathbf{H}_\angle\Delta) \cap \Pi_0(v_bT) \supseteq \Pi_0(\gcd(v_bT, v_eT))$. Moreover, $\supseteq$ is replaced by $\supset$ if v_b/v_e is rational.

While the elements of $N(\mathbf{H}_\angle)$ are easy to visualize as scaled antisymmetric functions for any $v_b/v_e > 1$, the elements of $N(\mathbf{H}_\angle\Delta)$ cannot usually be described in a straightforward way. The following is a rare exception.

Example Suppose the right edge of a moving object occludes an unknown surface moving twice as fast (Figure 2.13). When $v_b/v_e = 2$ the nullspace $N(\mathbf{H}_\angle\Delta) \cap \Pi_0(v_bT)$ can be determined explicitly by expressing a nullvector in $\Pi_0(v_bT)$ as

$$f_b(x) = \sum_{k \neq 0} a_k e^{j\frac{2\pi k}{v_bT}x}$$

and finding constraints on the a_k. Since

$$\Delta f_b(x) = \sum_{k \neq 0} \underbrace{a_k((-1)^k - 1)}_{c_k} e^{j\frac{2\pi k}{v_bT}x},$$

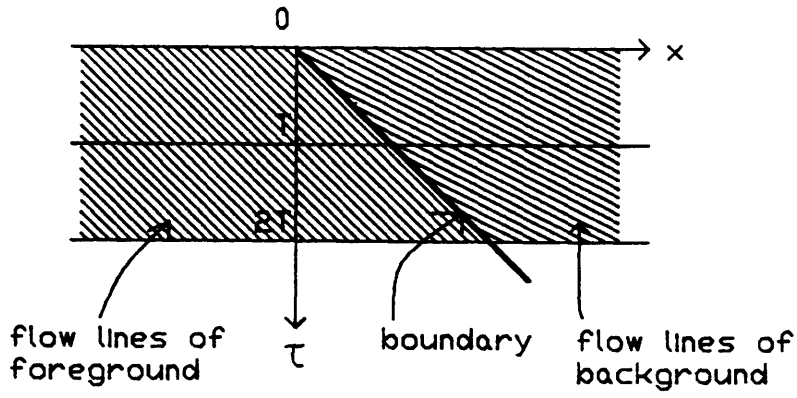

Figure 2.13: Space-time diagram for interframe, interregion reconstruction example

a_k is arbitrary if k is even. On the other hand, $\Delta f_b(x) \in N(\mathbf{H}_\angle) = \{\text{odd functions}\}$ requires $c_k = -c_{-k}$, so $a_k = -a_{-k}$ if k is odd. Therefore,

$$f_b(x) \in (\{\text{odd functions}\} \cap \Pi_0(v_b T)) \oplus \Pi_0(v_b T/2),$$

where the direct sum $X \oplus Y$ means the set of all signals equal to any function from X plus any function from Y. A natural basis for the unobservable subspace consists of all sines and cosines with periods $\frac{v_b T}{2}, \frac{v_b T}{4}, \frac{v_b T}{6}, \ldots$, along with the set of sinusoids with periods $v_b T, \frac{v_b T}{3}, \frac{v_b T}{5}, \ldots$ phased to cross zero at $x' = 0$, the intersection of the boundary with $\tau = 0$ (Figure 2.14).

2.4.3 Three or More Frames

Interregion reconstruction using three frames is no improvement over two frames when $v_b/v_e \leq 1$, while the third frame almost always eliminates some unobservable modes when $v_b/v_e > 1$. The situation is analogous to that of two-frame versus one-frame transition zone compensation.

Regardless of the velocity ratio or the number of frames observed, any background signal $f_b(x) \in \Pi_0(\text{gcd}(v_b T, v_e T))$ still forms a nullvector, since its displaced frame difference is zero. Therefore, the constraints provided by the third or following frames can do nothing to remove this class of unobservable modes. There still exists the possibility of affecting the

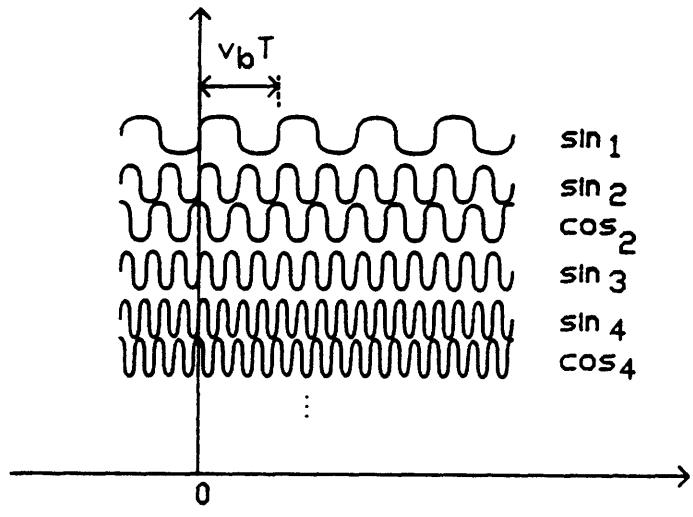

Figure 2.14: Nullvectors of interregion reconstruction when $v_b/v_e = 2$

nullvectors in $N(\mathbf{H}_\angle\Delta)\cap\Pi_0(v_bT)$, which are present only when $v_b/v_e > 1$. These nullvectors will now be re-examined.

Building upon the techniques of previous sections, the result can be obtained in short order. With three frames, a nullvector $f_b(x)$ must satisfy $\underline{\Delta}\, g_c(x,T) = 0$ in addition to $\underline{\Delta}\, g_c(x,0) = 0$, leading to the constraints

$$\begin{aligned} \Delta f_b(x) &\in N(\mathbf{H}_\angle) \\ \Delta f_b(x+(v_e-v_b)T) &\in N(\mathbf{H}_\angle) \\ \Delta f_b(x) &\in \Pi_0(v_bT;[2(v_e-v_b)T, v_eT]). \end{aligned}$$

Since these equations are of the same form as (2.13), Theorem 2.3.3 can be used to conclude that

$$\begin{cases} \Delta f_b(x) = 0, & \text{if } v_b/v_e \neq 2; \\ \Delta f_b(x) \in \{\text{odd functions}\} \cap \Pi_0(v_bT), & \text{if } v_b/v_e = 2. \end{cases} \tag{2.20}$$

The nullspace is exactly $\Pi_0(\gcd(v_bT, v_eT))$ as long as $v_b/v_e \neq 2$. The pathological exception of $v_b/v_e = 2$ could have been foreseen, knowing that frames beyond the second are redundant with respect to signals in the subspace $\Pi_0(v_bT)$. Consequently, all of the nullvectors from interregion reconstruction using two frames, as displayed in Figure 2.14, survive as nullvectors in the three-frame problem.

Theorem 2.4.3. For the interregion reconstruction problem using three or more frames, the unobservable modes are

$$N(\mathbf{H}) = \begin{cases} \Pi_0(\gcd(v_b T, v_e T)), & \text{if } v_b/v_e \neq 2; \\ (\{\text{odd functions}\} \cap \Pi_0(v_b T)) \oplus \Pi_0(v_b T/2), & \text{if } v_b/v_e = 2. \end{cases}$$

2.5 Summary

In any linear measurement-inversion problem, complete recovery of the unknown input signal is hindered by the existence of a nontrivial nullspace, i.e., unobservable subspace, because signal components within it are nulled out by the blurring system. For conventional intraframe, intraregion restoration of motion blur, a certain set of periodic signals is unobservable, and the benefits of additional information can be judged by how much the set is narrowed down. Therefore, it is important to predict the nullspace for each of the three prototype reconstruction problems, for image sequences with any number of frames. It is found that the nullspace depends on the velocities of surfaces and boundaries in a systematic manner.

The basic assumption underlying all the theorems in this chapter is that a noiseless and spatially continuous imaging system captures blurred, but otherwise ideal, frames by 100% temporal integration. The interframe, intraregion theory, which additionally requires piecewise constant velocities, concludes that the wavelength of unobservable modes drops to the greatest common divisor of the respective blurs in each frame. With luck, this gcd will be small or zero, and the visibility of missing-signal artifacts in the deblurred image will diminish.

Time-invariant surface and boundary velocities are assumed for the transition zone and interregion results. Transition zone compensation depends on prior knowledge of the contribution of one side to a transition zone so that it can be subtracted off at the outset. The interframe version seems to be the most successful reconstruction scheme since it can rule out all nullvectors except for one special combination of velocities.

The interregion theory does not require prior knowledge of one side. Instead, the boundary must move in lockstep with one of the adjacent surfaces, so that subtraction of consecutive frames offset by the boundary motion will totally cancel out the contribution of one side. This method is inferior to transition zone compensation, only because it does not recover periodic signals of wavelength equal to the greatest common divisor of the two surface blurs.

The pathology of $v_b/v_e = 2$, the critical point $v_b/v_e = 1$, and the violently discontinuous function $\gcd(z_1, z_2)$ figure prominently in this theory. Consequently, it appears that infinitesimal velocity perturbations could make structural changes to the nullspace. Such

sensitivity would be untenable for any results that are to be applied to physical problems. When §5.3.4 introduces noise into the analysis, however, it will be argued that a signal unobservable in theory for only a precise combination of velocities is unobservable in practice for a neighborhood of velocities. Therefore, the idealized results of this chapter should have some real-world significance.

Chapter 3

Generalization to Arbitrary Duty Cycle

Thus far, the theory has been presented assuming maximum camera integration [1]. The most general temporal integration function to be examined in this thesis will be a rectangular window of any duration up to T. The sequence recorded by the camera is now

$$g_c(x,t) = \frac{1}{DT}\int_t^{t+DT} f_c(x,\tau)\,d\tau,$$

where the duty cycle D must be positive and no greater than unity.

All the results for intraframe reconstruction problems follow directly from the previous work simply by replacing T with DT (redefining $\mathbf{H}_\angle$ suitably) because the symbol T was used there only to denote integration time, never frame period. The same is true for intraregion reconstruction from multiple frames. These problems need no further discussion, but are duly recorded in Figure 3.1. In contrast, the other interframe problems should be re-examined because the presence of time gaps between exposures changes the form of the linear mapping from surfaces to frames. Unfortunately, a complete characterization of the nullspace has not been obtained in every case.

[1] This chapter and the next may be skipped without loss of continuity. The reader may wish to proceed to Chapter 5, which discusses noise and sampling issues in the one-dimensional, 100% duty cycle framework.

Problem Classification	Special Assumptions	Frames	v_b/v_e	Duty cycle D	$N(\mathbf{H})$	Notes
Intraregion		M			$\Pi_0\big(\gcd(v_1 DT, \ldots, v_M DT)\big)$	$N(\mathbf{H}) = \{\mathbf{0}\}$ if $\exists i, j$ such that v_i/v_j =irrational
Transition Zone Compensation (one unknown region, one known region)		1	≤ 1		$\{\mathbf{0}\}$	
			> 1		$N(\mathbf{H}_{\angle}) \cap \Pi_0(v_b DT)$	
	constant velocities	≥ 2	$\neq 2$	$\geq \min(v_b/v_e - 1, 1)$	$\{\mathbf{0}\}$	
				$< \min(v_b/v_e - 1, 1)$	?	Only partial answers known
			$= 2$		{odd functions} $\cap \Pi_0\big(\gcd(v_b DT, v_b T)\big)$	$N(\mathbf{H}) = \{\mathbf{0}\}$ if D =irrational
Interregion (two unknown regions)		1			$\Pi_0(v_b DT)$	same as intraregion
	constant velocities, $v_f = v_e$	2	≤ 1		$\Pi_0\Big(\gcd\big(v_b DT, (v_e - v_b)T\big)\Big)$	$N(\mathbf{H}) = \{\mathbf{0}\}$ if $D/(v_b/v_e - 1)$ =irrational
			> 1		$N(\mathbf{H}_{\angle}\Delta) \cap \Pi_0(v_b DT)$	$N(\mathbf{H}) \supseteq \Pi_0\Big(\gcd\big(v_b DT, (v_e - v_b)T\big)\Big)$
		≥ 3	$\neq 2$	$\geq \min(v_b/v_e - 1, 1)$	$\Pi_0\Big(\gcd\big(v_b DT, (v_e - v_b)T\big)\Big)$	$N(\mathbf{H}) = \{\mathbf{0}\}$ if $D/(v_b/v_e - 1)$ =irrational
				$< \min(v_b/v_e - 1, 1)$	?	Only partial answers known
			$= 2$	$\neq m/n$, n odd	$\Pi_0\Big(\gcd\big(v_b DT, (v_e - v_b)T\big)\Big)$	$N(\mathbf{H}) = \{\mathbf{0}\}$ if $D/(v_b/v_e - 1)$ =irrational
				m/n, n odd	$\big(\{\text{odd functions}\} \cap \Pi_0(v_b T/n)\big)$ $\oplus \Pi_0\big(\gcd(v_b DT, v_b T/2)\big)$	

Figure 3.1: Unobservable subspaces of 1D reconstruction problems, $0 < D \leq 1$

$$(\mathbf{H}_{\angle} f)(x) = \frac{1}{v_b DT} \int_{(1-v_b/v_e)x}^{x} f(u)\, du, \quad x \in [0, v_e DT]$$

$$(\Delta f)(x) = f\big(x + (v_e - v_b)T\big) - f(x)$$

3.1 Transition Zone Compensation

Suppose two or more frames are observed. Since intraframe transition zone compensation is enough for unique reconstruction when $v_b/v_e \leq 1$, only the case of $v_b/v_e > 1$ needs to be discussed. Following the arguments leading up to (2.13), a nullvector $f_b(x)$ must satisfy

$$\begin{aligned} f_b(x) &\in N(\mathbf{H}_\angle) \\ f_b(x + (v_e - v_b)T) &\in N(\mathbf{H}_\angle) \\ f_b(x) &\in \Pi_0(v_b DT; [(1+D)(v_e - v_b)T, v_e DT]), \end{aligned} \tag{3.1}$$

where $\mathbf{H}_\angle$ is the linear transformation defined by

$$g_b(x,0) = \frac{1}{v_b DT} \int_{(1-v_b/v_e)x}^{x} f_b(u)\, du, \quad x \in [0, v_e DT]. \tag{3.2}$$

(See Figure 3.2). These simultaneous equations are studied in §A.4, where it is proved that the solution depends on v_b/v_e and D as follows:

1. If $v_b/v_e = 2$ and D can be expressed as the ratio of integers m/n in lowest terms, the set of solutions to (3.1) consists of all odd-symmetric signals in $\Pi_0(v_b T/n)$. But if D is irrational, the solution set contains only $\mathbf{0}$.

2. If $v_b/v_e < 2$ and $D \geq v_b/v_e - 1$, or if $v_b/v_e > 2$ and $D = 1$, the solution set contains only $\mathbf{0}$.

When the conditions of (2) are satisfied, the observed data in two frames is sufficient to recover the background surface. In the usual pathological case of $v_b/v_e = 2$, not all nullvectors from intraframe transition zone compensation necessarily survive as nullvectors in the two-frame problem (though they will if $m = 1$); $f_b(x)$ is restricted to the space $\Pi_0(v_b T/n)$, which can be narrower than $\Pi_0(v_b DT)$. Finally, additional observations do not eliminate any of these nullvectors, since frames beyond the second are redundant with respect to signals in the subspace $\Pi_0(v_b T/n)$.

Theorem 3.1. (Partial generalization of Theorem 2.3.3) After transition zone compensation in two or more frames, the unobservable modes are

$$N(\mathbf{H}) = \begin{cases} \{\mathbf{0}\}, & \text{if } v_b/v_e \neq 2 \text{ and } D \geq \min(\frac{v_b}{v_e} - 1, 1); \\ \{\text{odd functions}\} \cap \Pi_0(\gcd(v_b DT, v_b T)), & \text{if } v_b/v_e = 2. \end{cases}$$

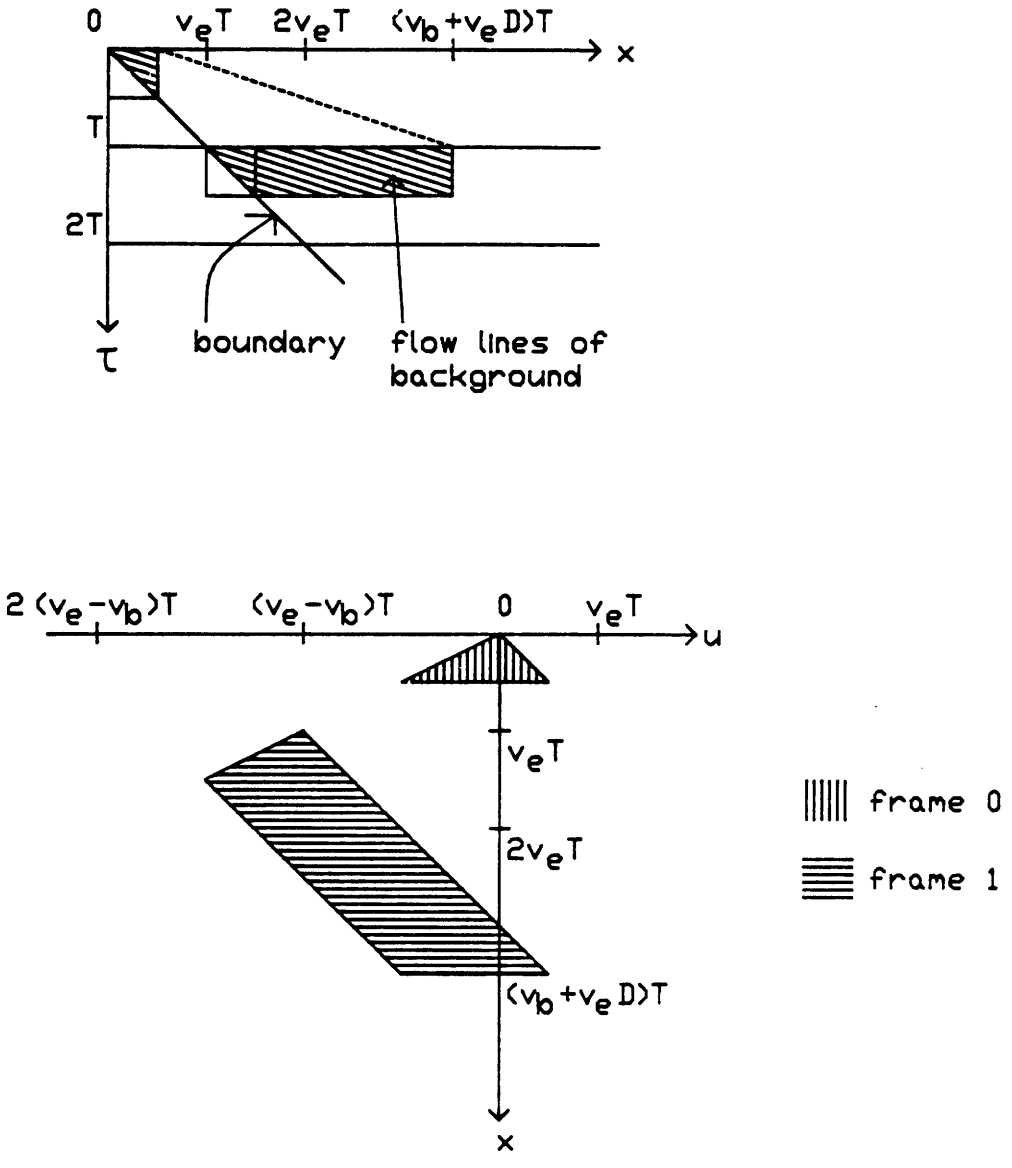

Figure 3.2: Transition zone compensation in two frames, $D < 1$: (top) Space-time diagram of relevant observation intervals, showing background contribution to g_c after compensation, cf. Figure 2.12; (bottom) corresponding integral operators for the observations in both frames.

The foregoing results are incomplete since they exclude the parameter range

$$\{(v_b/v_e, D) \mid v_b/v_e \neq 2, \quad 0 < D < \min(v_b/v_e - 1, 1)\}.$$

There is evidence to suggest that $N(\mathbf{H})$ is $\{\mathbf{0}\}$ or $N(\mathbf{H}_\angle) \cap \Pi_0(v_b DT)$ for a large subset of this range, but the subset is complicated to describe. Outside the subset, the nullspace is not presently known. Completion of the results appears to hinge on the iteration behavior of a certain nonlinear oscillator (§A.4).

3.2 Interregion Reconstruction

3.2.1 Two Frames

When two frames are observed, the general versions of (2.17) and (2.18) state that a nullvector $f_b(x)$ must satisfy

$$\begin{cases} \Delta f_b(x) = 0, & \text{if } v_b/v_e \leq 1; \\ \Delta f_b(x) \in N(\mathbf{H}_\angle), & \text{if } v_b/v_e > 1. \end{cases}$$

$\mathbf{H}_\angle$ is defined by (3.2), and $\Delta f_b(x)$ is still given by (2.16) independent of the duty cycle. Unless $D = 1$ and v_b/v_e is rational, it is not known if $N(\mathbf{H}_\angle\Delta) \cap \Pi_0(v_bDT)$ actually contains any signals outside of $\Pi_0\Big(\gcd(v_bDT, (v_e - v_b)T)\Big)$. The uncertainty means that the following theorem, like the result stated in the last chapter for $D = 1$, could perhaps be strengthened.

Theorem 3.2.1. (Generalization of Theorem 2.4.2) For the interregion reconstruction problem using two frames, the unobservable modes are

$$N(\mathbf{H}) = \begin{cases} \Pi_0\Big(\gcd(v_bDT, (v_e - v_b)T)\Big), & \text{if } v_b/v_e \leq 1; \\ N(\mathbf{H}_\angle\Delta) \cap \Pi_0(v_bDT), & \text{if } v_b/v_e > 1. \end{cases}$$

In fact, $N(\mathbf{H}_\angle\Delta) \cap \Pi_0(v_bDT) \supseteq \Pi_0\Big(\gcd(v_bDT, (v_e - v_b)T)\Big)$.

3.2.2 Three or More Frames

When three or more frames are observed, only the case of $v_b/v_e > 1$ needs to be discussed, since unobservable modes in $\Pi_0\Big(\gcd(v_bDT, (v_e - v_b)T)\Big)$ cannot be affected by frames beyond the second. Application of Theorem 3.1 to $\Delta f_b(x)$ implies that

$$\begin{cases} \Delta f_b(x) = 0, & \text{if } v_b/v_e \neq 2 \text{ and } D \geq \min(\frac{v_b}{v_e} - 1, 1); \\ \Delta f_b(x) = 0, & \text{if } v_b/v_e = 2 \text{ and } D = \text{irrational}; \\ \Delta f_b(x) \in \{\text{odd functions}\} \cap \Pi_0(v_bT/n), & \text{if } v_b/v_e = 2 \text{ and } D = m/n, \end{cases} \tag{3.3}$$

a generalization of (2.20).

When $v_b/v_e = 2$ and $D = m/n$, not all nullvectors from reconstruction with two frames necessarily survive as nullvectors in the three-frame problem (though they will if $m = 1$); $\Delta f_b(x)$ is restricted to the space $\Pi_0(v_bT/n)$, which can be narrower than $\Pi_0(v_bDT)$. The nullspace $N(\mathbf{H})$ can be determined explicitly by expressing a nullvector in $\Pi_0(v_bDT)$ as

$$f_b(x) = \sum_{k \neq 0} a_k e^{j\frac{2\pi kn}{mv_bT}x}$$

and finding constraints on the a_k. Since

$$\Delta f_b(x) = \sum_{k \neq 0} \underbrace{a_k(e^{-j\frac{\pi kn}{m}} - 1)}_{c_k} e^{j\frac{2\pi kn}{mv_bT}x},$$

a_k is arbitrary if kn/m is an even integer. On the other hand, $\Delta f_b(x) \in \{\text{odd functions}\} \cap \Pi_0(v_bT/n)$ requires $c_k = -c_{-k}$ if k is a multiple of m, and $c_k = 0$ otherwise. Therefore,

$$f_b(x) \in (\{\text{odd functions}\} \cap \Pi_0(v_bT/n)) \oplus \Pi_0(\gcd(v_bDT, v_bT/2)).$$

(Note that the first term of this direct sum is superfluous when n is even, for then $\Pi_0(v_bT/n) \subset \Pi_0(\gcd(v_bDT, v_bT/2))$.) Neither the third frame nor any additional observations can eliminate these nullvectors, since frames beyond the second are redundant with respect to signals in the subspaces $\Pi_0(v_bT/n)$ or $\Pi_0(v_bT/2)$. In conclusion, we may state this:

Theorem 3.2.2. (Partial generalization of Theorem 2.4.3) For the interregion reconstruction problem using three or more frames, the unobservable modes are

$$N(\mathbf{H}) = \begin{cases} \Pi_0\Big(\gcd(v_bDT, (v_e - v_b)T)\Big), \\ \qquad \text{if } v_b/v_e \neq 2 \text{ and } D \geq \min(v_b/v_e - 1, 1); \\ \Pi_0\Big(\gcd(v_bDT, (v_e - v_b)T)\Big), \\ \qquad \text{if } v_b/v_e = 2 \text{ and } D \neq m/n \text{ with } n \text{ odd}; \\ (\{\text{odd functions}\} \cap \Pi_0(v_bT/n)) \oplus \Pi_0(\gcd(v_bDT, v_bT/2)), \\ \qquad \text{if } v_b/v_e = 2 \text{ and } D = m/n \text{ with } n \text{ odd}. \end{cases}$$

Some values of $(v_b/v_e, D)$ are not mentioned in this theorem, for the same reason as in transition zone compensation.

3.3 Summary

This chapter has extended the analysis of unobservable subspaces to accommodate cameras that integrate light for only part of the time between frames.

There are two reasons why the presentation has been short on discussion and long on algebra. For one thing, many of the changes necessitated by permitting arbitrary duty cycle D are just a matter of replacing appropriate occurrences of T with DT. This rule is true for intraregion reconstruction from any number of frames. It also holds for intraframe transition zone compensation or interregion reconstruction in two frames; for both of these problems there is no point in adding more frames as long as $v_b/v_e \leq 1$.

For $v_b/v_e > 1$, on the other hand, additional frames are needed to achieve more complete reconstruction. Here the discussion has been limited because the results are mathematically incomplete. The nullspace is complicated to describe, not only because the variable D creates many subcases but also because the general solution of (3.1) is not yet known.

Chapter 4

Generalization to Two Dimensions

The assumption of maximum camera integration ($D = 1$) will now be reinstated in order to generalize the first set of image reconstruction results in a different way. It sometimes happens that signal processing theories in one dimension cannot be extended to higher dimensions for fundamental mathematical reasons (e.g., polynomial factorization). Fortunately, two-dimensional versions of the three classes of image reconstruction problems can be solved, under certain reasonable restrictions. Because the techniques needed to determine unobservable subspaces largely parallel those in one dimension, most of the results are correspondingly similar (Figure 4.1).

4.1 Intraregion Reconstruction

4.1.1 Intraframe

Suppose that the blurred image sequence $g_c(\vec{x}, t)$ is observed at $t = 0$ for $\vec{x} = (x, y)$ in an area that depends on a single surface moving with constant velocity vector $\vec{v} = (v_x, v_y)$. Let S be the domain in $f(\vec{x})$ that contributes to this area, and assume S is convex to avoid complications. This problem is essentially one-dimensional, since a coordinate system can be chosen to make one velocity component vanish; however, the result previously stated as Theorem 2.2.1 is now repeated for the sake of introducing useful notation. The nullspace can be characterized as the set of signals with DC-free periods of length $|\vec{v}|T$ in the $\vec{v}$ direction.

Problem Classification	Special Assumptions	Frames	$\vec{v}_b \cdot \hat{n} / \vec{v}_e \cdot \hat{n}$	$N(\mathbf{H})$	Notes
Intraregion		M		$\bigcap_{i=1}^{M} \Pi_0(\vec{v}_i T)$	$N(\mathbf{H}) = \{\mathbf{0}\}$ if $\exists i, j, k$ such that $[\vec{v}_i \vert \vec{v}_j]\vec{x} = \vec{v}_k$ has no rational solution
Transition Zone Compensation (one unknown region, one known region)	straight boundary	1	$\leq 1, \neq 0$	$\{\mathbf{0}\}$	
			> 1	$N(\mathbf{H}_{\angle}) \cap \Pi_0(\vec{v}_b T)$	
			$= 0$	$\Pi_0(\vec{v}_b D_1(\vec{x} \cdot \hat{n}) T)$	
	constant velocities, straight boundary	$M \geq 2$	$\neq 2, \neq 0$	$\{\mathbf{0}\}$	$N(\mathbf{H}) = \{\mathbf{0}\}$ in a band of width $(M-1)\vert\vec{v}_e\vert T$
			$= 2$	{odd functions} $\cap \Pi_0(\vec{v}_b T)$	
			$= 0$	$\Pi_0(\vec{v}_b D_M(\vec{x} \cdot \hat{n}) T)$	
Interregion (two unknown regions)		1		$\Pi_0(\vec{v}_b T)$	same as intraregion
	constant velocities, $\vec{v}_f = \vec{v}_e$, straight boundary	2	$\leq 1, \neq 0$	$\Pi_0(\vec{v}_b T) \cap \Pi(\vec{v}_e T)$	$N(\mathbf{H}) \supset \Pi_0(\vec{v}_b T) \cap \Pi(\vec{v}_e T)$
			> 1	$N(\mathbf{H}_{\angle \Delta}) \cap \Pi_0(\vec{v}_b T)$	
			$= 0$	$\{ f \mid \Delta f \in \Pi_0(\vec{v}_b D_1(\vec{x} \cdot \hat{n}) T) \}$	
		$M \geq 3$	$\neq 2, \neq 0$	$\Pi_0(\vec{v}_b T) \cap \Pi(\vec{v}_e T)$	
			$= 2$	$\{ f \mid \Delta f \in$ {odd functions} $\cap \Pi_0(\vec{v}_b T) \} \cap \Pi_0(\vec{v}_b T)$	$N(\mathbf{H}) \supset \Pi_0(\vec{v}_b T) \cap \Pi(\vec{v}_e T)$
			$= 0$	$\{ f \mid \Delta f \in \Pi_0(\vec{v}_b D_{M-1}(\vec{x} \cdot \hat{n}) T) \}$	$N(\mathbf{H}) = \Pi_0(\vec{v}_b T) \cap \Pi(\vec{v}_e T)$ in a band of width $(M-1)\vert\vec{v}_e\vert T$

$$(\Delta f)(\vec{x}) = f(\vec{x} + (\vec{v}_e - \vec{v}_b)T) - f(\vec{x})$$

Figure 4.1: Unobservable subspaces of 2D reconstruction problems, 100% duty cycle. See 1D results if $\vec{v}_b$ and $\vec{v}_f$ are parallel.

Definition.

$$\begin{aligned}\Pi(\vec{z}; S) &= \text{set of signals with periodicity vector } \vec{z} \text{ in the domain S} \\ &= \{f \mid f(\vec{x}) = f(\vec{x} + \vec{z}) \text{ whenever } \vec{x} \in S \text{ and } \vec{x} + \vec{z} \in S\}\end{aligned}$$

$\Pi(\mathbf{0}; S)$ is deemed to be the set of constant signals.

$$\begin{aligned}\Pi_0(\vec{z}; S) &= \text{set of signals whose average over any straight path } [\vec{x}, \vec{x} + \vec{z}] \text{ within } S \text{ is } 0 \\ &= \left\{ f \;\middle|\; \int_0^1 f(\vec{x} + \alpha\vec{z})\, d\alpha = 0 \text{ whenever } \vec{x} + \alpha\vec{z} \in S, \forall \alpha \in [0,1] \right\}\end{aligned}$$

Theorem 4.1.1. (Generalization of Theorem 2.2.1) For intraregion reconstruction in one frame, the unobservable modes are

$$\begin{aligned}N(\mathbf{H}) &= \Pi_0(\vec{v}T; S) \\ &= \Pi(\vec{v}T; S) \cap \left\{ f \;\middle|\; \text{on every line} \parallel \vec{v}, \quad \exists \vec{x} \text{ such that } \int_0^1 f(\vec{x} + \alpha\vec{v}T)\, d\alpha = 0 \right\}.\end{aligned}$$

A frequency-domain interpretation is available if S is the infinite two-dimensional plane. When the point spread function is a rectangular pulse of length $|\vec{v}|T$, the two-dimensional frequency response is the sinc function

$$H(\omega_x, \omega_y) = H(\vec{\omega}) = \frac{\sin \vec{\omega} \cdot \vec{v}T/2}{\vec{\omega} \cdot \vec{v}T/2},$$

whose zero contours are equally spaced lines perpendicular to $\vec{v}$ (Figure 4.2).

4.1.2 Interframe

Let the surface under observation have velocity $\vec{v}_i$ throughout the integration of frame i in a sequence of M frames, assuming that no two vectors are collinear. (If $\vec{v}_i$ and $\vec{v}_j$ are collinear, the pair of frames is equivalent to a single frame blurred by $\gcd(|\vec{v}_i|T, |\vec{v}_j|T)$ in the same direction.)

With just two frames, the set of unobservable frequencies is the intersection of two families of zero contours, and is typically a set of isolated points, as shown in Figure 4.3. The zero contours of a third frame may or may not intersect with any of those points, but if they don't then all frequency components of the input signal are observable.

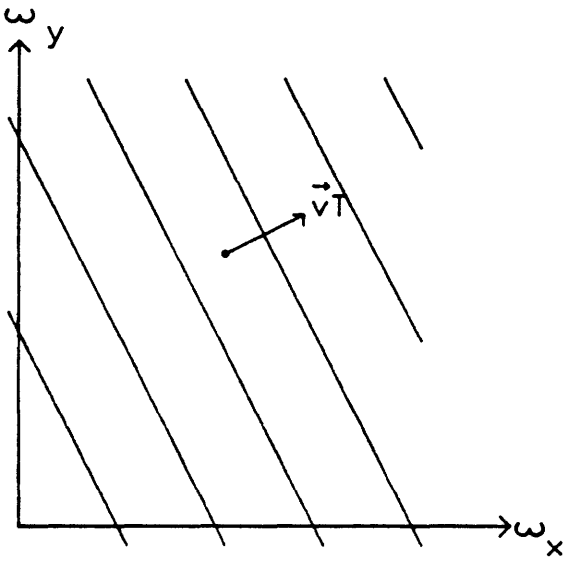

Figure 4.2: Zero contours of $H(\vec{\omega})$

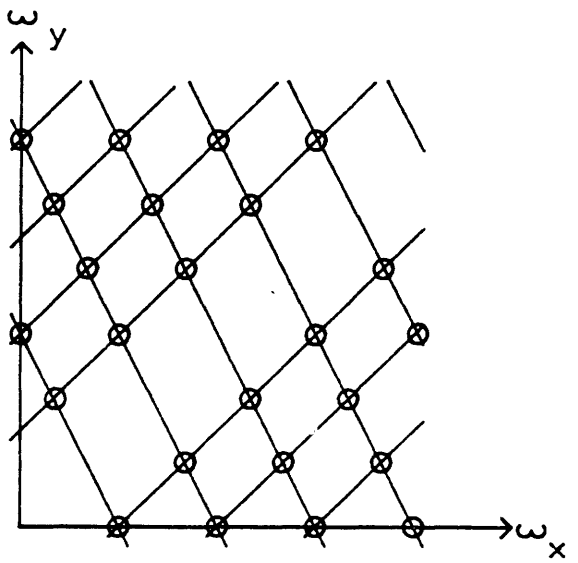

Figure 4.3: Intersections of two families of zero contours

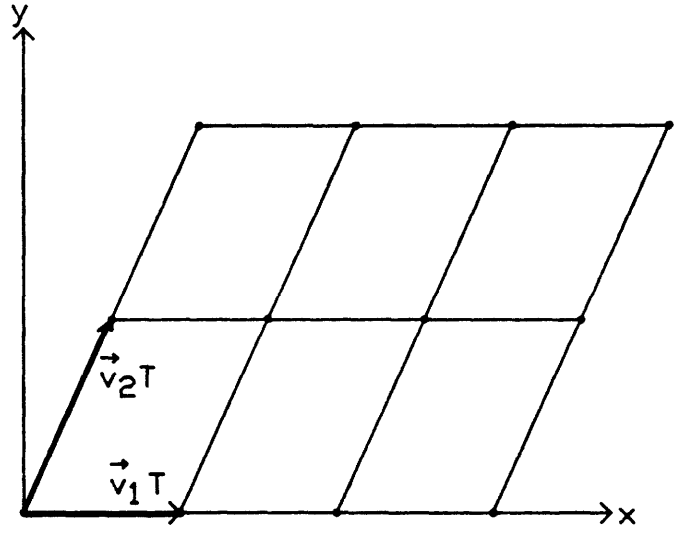

Figure 4.4: Lattice of fundamental period cells

Since the Fourier transform approach is, strictly speaking, not applicable when the observation domains are finite intervals, the same idea is now developed in the signal domain. The unobservable subspace is clearly

$$N(\mathbf{H}) = \bigcap_{i=1}^{M} \Pi_0(\vec{v}_i T).$$

When $M = 2$, a signal belonging to $N(\mathbf{H})$ will have periodicity matrix $P_2 = [\vec{v}_1 T | \vec{v}_2 T]$. Its period cells (Figure 4.4) contain no DC and have area $|\det P_2|$ [Dudgeon84]. Because a two-dimensional signal can easily be *biperiodic* (able to satisfy two periodicity constraints of the form $f(\vec{x}) = f(\vec{x} + \vec{z})$ simultaneously), the wavelength of the lowest-frequency unobservable signal is not reduced by combining two frames of data. Therefore, low-frequency artifacts may still be visible in the restored image. In contrast, when biperiodicity is forced on a one-dimensional signal the fundamental wavelength could be sharply reduced, i.e., $\gcd(v_1 T, v_2 T)$ can be much smaller than $v_1 T$ or $v_2 T$.

The constraints of additional frames can potentially eliminate the lowest-frequency null-vectors, because two-dimensional signals are not naturally triperiodic. As long as S, the region to be reconstructed on the basis of the observations, meets certain size and shape requirements, it can be shown that the periodicity matrix of a signal in the intersection set,

$N(\mathbf{H})$, "evenly divides" every $\vec{v}_i T$.

Definition. By analogy with the greatest common divisor of real numbers, let $\gcd(\vec{z}_1, \ldots, \vec{z}_M)$ of a set of real vectors be a matrix $\Lambda = [\vec{\lambda}_1 | \vec{\lambda}_2]$ of maximum determinant for which every $\vec{z}_i$ equals $\Lambda \vec{m}_i$ for some integer vector $\vec{m}_i$, or 0 if no such matrix exists. (Λ is not unique, for ΛQ also fulfills the conditions if Q is an integer matrix with unity determinant.)

Properties:

1. The vectors $\vec{m}_i$ are relatively prime, if they are defined.

2. $\det(\Lambda) \leq |\det[\vec{z}_i | \vec{z}_j]|$ for all i, j.

3. The gcd is zero if and only if the solution to $[\vec{z}_i | \vec{z}_j]\vec{x} = \vec{z}_k$ is irrational for some i, j, k.

A two-dimensional version of Theorem 2.2.2 will not be stated since analogous conditions on S have not been formulated in general. However, taking $M = 3$ as an example, let

$$S = \left\{ \sum_{i=1}^{3} \alpha_i \vec{v}_i T \,\middle|\, \alpha_i \in [0,1], \quad i = 1,2,3 \right\}.$$

This region suffices to generalize the argument in §A.1 and conclude that the unobservable subspace must have periodicity matrix $P_3 = \gcd(\vec{v}_1 T, \vec{v}_2 T, \vec{v}_3 T)$. A non-singular P_3 exists if the solution to $P_2 \vec{x} = \vec{v}_3 T$ is rational, in which case $|\det P_3|$ will turn out to be $\frac{1}{n}|\det P_2|$, where n is the denominator of $\vec{x} = [\frac{m}{n} \; \frac{m'}{n}]^{\mathrm{T}}$ expressed in lowest terms. Thus the area of the period cell is reduced by a factor of n. If, on the other hand, the solution $\vec{x}$ is irrational, the nullspace must be $\{\mathbf{0}\}$.

From this discussion we see that as few as three frames could be sufficient, in principle, to obtain unique reconstruction.

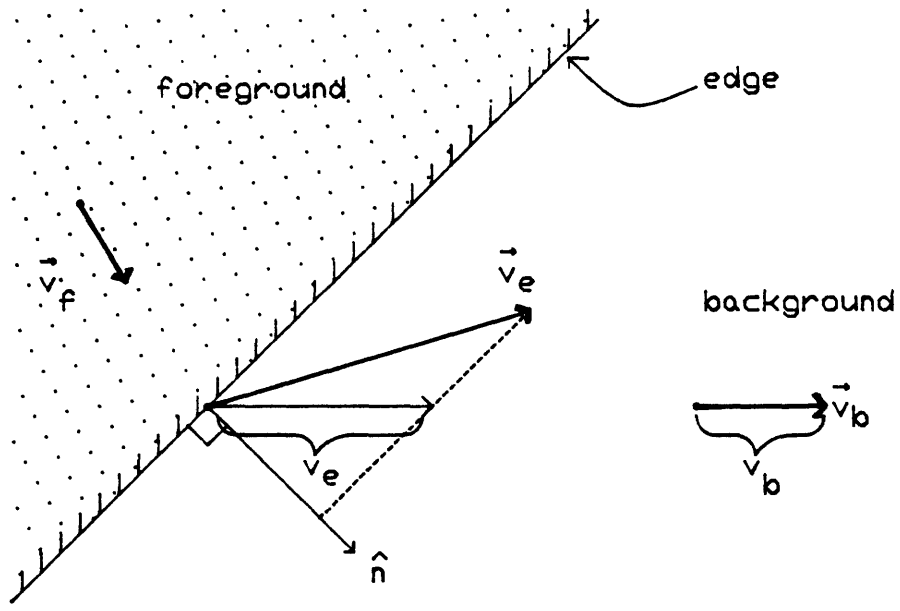

Figure 4.5: Vector velocities at a boundary

4.2 Transition Zone Compensation

Reconstruction of an unknown two-dimensional surface image after subtracting out the neighbor's contribution to a transition zone is essentially a one-dimensional problem. Assuming a constant velocity surface, there can be no interaction between points on different lines parallel to the motion; therefore, reconstruction could proceed independently on each parallel line. Depending on the scene configuration, however, the reconstruction problem reduces to either one-dimensional intraframe or one-dimensional transition zone compensation problems.

4.2.1 Definitions

Let the occluding boundary be an infinite straight line with unit normal $\hat{n}$ pointing towards the "background" surface. As shown in Figure 4.5, the three velocities of concern at a boundary are:

$\vec{v}_f$ = "foreground" surface velocity

$\vec{v}_b$ = "background" surface velocity

$\vec{v}_e$ = velocity of a point on the boundary (in general $\neq \vec{v}_b$ or $\vec{v}_f$).

These velocities are presumed time-invariant. Note that the component of $\vec{v}_e$ parallel to the boundary is arbitrary. It is required that $\vec{v}_e \cdot \hat{n} \neq 0$, for otherwise there is no transition zone to work with. In order to connect two-dimensional problems to the previous results, it is convenient to define the following associated scalars.

$$v_b = |\vec{v}_b| \text{sign}(\vec{v}_b \cdot \hat{n})$$

= speed of the background with positive sign for motion away from the foreground

$$v_e = \frac{\vec{v}_e \cdot \hat{n}}{|\vec{v}_b \cdot \hat{n}|/|\vec{v}_b|}$$

= speed of the boundary in the direction parallel to $\vec{v}_b$, using the same sign convention (undefined if $\vec{v}_b \cdot \hat{n} = 0$).

If the image is examined along a line parallel to $\vec{v}_b$, these scalars coincide with their definitions in one dimension (cf. §2.3.1). The usual velocity ratio v_b/v_e is equal to $\vec{v}_b \cdot \hat{n}/\vec{v}_e \cdot \hat{n}$.

4.2.2 Intraframe

Consider the foreground surface to be known and its contribution to the transition zone to be subtracted out. The background surface signal remains to be determined.

Suppose first that $\vec{v}_b \cdot \hat{n} \neq 0$, that is, the background does not move parallel to the boundary. As far as each line parallel to $\vec{v}_b$ is concerned (Figure 4.6a), the boundary appears to move at speed v_e, and the background signal contributes to the transition zone according to $\mathbf{H}_{\angle}$ or $\mathbf{H}_{\backslash\_}$, depending on v_b/v_e. Therefore, the one-dimensional transition zone compensation results from Theorem 2.3.2 are applicable. (Note that a straight boundary assures that v_e is time-invariant regardless of the direction of boundary motion; if $\vec{v}_e$ were parallel to $\vec{v}_b$ then a curved boundary would also work.)

In the special case of $\vec{v}_b \cdot \hat{n} = 0$, on the other hand, most lines parallel to $\vec{v}_b$ do not enter the transition zone (Figure 4.6b). Along a parallel passing through point $\vec{x}$, the background signal is convolved with a rectangular pulse of length $|\vec{v}_b| D_1(\vec{x} \cdot \hat{n}) T$, where $\vec{x} \cdot \hat{n}$ measures distance in the direction perpendicular to the boundary and $D_1(\vec{x} \cdot \hat{n})$ is a position-dependent duty cycle. $D_1(\vec{x} \cdot \hat{n})$ is 0 for $\vec{x}$ on the edge of the transition zone closest to the foreground, ramps linearly to 1 on the opposite edge, and stays at 1 for the rest of the background region. Accordingly, image reconstruction on any of the parallel lines is a one-dimensional intraregion problem.

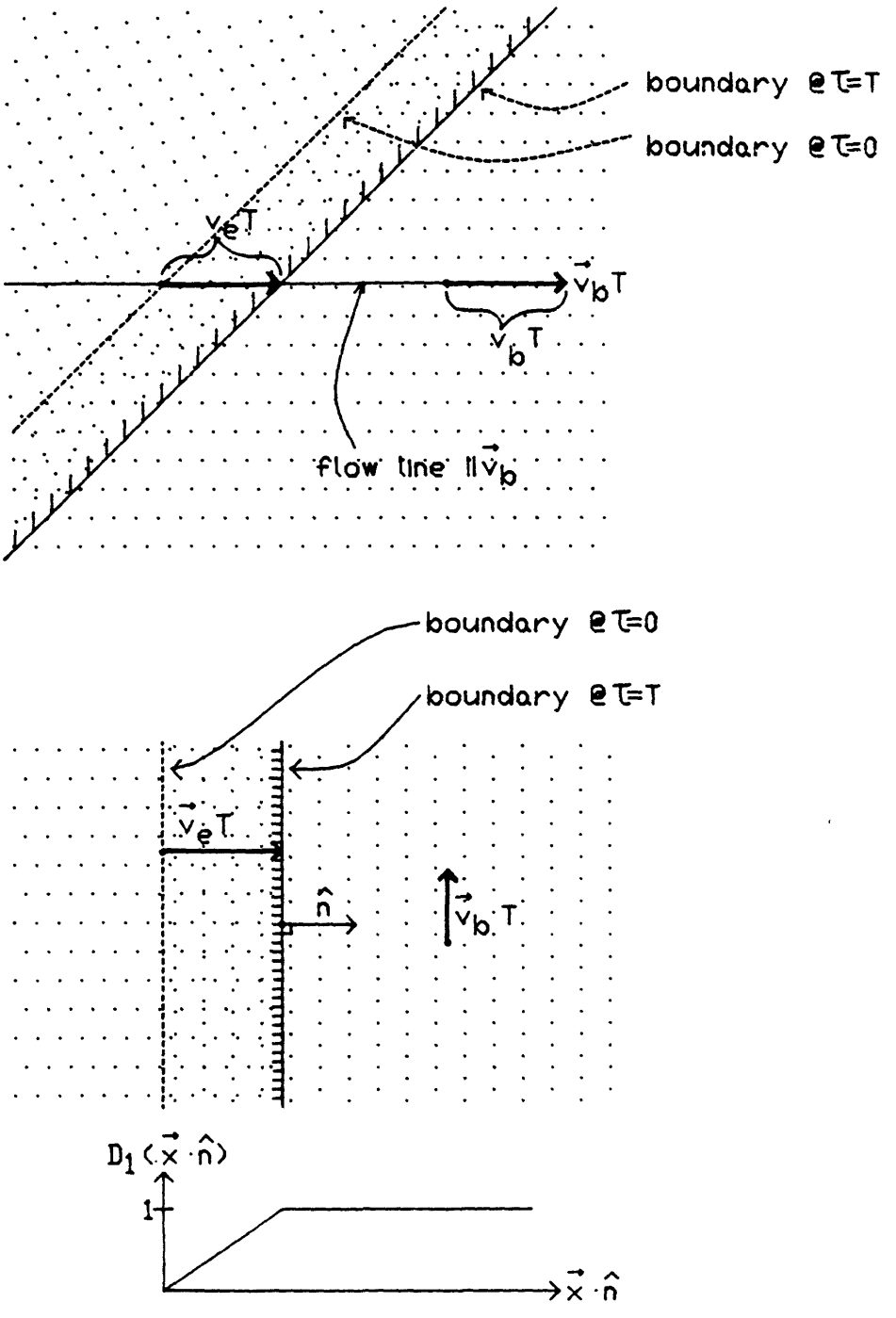

Figure 4.6: Image configuration at a boundary: (top) $\vec{v}_b \hat{n} \neq 0$; (bottom) $\vec{v}_b \hat{n} = 0$. D_1 is the effective duty cycle along each parallel of the background surface.

Theorem 4.2.2. (Generalization of Theorem 2.3.2) After transition zone compensation in one frame, the unobservable subspace along a line parallel to $\vec{v}_b$ passing through $\vec{x}$ is

$$N(\mathbf{H}) = \begin{cases} \{\mathbf{0}\}, & \text{if } \vec{v}_b \cdot \hat{n} / \vec{v}_e \cdot \hat{n} \leq 1, \neq 0; \\ N(\mathbf{H}_\angle) \cap \Pi_0(\vec{v}_b T), & \text{if } \vec{v}_b \cdot \hat{n} / \vec{v}_e \cdot \hat{n} > 1; \\ \Pi_0(\vec{v}_b D_1(\vec{x} \cdot \hat{n}) T), & \text{if } \vec{v}_b \cdot \hat{n} = 0. \end{cases}$$

$\mathbf{H}_\angle$ is understood to be the acute-triangular linear transformation replicated onto each parallel and appropriately positioned over the transition zone.

4.2.3 Interframe

As long as $\vec{v}_b \cdot \hat{n} \neq 0$, the results are simply copied from Theorem 2.3.3. An interesting new possibility arises, however, for the special case of $\vec{v}_b \cdot \hat{n} = 0$. When only frame i is observed, the nullspace is described by $\Pi_0\Big(\vec{v}_b D_1\big((\vec{x} - \vec{v}_e i T) \cdot \hat{n}\big) T\Big)$. The joint observation of M frames, therefore, narrows the nullspace to

$$\bigcap_{i=0}^{M-1} \Pi_0\Big(\vec{v}_b D_1\big((\vec{x} - \vec{v}_e i T) \cdot \hat{n}\big) T\Big) = \Pi_0(\vec{v}_b D_M(\vec{x} \cdot \hat{n}) T),$$

where

$$D_M(\vec{x} \cdot \hat{n}) = \gcd\Big(D_1(\vec{x} \cdot \hat{n}), D_1\big((\vec{x} - \vec{v}_e T) \cdot \hat{n}\big), \ldots, D_1\big((\vec{x} - \vec{v}_e (M-1) T) \cdot \hat{n}\big)\Big)$$

is the effective duty cycle. As depicted in Figure 4.7 for the case of three frames and an advancing foreground surface, M transition zones, each of width $|\vec{v}_e| T$, are formed over the course of M frames. $D_M(\vec{x} \cdot \hat{n}) = 1$ if $\vec{x}$ is continuously covered by the background during the M frames, and $D_M(\vec{x} \cdot \hat{n})$ ramps between 0 and 1 within the transition zone formed during frame $i = 0$.

Suppose now that $\vec{x}$ lies in the transition zone formed during frame i, $1 \leq i \leq M - 1$. The background signal along the parallel through $\vec{x}$ is blurred by $|\vec{v}_b| D_1\big((\vec{x} - \vec{v}_e i T) \cdot \hat{n}\big) T$ during frame i, is blurred by $|\vec{v}_b| T$ in all earlier frames, and is occluded in later frames. The nullspace along a parallel is $\Pi_0\Big(\vec{v}_b \gcd\big(T, D_1\big((\vec{x} - \vec{v}_e i T) \cdot \hat{n}\big) T\big)\Big)$, but this is $\{\mathbf{0}\}$ unless $D_1\big((\vec{x} - \vec{v}_e i T) \cdot \hat{n}\big)$ happens to be rational—a condition attained on a set of parallels whose total area is zero in the Lebesgue measure. Consequently, the projection of any finite two-dimensional signal in this transition zone onto $N(\mathbf{H})$ has zero energy. In conclusion, the

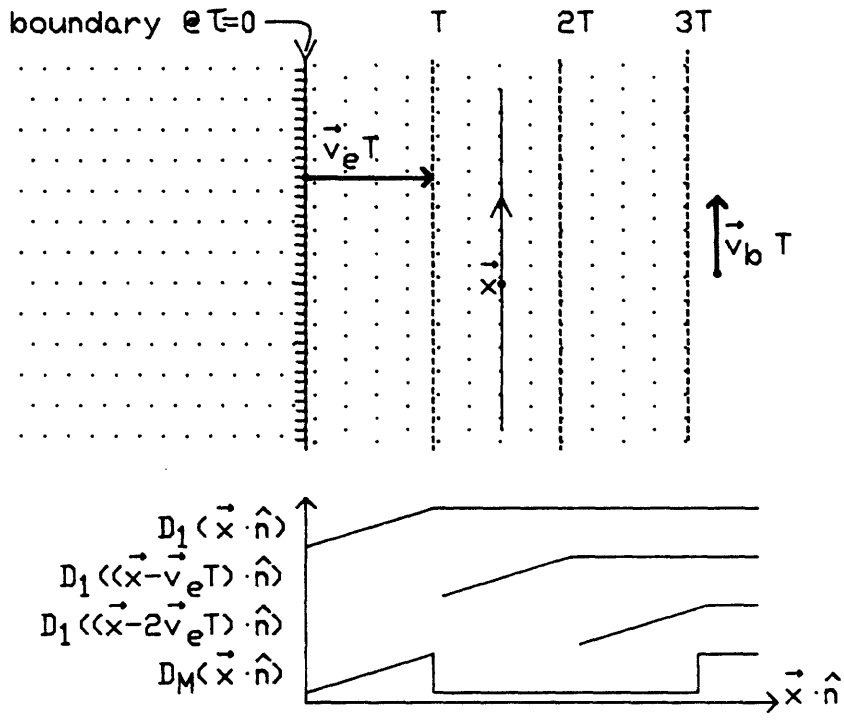

Figure 4.7: Interframe transition zone compensation, $\vec{v}_b \cdot \hat{n} = 0$. D_M is the effective duty cycle along each parallel of the background surface, taking all three frames into consideration.

effective duty cycle may be simplified to $D_M(\vec{x}\cdot\hat{n}) = 0$ in a band of width $(M-1)|\vec{v}_e|T$. As more frames are collected, the uniquely reconstructible area of the background expands.

Theorem 4.2.3. (Generalization of Theorem 2.3.3) After transition zone compensation in $M = 2$ or more frames, the unobservable modes are

$$N(\mathbf{H}) = \begin{cases} \{\mathbf{0}\}, & \text{if } \vec{v}_b\cdot\hat{n}/\vec{v}_e\cdot\hat{n} \neq 2, \neq 0; \\ \{\text{odd functions}\} \cap \Pi_0(\vec{v}_b T), & \text{if } \vec{v}_b\cdot\hat{n}/\vec{v}_e\cdot\hat{n} = 2; \\ \Pi_0(\vec{v}_b D_M(\vec{x}\cdot\hat{n})T), & \text{if } \vec{v}_b\cdot\hat{n} = 0. \end{cases}$$

4.3 Interregion Reconstruction

Prior knowledge of the foreground surface is now replaced with the condition $\vec{v}_e = \vec{v}_f$ so that the foreground surface contribution will vanish in the displaced frame difference. For argument's sake assume that $\vec{v}_e \cdot \hat{n} > 0$.

4.3.1 Intraframe

With a single-frame observation, the unobservable subspace for the background surface is $\Pi_0(\vec{v}_b T)$. Given any $f_b(\vec{x}) \in \Pi_0(\vec{v}_b T)$ it is possible to find $f_f(\vec{x})$ to make $g_c(\vec{x}) = 0$ in the transition zone and everywhere else. Once $g_b(\vec{x}, 0)$ is given, the determination of $f_f(\vec{x})$ is a one-dimensional problem along lines parallel to $\vec{v}_f$. Recalling §2.4.1, choose

$$f_f(\vec{x}) = \begin{cases} |\vec{v}_f| T \, \nabla_{\vec{v}_f} g_b(\vec{x} + \vec{v}_f T, 0), & \text{if } \vec{x} \in \text{transition zone;} \\ f_f(\vec{x} + \vec{v}_f T), & \text{otherwise.} \end{cases}$$

$\nabla_{\vec{v}_f}$ denotes the derivative in the $\vec{v}_f$ direction with respect to $\vec{x}$. Any such pair (f_b, f_f) is a nullvector for the two-dimensional intraframe, interregion reconstruction problem.

4.3.2 Two Frames

It can be shown that the displaced-frame-difference image

$$\triangle g_c(\vec{x}, t) = g_c(\vec{x} + \vec{v}_e T, t + T) - g_c(\vec{x}, t)$$

is independent of the foreground signal $f_f(\vec{x})$ and depends only on the background difference signal

$$\Delta f_b(\vec{x}) = f_b(\vec{x} + (\vec{v}_e - \vec{v}_b)T) - f_b(\vec{x}).$$

Not surprisingly, this dependence is identical to the relationship between $g_c(\vec{x}, t)$ and $f_b(\vec{x})$ in the transition zone compensation problem. Therefore, Theorem 4.2.2 implies that a nullvector $f_b(x)$ must satisfy

$$\begin{cases} \Delta f_b(\vec{x}) = 0, & \text{if } \vec{v}_b \cdot \hat{n} / \vec{v}_e \cdot \hat{n} \leq 1, \neq 0; \quad (4.1) \\ \Delta f_b(\vec{x}) \in N(\mathbf{H}_\angle) \cap \Pi_0(\vec{v}_b T), & \text{if } \vec{v}_b \cdot \hat{n} / \vec{v}_e \cdot \hat{n} > 1; \quad (4.2) \\ \Delta f_b(\vec{x}) \in \Pi_0(\vec{v}_b D_1(\vec{x} \cdot \hat{n}) T), & \text{if } \vec{v}_b \cdot \hat{n} = 0. \quad (4.3) \end{cases}$$

Condition (4.1) translates to $f_b(\vec{x}) \in \Pi((\vec{v}_e - \vec{v}_b)T)$; therefore, the nullspace is narrowed from $\Pi_0(\vec{v}_b T)$ to $\Pi_0(\vec{v}_b T) \cap \Pi((\vec{v}_e - \vec{v}_b)T) = \Pi_0(\vec{v}_b T) \cap \Pi(\vec{v}_e T)$ by the information in the

second frame. (Note that we do not write $\Pi_0(\vec{v}_e T)$, since $\Pi_0(\vec{z}) \cap \Pi(\vec{z}') \neq \Pi_0(\vec{z}) \cap \Pi_0(\vec{z}')$ in two dimensions.) Because two-dimensional signals can naturally support biperiodicity, this intersection set never degenerates to $\{\mathbf{0}\}$.

Unlike the one-dimensional problem (into which this problem degenerates if $\vec{v}_b$ is parallel to $\vec{v}_e$), there is no doubt as to the existence of functions $f_b(\vec{x})$ satisfying (4.2) but not (4.1), because here Δ subtracts a pair of one-dimensional signals on different lines parallel to $\vec{v}_b$, not one signal from itself. $N(\mathbf{H})$ is thus the direct sum of these interesting solutions with $\Pi_0(\vec{v}_b T) \cap \Pi(\vec{v}_e T)$.

Finally, condition (4.3) states that the background image along a parallel in the transition zone closest to the foreground is equal to the signal on the parallel $(\vec{v}_e - \vec{v}_b)T$ away, plus an arbitrary function in $\Pi_0(\vec{v}_b D_1(\vec{x}\hat{n})T)$. On all other parallels in the background, the condition is redundant since $D_1(\vec{x}\cdot\hat{n}) = 1$ and $f_b(\vec{x}) \in \Pi_0(\vec{v}_b T)$ already implies $\Delta f_b(\vec{x}) \in \Pi_0(\vec{v}_b T)$. Therefore, $N(\mathbf{H})$ does contain some signals in addition to all those in $\Pi_0(\vec{v}_b T) \cap \Pi(\vec{v}_e T)$.

Theorem 4.3.2. (Generalization of Theorem 2.4.2) For the interregion reconstruction problem using two frames, the unobservable modes are

$$N(\mathbf{H}) = \begin{cases} \Pi_0(\vec{v}_b T) \cap \Pi(\vec{v}_e T), & \text{if } \vec{v}_b\cdot\hat{n}/\vec{v}_e\cdot\hat{n} \leq 1, \neq 0; \\ N(\mathbf{H}_{\angle}\Delta) \cap \Pi_0(\vec{v}_b T), & \text{if } \vec{v}_b\cdot\hat{n}/\vec{v}_e\cdot\hat{n} > 1; \\ \{f \mid \Delta f \in \Pi_0(\vec{v}_b D_1(\vec{x}\cdot\hat{n})T)\}, & \text{if } \vec{v}_b\cdot\hat{n} = 0. \end{cases}$$

4.3.3 Three or More Frames

When $M = 3$ or more frames are observed, application of Theorem 4.2.3 to $\Delta f_b(\vec{x})$ leads to the result stated below. If $\vec{v}_b\cdot\hat{n} = 0$, there will be a band of width $(M-1)|\vec{v}_e|T$ in which a nullvector must belong to $\Pi_0(\vec{v}_b T) \cap \Pi(\vec{v}_e T)$. This band expands as more frames are collected. If $\vec{v}_b\cdot\hat{n}/\vec{v}_e\cdot\hat{n} = 2$, additional frames are redundant and cannot reduce the unobservable subspace.

Theorem 4.3.3. (Generalization of Theorem 2.4.3) For the interregion reconstruction problem using $M = 3$ or more frames, the unobservable modes are

$$N(\mathbf{H}) = \begin{cases} \Pi_0(\vec{v}_b T) \cap \Pi(\vec{v}_e T), & \text{if } \vec{v}_b\cdot\hat{n}/\vec{v}_e\cdot\hat{n} \neq 2, \neq 0; \\ \{f \mid \Delta f \in \{\text{odd functions}\} \cap \Pi_0(\vec{v}_b T)\} \cap \Pi_0(\vec{v}_b T), & \text{if } \vec{v}_b\cdot\hat{n}/\vec{v}_e\cdot\hat{n} = 2; \\ \{f \mid \Delta f \in \Pi_0(\vec{v}_b D_{M-1}(\vec{x}\cdot\hat{n})T)\}, & \text{if } \vec{v}_b\cdot\hat{n} = 0. \end{cases}$$

4.4 Summary

The nullspaces for reconstruction of motion-blurred surfaces in two dimensions have been determined in this chapter, most results being obvious generalizations of their one-dimensional counterparts. Two-dimensional reconstruction differs from the one-dimensional case because the maximum number of independent periodicity vectors is equal to the number of dimensions. By assuming a straight-line boundary, the one-dimensional theorems on transition zone compensation and interregion reconstruction can be applied along parallels in the direction of surface motion to obtain results for two dimensions. The main new feature is an additional special case to treat a surface moving parallel to the boundary.

Compared to the original one-dimensional, 100% duty cycle theory, the results for arbitrary duty cycle and for motion in two dimensions are incomplete. In the sequel, there will be no further mention of these extensions. Nevertheless, this digression to generalize Chapter 2 has enhanced the understanding of the original theory in two ways. First, the parallel development of Chapters 2–4 created a consistent notation. Second, the findings negate the hypothesis that reconstruction of one-dimensional images with 100% duty cycle is entirely a pathological case; on the contrary, they suggest that the unobservable modes predicted by the original theory will survive in more general scene configurations.

Chapter 5

Noise and Sampling

Conditions for unique reconstruction have been derived by considering the nullspace of a linear transformation from one spatially continuous signal to another, but many issues must be resolved before reconstruction can be carried out with blurred sequences recorded by a real camera. First of all, the proofs alone do not suggest how to actually construct a unique or non-unique solution. Second, the impact of noise on observability has yet to be determined. Third, digital processing requires that continuous images be represented by finite sets of coefficients; it is possible that sampling the blurred data will destroy information vital to unique reconstruction. Finally, except in artificial situations the linear transformation $\mathbf{H}$ is unknown and must be estimated from the blurred image sequence itself—the problem of blind image restoration.

In order to address the first three concerns, this chapter adopts the approach of linear least squares, i.e. Wiener, estimation. The pertinent equations are reviewed, and the appropriateness of the Wiener approach is considered. Subsequently, the minimum achievable mean-square error is calculated for a single-pole input signal spectrum over a wide range of scene parameters. The MSE experiments serve two purposes: first, they corroborate the analytical results previously derived, linking theory to the physical world; second, they indicate the quality of reconstruction possible using noisy and/or sampled data, thereby assessing the relative benefits of interframe and interregion constraints. Furthermore, the numerical results are supported by examples of restored pictures.

Consider a first-kind Fredholm integral equation

$$g(x) = \int h(x,u) f(u)\, du,$$

where $h(x,u)$ is any square-integrable kernel, not necessarily one arising from observing a motion-blurred scene. In terms of linear transformations between infinite dimensional vector spaces, this can be represented abstractly by $\mathbf{g} = \mathbf{H}\mathbf{f}$. It is well known that inversion of such a linear system to recover $\mathbf{f}$ is an ill-posed problem [Root87]. $\mathbf{H}$ can be characterized by its singular values (square root of eigenvalues of $\mathbf{H}^{\mathrm{T}}\mathbf{H}$). The closure of the set of singular values always includes 0; in other words, if 0 is not itself a singular value then at least there is a sequence of singular values that converges to 0 [Tricomi85, Devles85]. Consequently, whether or not $\mathbf{H}$ possesses exact nullvectors, there will always exist modes attenuated so much by the system that noise will render them effectively unobservable. From this perspective, focusing attention on the nullspace alone, as in the preceding chapters, is like missing the forest for the trees.

Perhaps there is some justification for overlooking the forest. By the nature of motion blur, any eigenvector that corresponds to a small singular value must be close to being periodic with DC-free periods of wavelength vT (or else be a high frequency signal beyond the passband of interest). The system response to such eigenvectors cannot be too different from the response to pure sinusoids of period $vT, vT/2, vT/3, \ldots$. If the latter become more easily observable given additional information, so does an approximately periodic signal. Thus, the behavior of exact nullvectors should be representative of the behavior of near-nullvectors. The preceding argument is merely a heuristic, and the best justification is that all experimental results can be explained by considering only exact nullvectors.

In this chapter, the duty cycle of camera integration is again assumed to be $D = 1$, and only one-dimensional signals are discussed. As a result, if motion blur and reconstruction occur in the horizontal direction, vertical correlations in the image will be completely disregarded. Extensions to two-dimensional motion were not pursued in this thesis investigation since the computational approach developed for one-dimensional signals with L samples becomes impractical for two-dimensional signals with L^2 samples. Extensions to arbitrary duty cycle were not studied experimentally, either. In most cases, the only effect of D is to scale the wavelengths of unobservable modes, so those results are not in doubt once the $D = 1$ results have been verified. On the other hand, further experiments would be useful where the $D < 1$ theory is incomplete.

5.1 Linear Least Squares Estimation

Let $\mathbf{f}$ and $\mathbf{n}$ be uncorrelated zero-mean random vectors with covariances $\mathbf{\Lambda}_f$, $\mathbf{\Lambda}_n$. The general noisy linear observation equation is

$$\mathbf{g} = \mathbf{H}\mathbf{f} + \mathbf{n}. \tag{5.1}$$

The Wiener estimator of $\mathbf{f}$, defined as the linear function $\hat{\mathbf{f}} = \mathbf{K}\mathbf{g}$ minimizing the expected mean squared error $\mathrm{E}\left\{\left\|\hat{\mathbf{f}} - \mathbf{f}\right\|^2\right\}$, is given by

$$\hat{\mathbf{f}}(\mathbf{g}) = \mathbf{P}\mathbf{H}^{\mathrm{T}}\mathbf{\Lambda}_n^{-1}\mathbf{g}, \tag{5.2}$$

where

$$\mathbf{P} = \left(\mathbf{H}^{\mathrm{T}}\mathbf{\Lambda}_n^{-1}\mathbf{H} + \mathbf{\Lambda}_f^{-1}\right)^{-1}. \tag{5.3}$$

$\mathbf{P}$ is the covariance of the estimation error $\hat{\mathbf{f}} - \mathbf{f}$, and a spatially averaged normalized error can be defined as MSE=tr($\mathbf{P}$)/tr($\mathbf{\Lambda}_f$). This ratio is always between 0 and 1, and will serve as a performance criterion in the sequel.

5.1.1 Justification for Wiener Estimation

The introduction of Wiener estimation, which depends on a statistical model of the input signal, seems to conflict with the goal of reconstructing $\mathbf{f}_{\text{unobs}}$ deterministically, using interframe and interregion constraints. It turns out, however, that $\mathbf{\Lambda}_f$ primarily assists in noise reduction and has almost no effect on resolving underdeterminacy. If the input signal basis is chosen so that $\mathbf{f}$ is partitioned into

$$\begin{bmatrix} \mathbf{f}_{\text{obs}} \\ \mathbf{f}_{\text{unobs}} \end{bmatrix},$$

then the system matrix must be $\mathbf{H} = [\mathbf{H}_1\ \mathbf{0}]$, with $\mathbf{H}_1^{\mathrm{T}}\mathbf{H}_1$ full rank. Partition $\mathbf{\Lambda}_f$ likewise as

$$\begin{bmatrix} \mathbf{\Lambda}_1 & \mathbf{\Lambda}_{21}{}^{\mathrm{T}} \\ \mathbf{\Lambda}_{21} & \mathbf{\Lambda}_2 \end{bmatrix}.$$

Then, in accordance with Figure 5.1, the Wiener estimator for $\hat{\mathbf{f}}$ can be decomposed as

$$\hat{\mathbf{f}} = \underbrace{\begin{bmatrix} \mathbf{I} \\ \mathbf{\Lambda}_{21}\mathbf{\Lambda}_1^{-1} \end{bmatrix}}_{\text{prediction}} \underbrace{\left(\mathbf{H}_1^{\mathrm{T}}\mathbf{H}_1\right)^{-1}\mathbf{H}_1^{\mathrm{T}}}_{\text{reconstruction}} \underbrace{\mathbf{H}\mathbf{\Lambda}_f\mathbf{H}^{\mathrm{T}}\left(\mathbf{H}\mathbf{\Lambda}_f\mathbf{H}^{\mathrm{T}} + \mathbf{\Lambda}_n\right)^{-1}}_{\text{noise reduction}}\mathbf{g}.$$

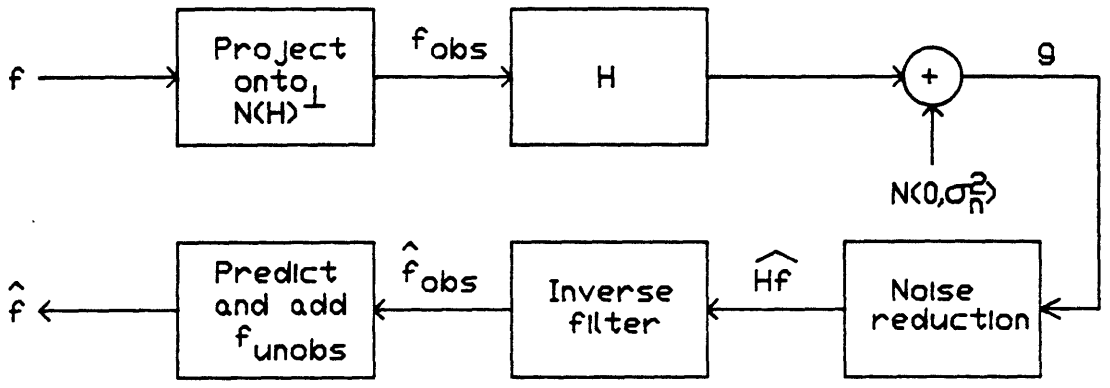

Figure 5.1: Decomposition of signal degradation and restoration into stages

The third factor is the Wiener filter for estimating $\mathbf{Hf}$. The second factor is the inverse filter for reconstructing $\mathbf{f}_{\text{obs}}$ given a noiseless observation of $\mathbf{Hf}$. The first factor contains the optimal predictor of $\mathbf{f}_{\text{unobs}}$ given a noiseless observation of $\mathbf{f}_{\text{obs}}$. $N(\mathbf{H})$ and $N(\mathbf{H})^{\perp}$ occupy roughly disjoint bands of frequency and are therefore uncorrelated as long as $f(x)$ is wide-sense stationary. Hence, $\mathbf{\Lambda}_{21} \approx \mathbf{0}$, $\mathbf{f}_{\text{unobs}}$ is poorly estimated from $\mathbf{g}$, and the mean energy of $\mathbf{f}_{\text{unobs}}$ is an approximate lower bound on the error energy, i.e., the irreducible error. For these reasons, it is fair to say that the addition of a second-order signal model does not represent a major departure from the approach of this investigation.

Even when its role is limited to noise reduction, however, Wiener filtering of images has been criticized on at least two counts. Some researchers avoid Bayesian approaches, maintaining that a random process is a dubious way to model real image signals. A more practical problem with Wiener filters based on stationary models is subjectively suboptimal performance in typically non-homogeneous pictures.

To answer the first criticism, it is sufficient to find plausible derivations of the Wiener equations that view $\mathbf{f}$ as a deterministic but unknown signal. Solutions produced by various regularization techniques are intimately connected to (5.2) and (5.3).

Wiener estimation is equivalent to minimizing the cost function

$$J_{\Sigma}(\mathbf{f}|\mathbf{g}) = \mathbf{f}^{\mathrm{T}}\mathbf{\Lambda}_f^{-1}\mathbf{f} + (\mathbf{g} - \mathbf{Hf})^{\mathrm{T}}\mathbf{\Lambda}_n^{-1}(\mathbf{g} - \mathbf{Hf}) \tag{5.4}$$

with respect to $\mathbf{f}$. In constrained least squares, $\mathbf{\Lambda}_f^{-1}$ is simply viewed as a weighting matrix

that penalizes non-smooth solutions [Hunt73]. The estimate is a tradeoff between smoothness of $\hat{\mathbf{f}}$ and closeness of $\mathbf{H}\hat{\mathbf{f}}$ to $\mathbf{g}$. The covariance of $\hat{\mathbf{f}}$, which consists solely of amplified observation noise, is not given by (5.3) in this example.

Another approach to regularization is to choose the linear estimator that minimizes the maximum error covariance as the true $\mathbf{f}$ wanders over the a priori set of possible signals [Root87]. Specifically, suppose $\mathbf{f}$ is known to lie in a rectangular parallelepiped of the form

$$\mathcal{F} = \left\{ \sum_{k=0}^{\infty} f_k \phi_k \middle| |f_k| < b_k, \forall k \right\},$$

where the b_k's are arbitrary constants and the ϕ_k's are orthonormal eigenvectors of $\mathbf{H}^{\mathrm{T}}\mathbf{H}$ corresponding to nonzero eigenvalues. Replace $\mathbf{\Lambda}_f$ in the Wiener filter by $\sum_{k=0}^{\infty} b_k^2 \phi_k \phi_k^{\mathrm{T}}$. It then turns out that the optimum linear estimator $\hat{\mathbf{f}}$ minimizing $\max_{\mathbf{f}\in\mathcal{F}} \mathrm{E}\left\{ \left\| \hat{\mathbf{f}} - \mathbf{f} \right\|^2 \right\}$ is (5.2), and the minimax value of squared error is (5.3).

It is not necessary to elaborate on these techniques. The main point is that the Wiener equations are identical to, or serve as prototypes for, many alternative estimation methods, both Bayesian and deterministic.

The second criticism is a more significant issue in practice. Nonadaptive Wiener filters tend to perform more noise reduction around edges and busy areas than necessary for the optimum subjective tradeoff between noise and sharpness. Superior pictures have been obtained by noise reduction filters adapting to local image activity and direction (for example, [Anderson76, Powell82, Abramatic82, Knuttson83, Bovik85]), although no applications to blur restoration have been demonstrated. Ideally, such approaches should be used for the noise reduction stage of a complete system to restore motion-blurred sequences. However, further discussion of this subject lies beyond the scope of this research and is not directly related to the main problem of unobservable modes.

5.1.2 Alternate Performance Criteria

Several reasons for using the Wiener estimator to implement reconstructions in this thesis have now been advanced. Still, the error covariance (5.3) may not seem like a sound basis for a performance criterion. An ensemble average quantity like MSE is not too meaningful if $\mathbf{f}$ is a deterministic signal. On the other hand, more important than the absolute magnitude of the estimation error is how it varies as $\mathbf{H}$ is changed, and it is presumed that this variation is similar whether $\mathbf{f}$ is fixed or random. Furthermore, $\mathrm{tr}(\mathbf{P})$ equals the sum of reciprocal

eigenvalues of $\mathbf{H}^{\mathrm{T}}\mathbf{\Lambda}_n^{-1}\mathbf{H} + \mathbf{\Lambda}_f^{-1}$ and is therefore sensitive to the number and magnitude of small singular values of $\mathbf{H}$, which indicate unobservable modes.

Another possible criterion to monitor is the condition number, or eigenvalue ratio, of $\mathbf{H}^{\mathrm{T}}\mathbf{\Lambda}_n^{-1}\mathbf{H} + \mathbf{\Lambda}_f^{-1}$. Since the maximum eigenvalue is basically fixed by the signal to noise ratio, the condition number varies with the minimum singular value of $\mathbf{H}$. A large change in condition number does not always imply changes to all small singular values of $\mathbf{H}$, and for this reason it may not be as relevant to overall performance as MSE.

Finally, an information-theoretical approach might measure the quality of reconstruction by the conditional entropy of $\mathbf{f}$ given $\mathbf{g}$,

$$\mathcal{H}(\mathbf{f}|\mathbf{g}) = \mathcal{H}(\mathbf{f}) - \mathcal{I}(\mathbf{f};\mathbf{g}).$$

$\mathcal{H}(\mathbf{f})$ is the entropy of $\mathbf{f}$. $\mathcal{I}(\mathbf{f};\mathbf{g})$ is the average mutual information between $\mathbf{f}$ and $\mathbf{g}$, which reflects how useful the noisy blurred observation is for estimating the input signal [Gallager68]. For example, if $\mathbf{f}$ and $\mathbf{n}$ are independent zero-mean Gaussian random vectors, then

$$\mathcal{I}(\mathbf{f};\mathbf{g}) = \frac{1}{2}\log\frac{\det(\mathbf{H}\mathbf{\Lambda}_f\mathbf{H}^{\mathrm{T}} + \mathbf{\Lambda}_n)}{\det\mathbf{\Lambda}_n};$$

thus, $\mathcal{H}(\mathbf{f}|\mathbf{g})$ is sensitive to the singular values of $\mathbf{H}$ via the determinant of $\mathbf{H}\mathbf{\Lambda}_f\mathbf{H}^{\mathrm{T}} + \mathbf{\Lambda}_n$. This approach will not be pursued any further.

5.2 Experimental Setup

With a fixed intraframe, intraregion reconstruction problem designated as a benchmark, the general plan of this series of experiments is to compare the MSE reductions achievable using different sets of additional constraints. The surface velocity of this original observation will be held constant.

- For the class of intraregion reconstruction problems, the observation domain will be extended spatially in the same frame or temporally to a new frame. The optimum MSE will be determined as a function of the extended interval length in the former case; of the surface velocity during the new frame, in the latter.

- For transition zone compensation, the original observation will be extended spatially to encompass a transition zone, in which the contribution of the adjacent surface has

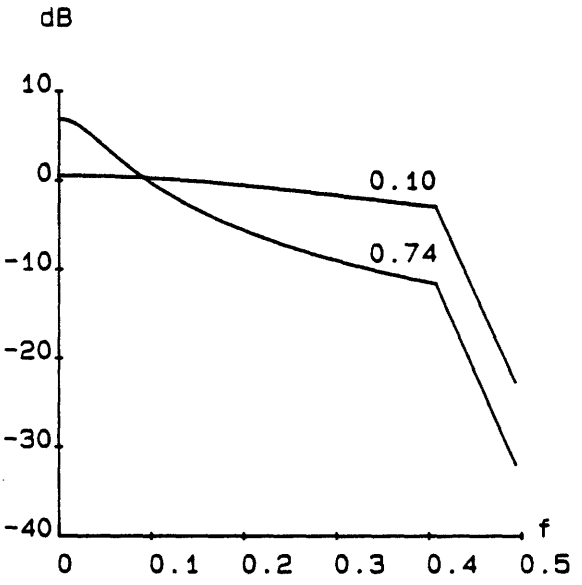

Figure 5.2: Single-pole signal spectra: each surface is modeled by a single-pole power spectrum, with $\rho = 0.74$ or $\rho = 0.10$, multiplied by a window with infinite attenuation above $\omega = \pi$ (i.e., $f = 0.5$).

already been subtracted out. The MSE will be evaluated as a function of the boundary velocity. New frames will also be added.

- The interregion reconstruction experiments will be conducted similarly, except no prior subtraction is assumed.

Each unknown surface image is modeled as a segment of a spatially continuous, stationary random process with single-pole power spectrum, multiplied by a bandlimiting window (Figure 5.2). SNR is defined as the input signal power divided by the height of the output white noise spectrum, i.e., SNR=$\mathrm{Var}(f(x))/N_0$.

Since a signal segment of length L may be represented by the cosine series

$$f(x) = \sqrt{\frac{1}{L}} f_0 + \sqrt{\frac{2}{L}} \sum_{k=1}^{\infty} f_k \cos \frac{\pi k}{L} x, \quad x \in [0, L],$$

the following computational simplifications are used. Because the cosine transform approximates the ideal Karhunen-Loève expansion for this process [Hou87, Clarke81], the cross-correlations $\mathrm{E}\{f_k f_l\} \approx 0$ are set to 0. Also, if $S_f(\omega)$ is the signal power spectrum then

$\mathrm{Var}(f_k) \approx S_f(\pi k/L)$. Since $f(x)$ is bandlimited, only a finite number of terms are nonzero; accordingly, the input side of the linear system $\mathbf{H}$ in (5.1) becomes finite dimensional, and $\mathbf{\Lambda}_f$ in this basis is a diagonal matrix. $\mathbf{H}$ itself is not diagonal, however.

The preceding method of discretizing $f(x)$ is preferable to Nyquist sampling because accurately computing the coefficients of $\mathbf{H}$ in the basis of shifted sinc functions is very expensive; it was found that even a tiny amount of aliasing could change the zero eigenvalues of $\mathbf{H}$, masking its truly singular nature. Another advantage of this representation is that the diagonal of $\mathbf{P}$ has a frequency-domain interpretation—it is something like the power spectrum of the estimation error. The main drawback—that the MSE for a subinterval of $[0, L]$ is not immediately accessible—is outweighed by the advantages.

In keeping with the theoretical analysis of the previous chapters, blurred frames are considered to be spatially continuous and observed with infinite bandwidth, only now corrupted by additive white noise. Therefore, the optimum MSE values to be calculated serve as lower bounds on the actual MSE achievable with discrete and finite bandwidth observations (to be discussed in §5.5). Since $\mathbf{H}^{\mathrm{T}}\mathbf{\Lambda}_n^{-1}\mathbf{H}$ is finite dimensional and can be calculated analytically, no discrete approximation is involved for the output side of the linear system.

5.3 Confirmation of Theory

The performance of the optimum Wiener estimates is found to be in excellent agreement with the theory, in the sense that all differences can be ascribed to observation noise or the finite bandwidth signal model. Refer back to Figure 2.1 for a summary of the predicted nullspaces.

5.3.1 Intraregion

5.3.1.1 Intraframe

When the SNR of the data is high, the estimation error in the benchmark problem is dominated by the irreducible error of unobservable modes rather than amplified observation noise. As shown in Figure 5.3b, the error energy in the cosine transform domain is concentrated around basis functions with periods vT/k, $k = 1, 2, 3, \ldots$. Consequently, the error autocorrelation in the signal domain is nearly periodic, with period equal to the blur distance (Figure 5.3c). These results agree with the theoretical nullspace $N(\mathbf{H}) = \Pi_0(vT)$.

There is an intuitive reason that errors at samples spaced $vT, 2vT, 3vT, \ldots$ apart are highly correlated. Ignoring noise, $f(x)$ is related deterministically to $f(x - vT)$ via the difference equation (1.1) once $g(x)$ is observed.

As an aside, one would typically expect better performance in the middle of a finite interval estimation problem than at the ends. A trend of this sort is evident from Figure 5.3d, but the difference is almost negligible.

5.3.1.2 Interframe

A corresponding interval is now made available from another frame. The surface displacements during successive frames, v_1T and v_2T, will ordinarily be very close, but we will examine a wide range of v_2/v_1 in order to allow non-consecutive frames as well. The broken curves in Figure 5.4 are the optimum MSE's achievable when either of the two frames is observed alone. v_2/v_1 is varied while $v_1T = 11$ is held constant. The solid curve is the MSE when the two observations are combined, and obviously has to stay below both broken curves.

Two salient features should be noted. First, the peaks in the interframe MSE are in

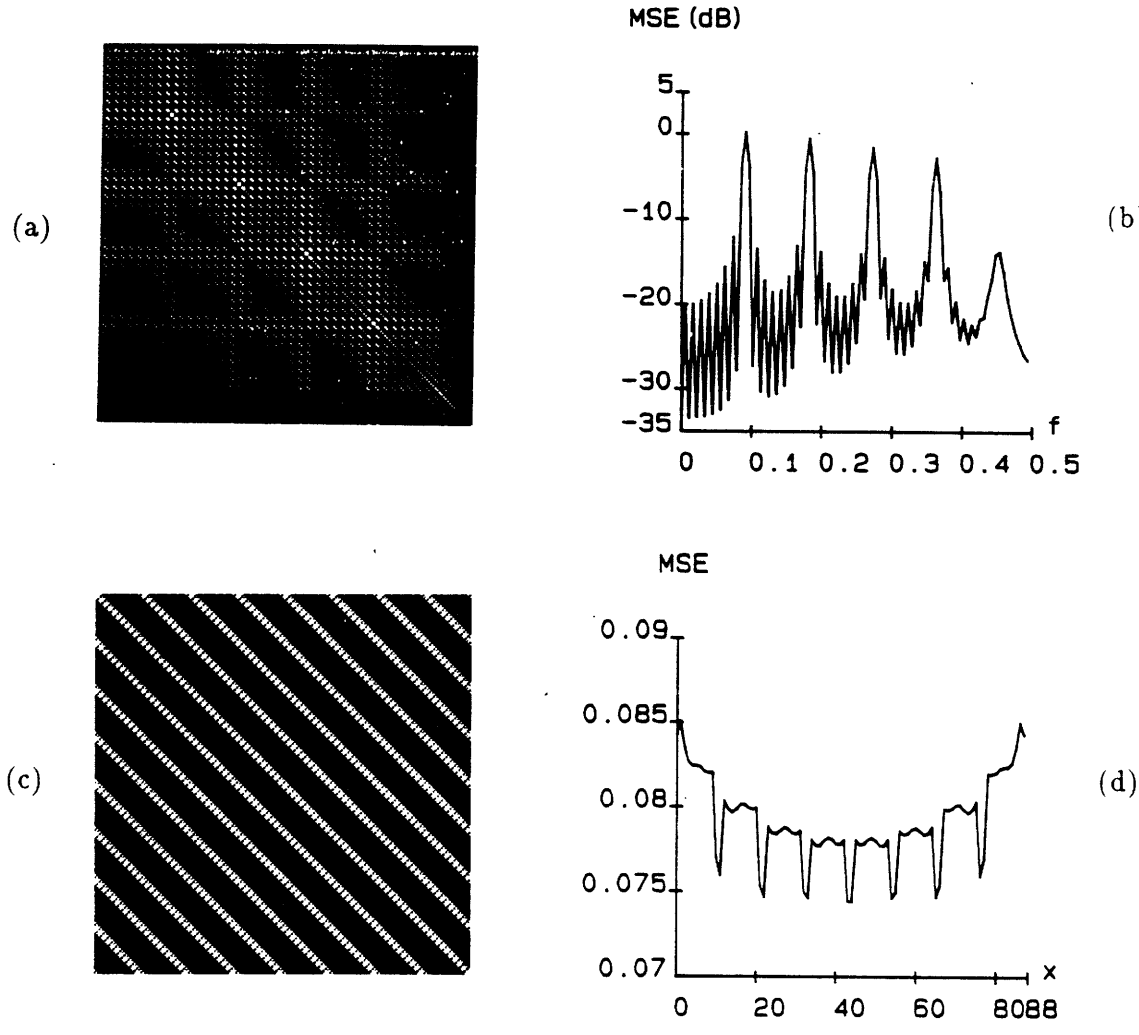

Figure 5.3: Error covariance of optimum intraframe, intraregion reconstruction. $\rho = 0.10$, SNR=50 dB, $vT = 11$, $L = 88$.
(a) Covariance $\mathbf{P}$ in cosine transform domain (log magnitude);
(b) Diagonal elements of $\mathbf{P}$;
(c) Covariance in signal domain;
(d) Diagonal of (c), with greatly exaggerated vertical scale.

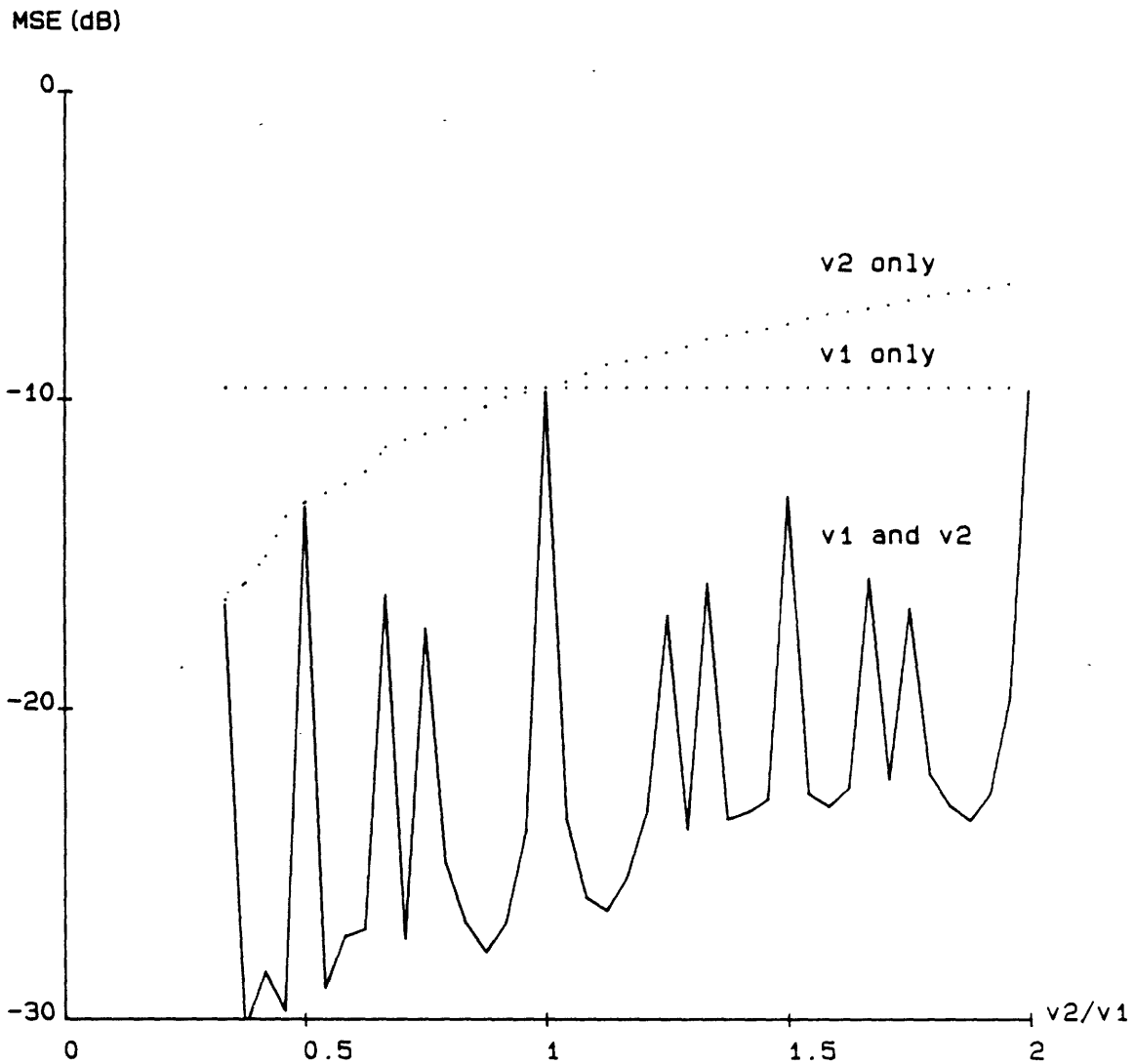

Figure 5.4: MSE of intraregion reconstruction vs. v_2/v_1: $v_1T = 11$ is fixed.
$\rho = 0.10$, SNR=50 dB, $L = 88$.
(dotted) reconstruction using single frame of blur v_1T or v_2T individually;
(solid) reconstruction using both frames.

one-to-one correspondence with the set of velocity combinations that satisfy

$$\gcd(v_1T, v_2T) \geq 2\pi/\omega_{\max}, \tag{5.5}$$

where $\omega_{\max}$ is about 0.7π. Specifically, peaks are located at

$$v_2T = \frac{11}{3}, \frac{11}{2}, \frac{22}{3}, \frac{33}{4}, 11, \frac{55}{4}, \frac{44}{3}, \frac{33}{2}, \frac{55}{3}, \frac{77}{4}, \text{ and } 22.$$

Second, the height of a peak is directly related to the magnitude of $\gcd(v_1T, v_2T)$, and the arrangement of peaks resembles Figure 2.5. For example, the peak at $v_2/v_1 = 2/3$ is higher than the one at $v_2/v_1 = 3/4$; the gcd's are 11/3 and 11/4, respectively.

Both properties could have been predicted by the theory. In principle the nullspace is $\Pi_0(\gcd(v_1T, v_2T))$, nonempty for all rational v_2/v_1, but in practice the only nullvectors that matter are those with frequencies well within the low-pass signal spectrum $S_f(\omega)$. Peaks appear only when $\gcd(v_1T, v_2T)$ is sufficiently large (the nominal cutoff frequency $\omega_{\max}$ in (5.5) is lower than π due to the spectral window), and the nullspace is essentially empty for almost every velocity ratio, even rational ones. Finally, the peaks are highest whenever $N(\mathbf{H})$ contains nullvectors of lower frequencies, because $S_f(\omega)$ is a decreasing function of frequency.

The idealized theory would predict infinitesimally narrow peaks, but observation noise prevents this from occurring. Although the signals in $\Pi_0(\gcd(v_1T, v_2T))$ are no longer exact nullvectors as v_2T is perturbed away from a peak, they will still be attenuated so much by $\mathbf{H}$ that they remain effectively unobservable and continue to cause high MSE.

5.3.2 Transition Zone Compensation

5.3.2.1 Intraframe

As in Chapter 2 the unknown surface will be regarded as "background" and the known adjacent surface, whose contribution is perfectly subtracted out of the transition zone, is "foreground". Assuming that the original intraregion domain of observation abuts a transition zone, the zone is now appended to the data available to the reconstruction algorithm. v_b/v_e is varied while $v_bT = 11$ is held constant. (In particular, the condition $v_b/v_e = 1$ could represent the situation where the "background" is really an object moving in front of a known stationary surface.)

The broken line in Figure 5.5 is the MSE of the benchmark intraframe, intraregion

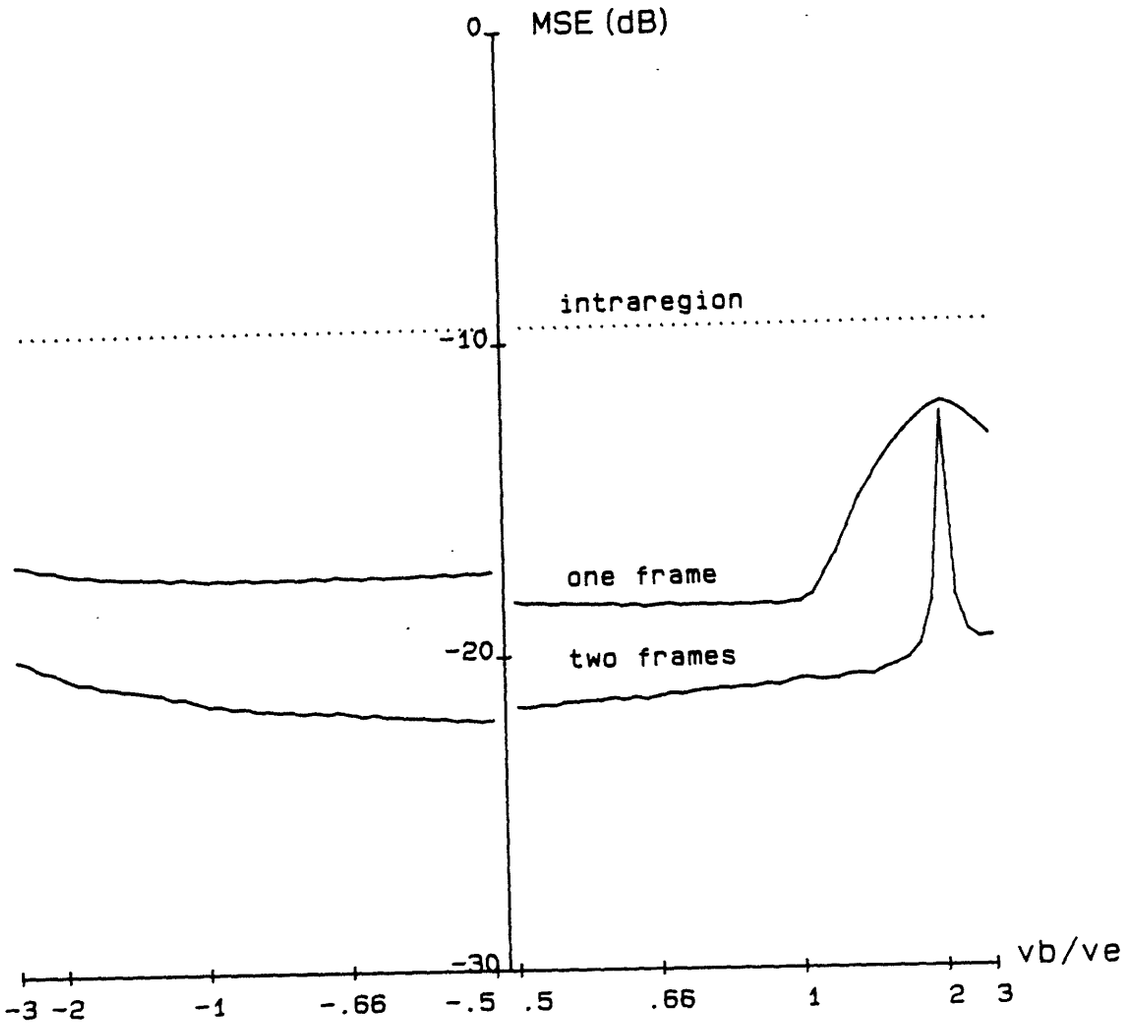

Figure 5.5: MSE of transition zone compensation vs. v_b/v_e: $v_bT = 11$ is fixed.
$\rho = 0.10$, SNR=50 dB, $L = 88$.
(dotted) intraframe, intraregion reconstruction for comparison;
(solid) transition zone compensation using one or two frames.

reconstruction problem. The upper solid curve demonstrates that intraframe transition zone compensation is markedly less effective when $v_b/v_e > 1$, confirming the existence of the nullspace $N(\mathbf{H}_\angle) \cap \Pi_0(v_bT)$ for this range of velocity ratios.

Notice that the MSE gradually decreases from the peak at $v_b/v_e = 2$. This shallow skirt can be explained by the low-pass nature of $S_f(\omega)$. At the peak, the region of support of $\mathbf{H}_\angle$ is an isosceles triangle, and a period-v_bT nullvector in $N(\mathbf{H}_\angle)$ can be a pure sinusoid of wavelength v_bT. As v_b/v_e moves away from 2 in either direction, the triangle becomes more and more asymmetrical; this requires period-v_bT nullvectors to contain higher frequency harmonics, which are lower in energy.

Another feature is a gradual rise in MSE as $|v_eT|$, the width of the transition zone, decreases (evident in the graphs only for $v_b/v_e < 0$ since the effect is obscured by the peak at $v_b/v_e = 2$). Because the total energy due to $f_b(x)$ in the transition zone is declining quadratically with $|v_eT|$ while the total noise energy in the zone is declining only linearly, the quality of the boundary condition suffers. In the limit as $|v_eT| \to 0$, of course, the transition zone vanishes and the MSE must approach that of intraregion reconstruction.

5.3.2.2 Interframe

The corresponding interval in an adjacent frame is added to the previous observation domain, choosing the previous frame if the boundary and background surface are moving apart, or the following frame if they are converging. This procedure avoids adding more new portions of $f_b(x)$ to the set of unknowns.

The lower solid curves in Figure 5.5 exhibit only a narrow peak at $v_b/v_e = 2$, as the theory would predict. The constraints provided by the second frame of transition zone compensation rule out unobservable modes in $N(\mathbf{H}_\angle) \cap \Pi_0(v_bT)$, except around one pathological velocity ratio.

5.3.3 Interregion Reconstruction

The interregion reconstruction problem uses the same surface and observation configurations as transition zone compensation. However, prior knowledge of the foreground contribution $g_f(x,t)$ within the transition zone is replaced, in effect, by the interframe constraint $g_f(x + v_eT, t+T) - g_f(x,t) = 0$.

5.3.3.1 Intraframe

Interregion reconstruction is impossible using one frame, as shown by the top solid curves in Figure 5.6.

5.3.3.2 Two frames

The middle solid curves display properties of both intraregion and transition zone compensation problems. In the range $v_b/v_e > 1$ the MSE broadly peaks at $v_b/v_e = 2$. This agrees with the prediction of nullspace $N(\mathbf{H}_{\angle}\Delta) \cap \Pi_0(v_bT)$ for this range of velocity ratios. Asymmetry in $\mathbf{H}_{\angle}$ should again account for the shallow skirt.

Every narrow peak in the MSE corresponds to a velocity combination for which

$$\gcd(v_bT, v_eT) \geq 2\pi/\omega_{\max},$$

where $\omega_{\max}$ is roughly 0.7π. The height of a peak is directly related to the magnitude of $\gcd(v_bT, v_eT)$. These peaks support the prediction of nullvectors in $\Pi_0(\gcd(v_bT, v_eT))$.

Notice, however, the absence of a peak at $v_b/v_e = 3$ and the scarcity of peaks for negative v_b/v_e. It appears that v_b, v_e must also satisfy

$$\frac{\gcd(v_bT, v_eT)}{1 - v_b/v_e} \geq \frac{2\pi}{\omega_{\max}} \tag{5.6}$$

to produce a peak, and this is violated by $v_eT = 11/3$ as well as most of the potential peak velocities in the range $v_eT < 0$.

This extra requirement can be explained by the signal spectrum of the *foreground* surface, which constrains the set of possible background surface nullvectors even though it is not being estimated. Suppose the pair (f_b, f_f) makes a nullvector. From (2.14), $f_f(x)$ in the transition zone is the scaled derivative of $g_b(x, 0)$, which is related to $f_b(x)$ through $\mathbf{H}_{\angle}$ or $\mathbf{H}_{\backslash}$ (2.7):

$$g_b(x, 0) = \frac{1}{v_bT} \int_{(1-v_b/v_e)x}^{x} f_b(u)\, du, \quad x \in [0, v_eT]. \tag{5.7}$$

An input signal component at frequency ω produces an output containing frequency $(1 - v_b/v_e)\omega$ as well as ω itself. The inequality (5.6) just means that $f_f(x)$ cannot contain frequencies beyond the nominal bandwidth.

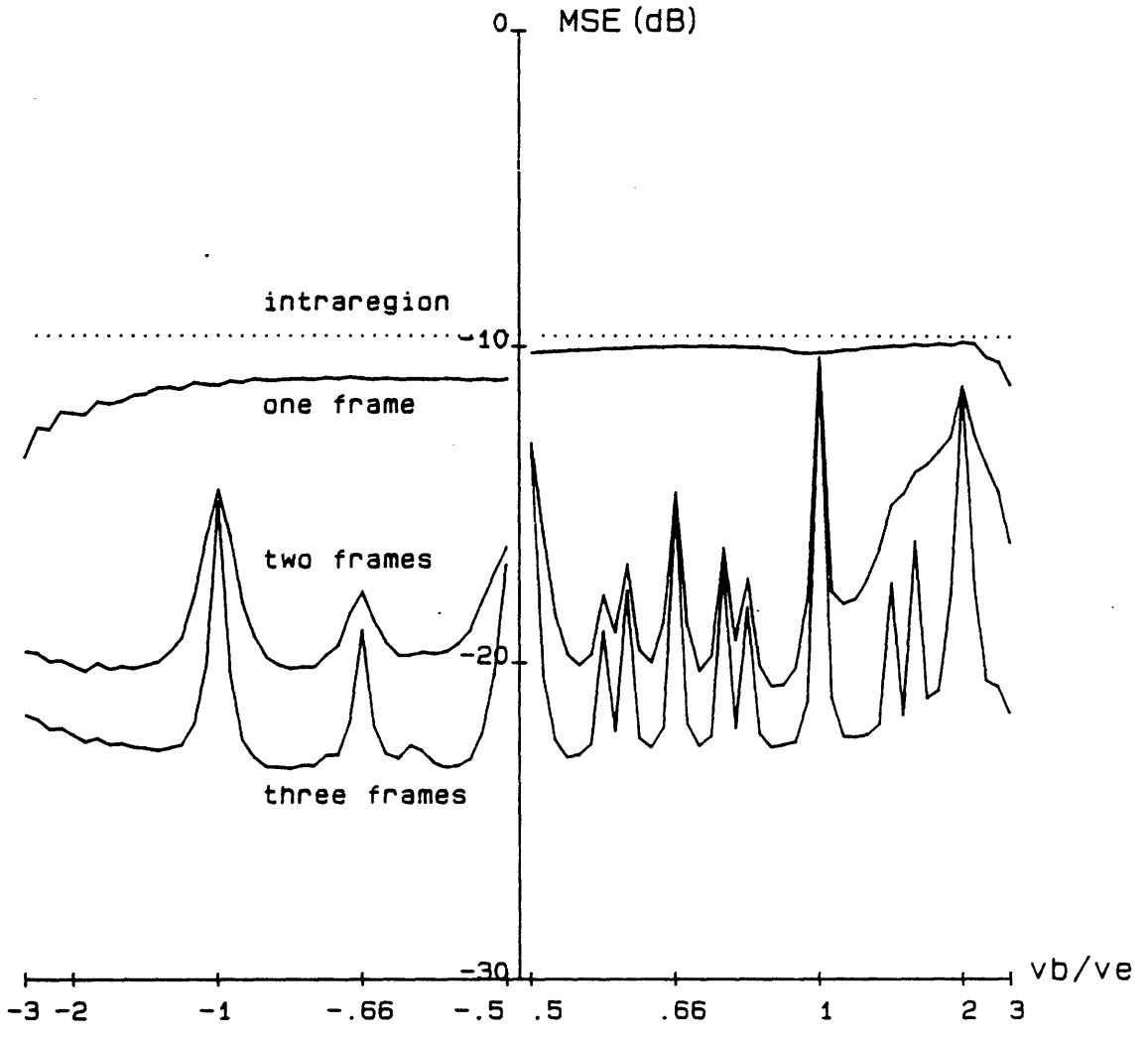

Figure 5.6: MSE of interregion reconstruction vs. v_b/v_e: $v_bT = 11$ is fixed.
$\rho = 0.10$, SNR=50 dB, $L = 88$.
(dotted) intraframe, intraregion reconstruction for comparison;
(solid) interregion reconstruction using one to three frames.

5.3.3.3 Three frames

The main effect of adding a third frame is to discard the shallow skirt to reveal two smaller peaks, which correspond to modes in $\Pi_0(\gcd(v_bT, v_eT))$. The tall peak at $v_b/v_e = 2$ reflects the usual pathological case. §2.4.2 questioned whether signals in the nullspace $N(\mathbf{H}_{\angle}\Delta) \cap \Pi_0(v_bT)$ but not also in $\Pi_0(\gcd(v_bT, v_eT))$ actually exist; the clear difference in MSE between two and three frames for velocities in the range $v_b/v_e > 1$ indicates that they do.

5.3.4 Discussion

To summarize, the foregoing experiments confirm that the structure of the nullspace is determined by interregion or interframe velocity ratios in accordance with theory, modified by the signal model and the existence of observation noise. No specific nullvectors were actually calculated to verify that $N(\mathbf{H})$ is really $\{\text{odd functions}\} \cap \Pi_0(v_bT)$ or $N(\mathbf{H}_{\angle}\Delta) \cap \Pi_0(v_bT)$, for example, but the results offer no evidence to the contrary. When properly interpreted, the results of Chapters 2–4, which might have been dismissed as merely mathematical curiosities, reflect the actual performance under more realistic assumptions.

The set of unfavorable velocity combinations is less extensive than predicted by theory because the shorter wavelength functions in $N(\mathbf{H})$ become irrelevant when $S_f(\omega)$ is a low-pass spectrum. For all intents and purposes, a subspace of the form $\Pi_0(\gcd(z_1, z_2))$ is nonempty not for the dense set of all rational z_1/z_2 but only for the sparse set of $z_1/z_2 = m/n$ where m, n are small integers. Velocities are in effect incommensurate whenever inequalities like (5.5) and (5.6) are violated.

On the other hand, the set of unfavorable velocities is expanded by the presence of observation noise. A signal component in $N(\mathbf{H})$ at one specific velocity will remain essentially unobservable for a range of neighboring velocities, since its system response remains buried in noise. Noise keeps infinitesimal velocity perturbations from causing discontinuous changes in the behavior of reconstruction.

In a Bayesian approach like Wiener estimation, one aspect of proper interpretation includes defining what is meant by "observability". After all, noise always prevents perfect estimation, even when far away from an MSE peak, and the signal model prevents total ignorance. An "observable mode" is one that can be estimated relatively well from the

data, while an "unobservable mode" can only be poorly estimated; i.e., the data gives little information and a priori knowledge is heavily weighted.

In light of this discussion, it is vital to reassess the relevance of the unsolved theoretical problems raised in earlier chapters. The discussion of Theorem 2.4.2 questioned the existence of "interesting" nullvectors for irrational values of v_b/v_e, but the question is moot since they do exist for neighboring rational values. In connection with Theorem 3.1, §A.4 speculates that $N(\mathbf{H}) = \{\mathbf{0}\}$ or $N(\mathbf{H}_\angle) \cap \Pi_0(v_b DT)$ for almost all points in the (α, δ) plane, except in a certain set where the nullspace is not yet known. Despite the small area of that subset, it is still important to determine the nullvectors, if any: in the presence of noise they affect observability at neighboring values of (α, δ) which were theoretically free of nullvectors.

5.4 Comparison of Reconstructions

In order to best illustrate the theory, the signal and noise statistics were fixed in the preceding section. Here, these parameters are allowed to vary, and the performance of intraregion, transition zone compensation, and interregion restorations is compared. The benchmark reconstruction problem is the intraframe observation of a surface segment of length $L = 88$, blurred by displacement $v_bT = 11$; the signal spectra are those of Figure 5.2.

Although MSE is a convenient figure of merit, the numbers should not be taken too seriously. After all, typical natural scenes do not resemble samples of a homogeneous random process. Moreover, residual blur, random-looking noise, and periodic artifacts all contribute to this error metric, but it is unlikely that the subjective visibility of these disparate distortions combine by simple addition. For this reason, test images will supplement the numerical results. Figure 5.7a shows the original background surface along with a narrow strip of the foreground. The estimated correlation between points horizontally spaced 1 unit apart is $\rho = 0.88$. The blurred image from one frame is depicted in Figure 5.7b,c, with background displacement $v_bT = 11$. The transition zone on the left margin is seen to contain some signal from the foreground, whose displacement is $v_fT = v_eT = \pm 8$.

5.4.1 Effects of ρ and SNR

Figures 5.9,5.13,5.17 cover the three classes of reconstruction problems with three levels of noise. As a check on the calculations, it is verified that increasing the amount of information—e.g., increasing ρ, SNR, number of frames, or spatial extent of observation, or performing subtraction in the transition zone—never increased the MSE.

The effect of ρ on MSE is negligible when the MSE itself is very low, because the a priori information of signal statistics is not heavily weighted. At high levels of MSE, decreasing the correlation from $\rho = 0.74$ to 0.10 increases MSE by 3 dB or so (Figure 5.8). Qualitatively, the performance curves are unchanged and so only $\rho = 0.74$ data will be shown and discussed.

The noise level, on the other hand, greatly affects the shape of the curves. The highly peaked behavior at 50 dB SNR caused by the changing nullspace structure is diminished at 40 and 30 dB. The valleys are rapidly lifted by an increase in noise because at those velocity ratios the estimation of signals close to the nullspace depends heavily on data, while the

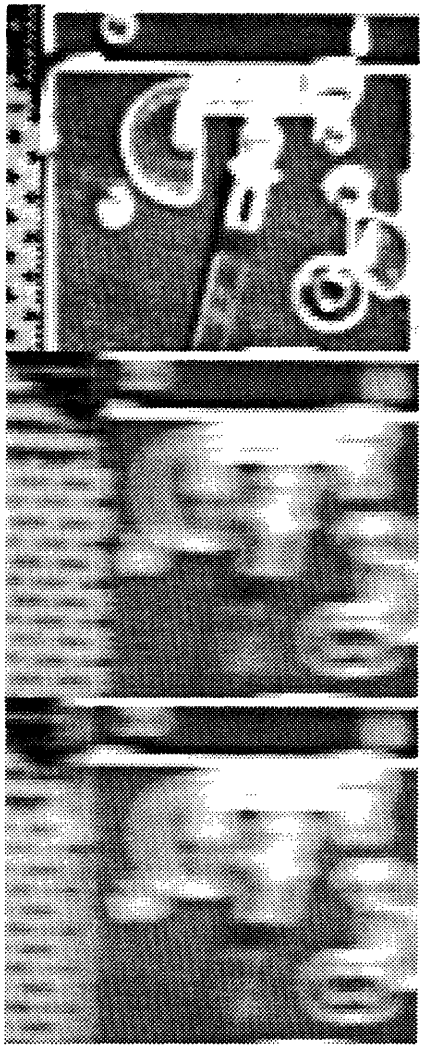

(a)
Original

$v_f T = -8$

(b)
$v_b T = 11$

$v_f T = 8$

(c)
$v_b T = 11$

Figure 5.7: Original and blurred test images:
(a) original background surface from "cman" ($L = 89$) and foreground surface from "quilt", which appears as a narrow strip on the left;
(b) background blurred by displacement $v_b T = 11$ and foreground surface blurred by displacement $v_e T = v_f T = -8$;
(c) $v_e T = v_f T = 8$.

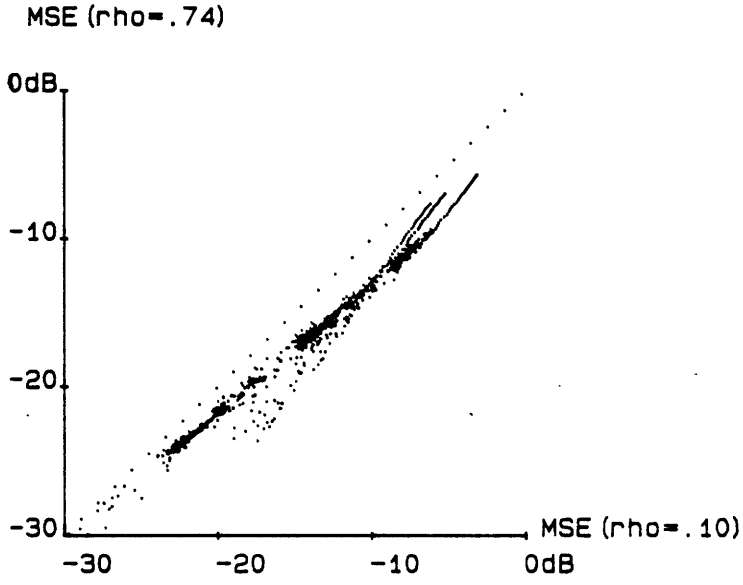

Figure 5.8: MSE at $\rho = 0.10$ vs. MSE at $\rho = 0.74$. Data points combined from intraregion, transition zone compensation, and interregion at all velocity ratios and SNR levels.

peaks rise slowly because the data at those velocity ratios is not too useful for estimating near-nullvectors.

5.4.2 Intraregion

The MSE for the benchmark problem of intraframe, intraregion restoration ranges from -9 to -13 dB as the SNR of the observation varies from 30 to 50 dB (Figure 5.9). Compared to -4 dB, the MSE of the blurred frame without any processing, the gains are moderate to large. The subjective improvement is significant if a sharp image with artifacts (Figure 5.10a) or artifacts plus noise (Figure 5.10c) is considered better than a blurred one with no artifacts or noise. Even so, both the theoretical performance and the visible artifacts leave something to be desired.

The Wiener MSE for the high SNR observation comes within 0.1 dB of the MSE of a noiseless pseudoinverse reconstruction, i.e., the variance of $f_{\text{unobs}}(x)$. Moreover, the reconstruction in Figure 5.10a is very close to the calculated observable component, Figure 1.2d. This is reasonable because of the weak correlation between $\mathbf{f}_{\text{unobs}}$ and $\mathbf{f}_{\text{obs}}$: at its best (at high SNR) the Wiener estimator recovers only the observable part.

5.4.2.1 Extending the observation spatially

The most straightforward method of improving the benchmark reconstruction is to expand the length of observation. Since $g(x)$ is correlated even if $f(x)$ is not, the performance must improve. However, the MSE declines slowly with L (Figure 5.11). Doubling L from 88 to 176 gives less than 2 dB improvement at SNR of 50 dB; only in the limit as $L \to \infty$ does the attainable MSE rival that of reconstructions involving the compensated or uncompensated transition zone. This approach is not promising because the burden of computation grows and because regions have limited size.

5.4.2.2 Interframe with unequal velocities

Among the three classes of reconstruction problems, the greatest potential MSE reduction results from multiple velocity observations of a single surface. Object velocities do not often change much over the course of a few frames, so the most relevant part of Figure 5.9 is the neighborhood around $v_2/v_1 = 1$. At 50 dB SNR, adding a frame in which the displacement is $v_2T = 9.6$ makes the MSE drop by 16 dB to reach -28 dB. As demonstrated in

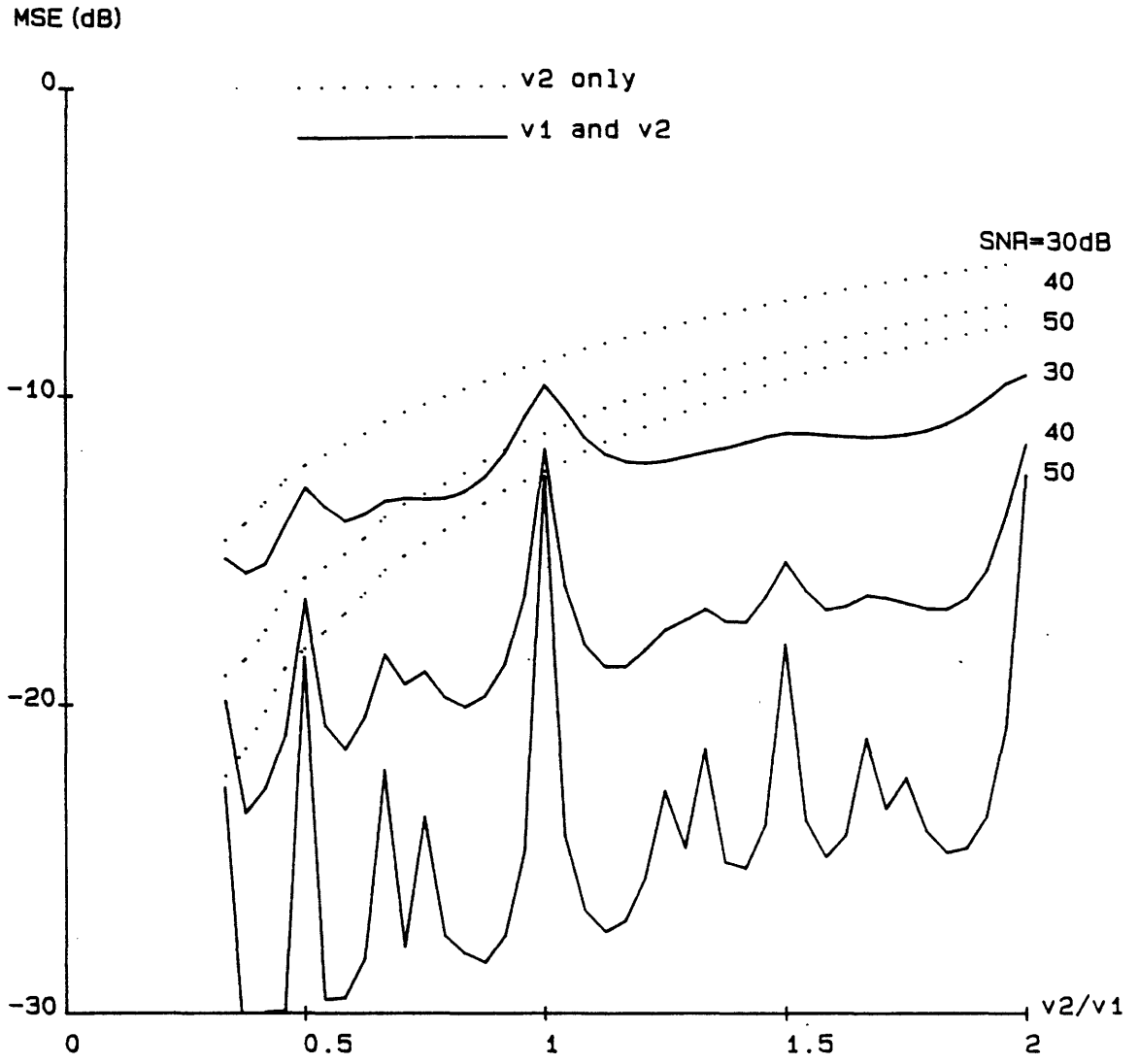

Figure 5.9: MSE of intraregion reconstruction vs. v_2/v_1 and SNR. $v_1T = 11$ is fixed. $L = 88$, $\rho = 0.74$.
(dotted) intraframe reconstruction using single frame of blur v_2T;
(solid) reconstruction using both frames.

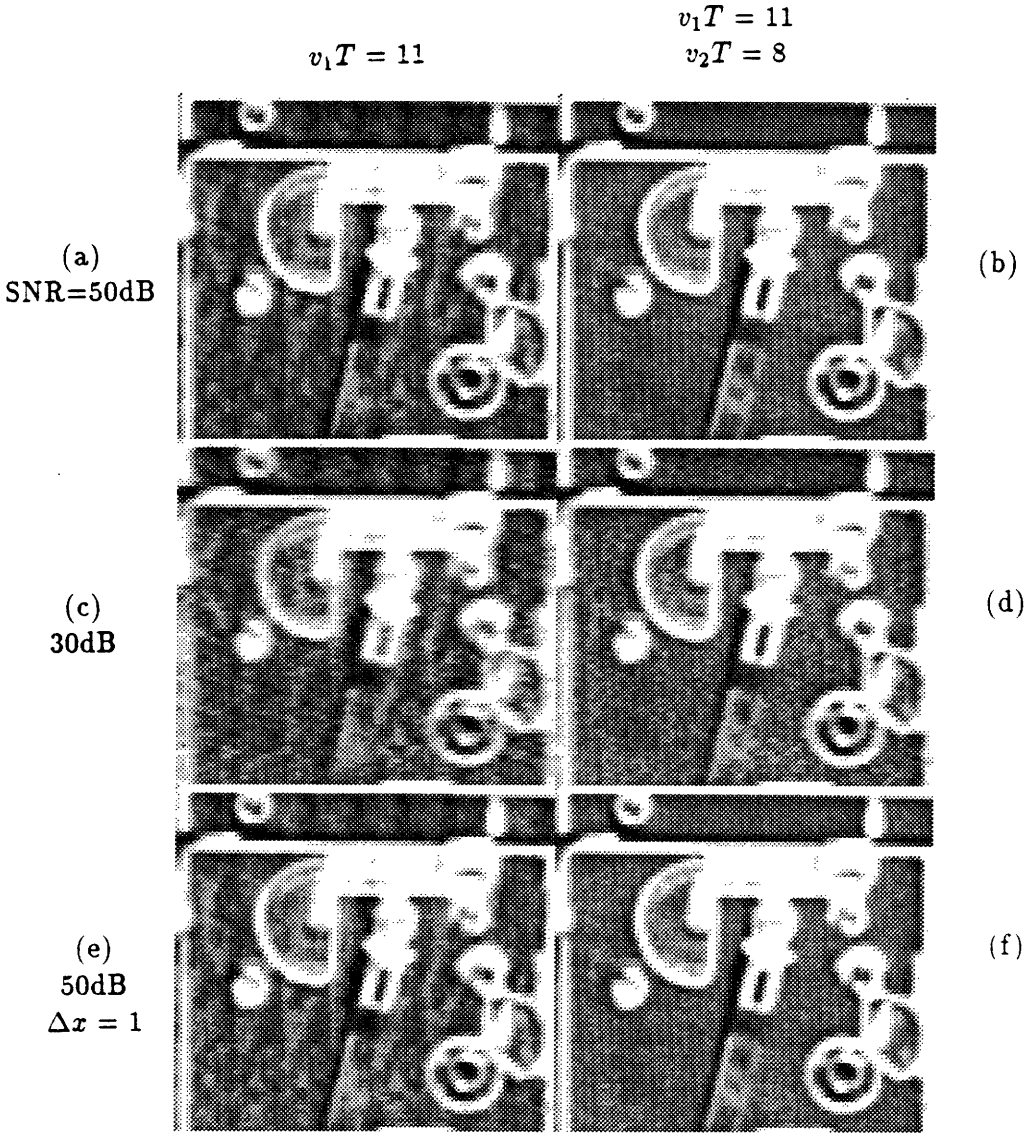

Figure 5.10: Intraregion reconstruction of an image: (left) using one frame, $v_1T = 11$; (right) using two frames, $v_1T = 11$, $v_2T = 8$.
(a-d) continuous observation;
(e-f) discrete observation, $\Delta x = 1$.

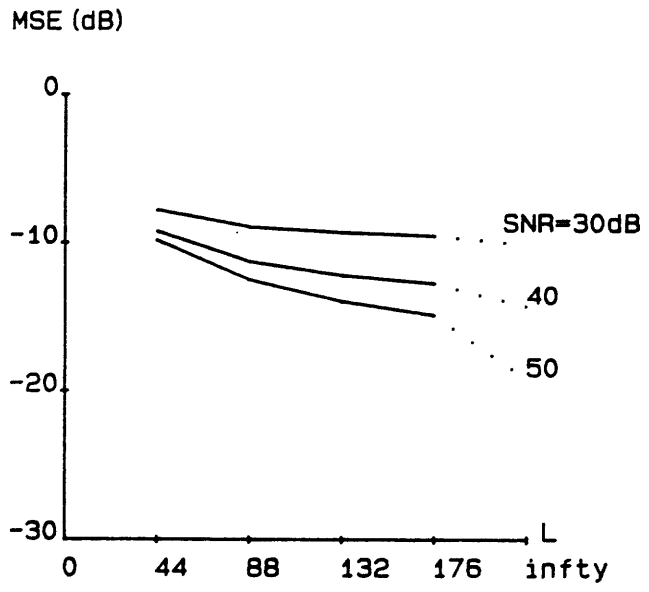

Figure 5.11: MSE of intraframe, intraregion reconstruction vs. L and SNR. $vT = 11$, $\rho = 0.74$.

Figure 5.10b, the periodic component in $\Pi_0(v_1 T)$ is completely recovered and the reconstruction is virtually indistinguishable from the original. At 30 dB SNR the predicted MSE improvement is not impressive, but the subjective improvement is still good (Figure 5.10d).

The principal limitation of this approach is that performance is highly variable, degrading when v_2/v_1 is close to a ratio of small integers. In Figure 5.12a the velocity ratio is 3/2 and the interframe reconstruction is missing a periodic component of fundamental wavelength $\gcd(16.5, 11) = 5.5$.

5.4.3 Transition Zone Compensation

5.4.3.1 Intraframe

Transition zone compensation is not very useful when a nontrivial nullspace is present ($v_b/v_e > 1$) or when the SNR is worse than 40 dB or so (Figure 5.13). When $v_b/v_e \leq 1$ and SNR=50 dB, though, an improvement up to 8 dB over the benchmark is possible. That brings the MSE down to -21 dB, which is far worse than the potential performance of two-frame intraregion processing, above.

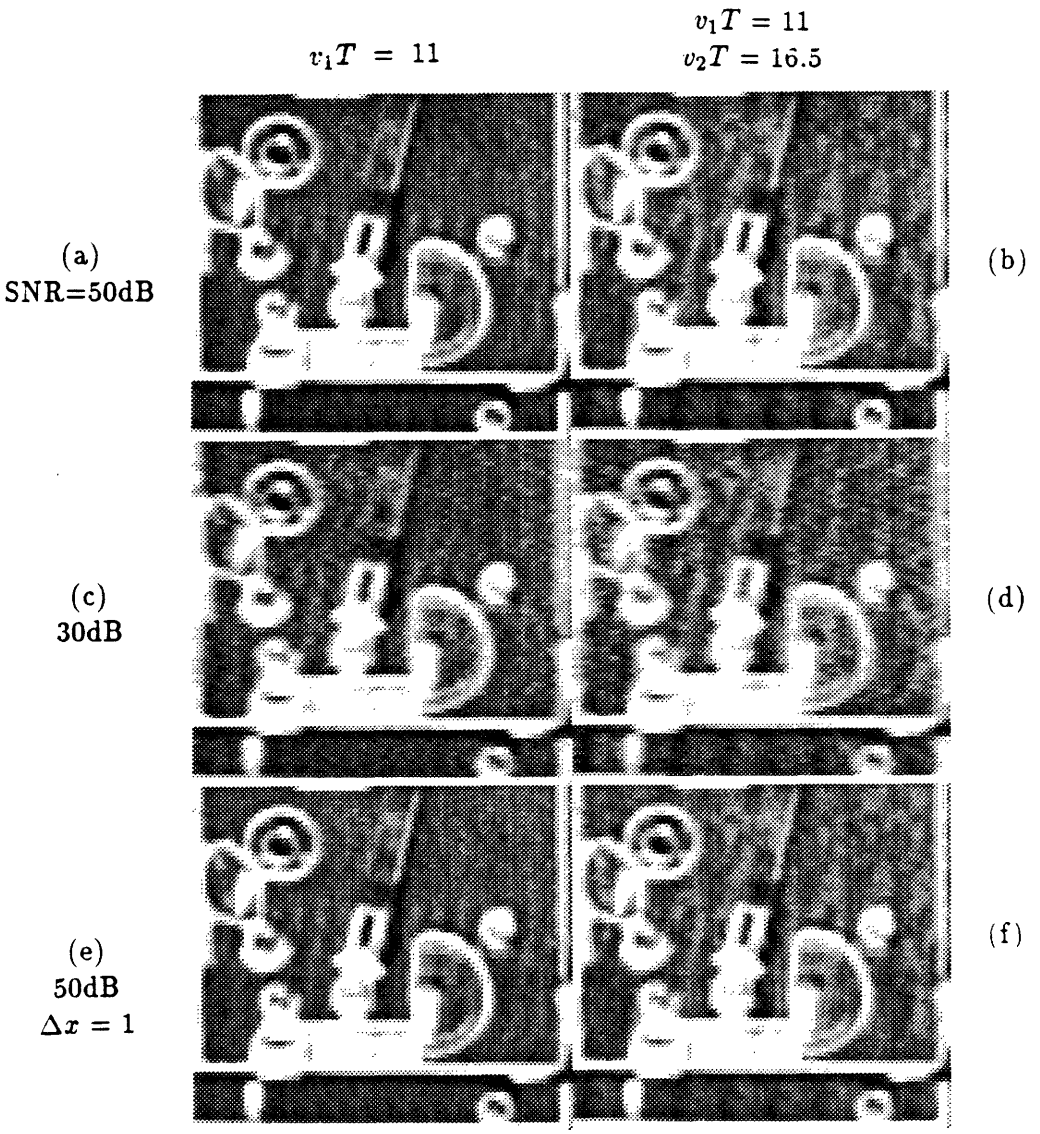

Figure 5.12. Intraregion reconstruction of an image when v_1/v_2 is ratio of small integers: (left) using one frame, $v_1T = 11$; (right) using two frames, $v_1T = 11$, $v_2T = 16.5$.
(a-d) continuous observation;
(e-f) discrete observation, $\Delta x = 1$.

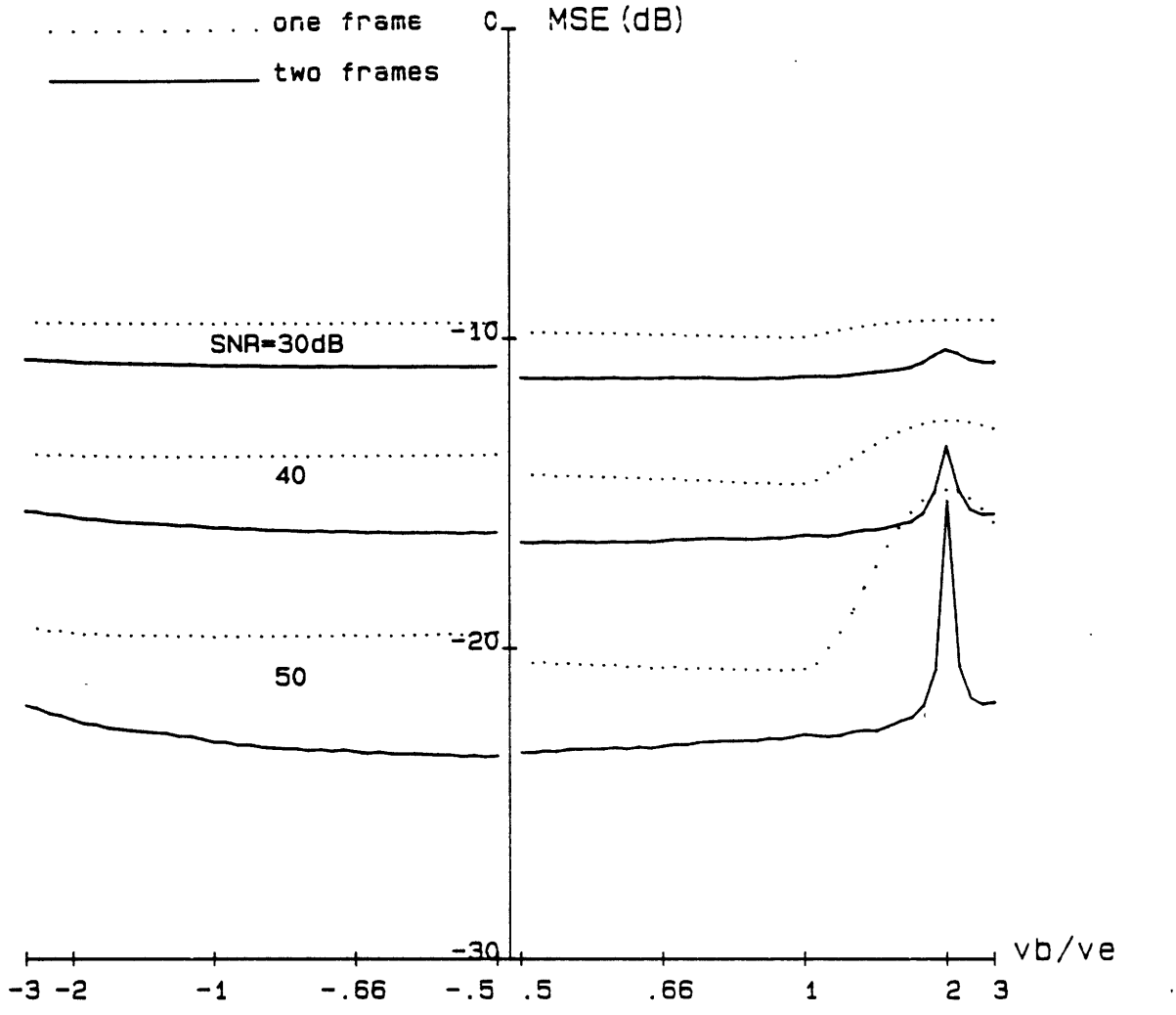

Figure 5.13: MSE of transition zone compensation vs. v_b/v_e and SNR. $v_bT = 11$ is fixed. $L = 88$, $\rho = 0.74$.
(dotted) transition zone compensation in one frame;
(solid) in two frames.

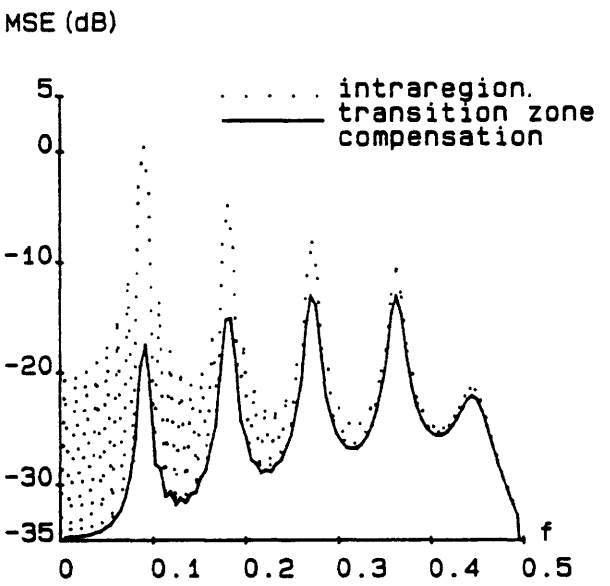

Figure 5.14: Error spectra of intraregion reconstruction and transition zone compensation in cosine transform domain. $\rho = 0.74$, SNR=50 dB, $v_bT = 11$, $v_eT = 15.1$, $L = 88$.

Since transition zone compensation theoretically eliminates all unobservable modes when $v_b/v_e \leq 1$, these predictions are disappointing. Even at 50 dB SNR, the culprit is probably noise. The boundary condition created after subtracting out the foreground surface is a reasonably good constraint on the lowest frequency nullvectors (period v_bT), but a poor constraint on higher frequency ones since they are attenuated more by $\mathbf{H}_{\backslash}$. Thus, the MSE tends to be dominated by the latter (Figure 5.14).

On the other hand, the subjective improvement could still be worthwhile. Sample pictures confirm that transition zone compensation is very effective in removing artifacts of unobservable modes when the SNR is high and $v_b/v_e < 1$ (Figure 5.15a). At 30 dB SNR the artifacts can be reduced only slightly (Figure 5.15c). As expected, modes in $N(\mathbf{H}_{\angle}) \cap \Pi_0(v_bT)$, for $v_b/v_e > 1$, cannot be removed by transition zone compensation (Figure 5.16a). However, since the rest of the signal in $\Pi_0(v_bT)$ has been recovered, the artifacts are less severe.

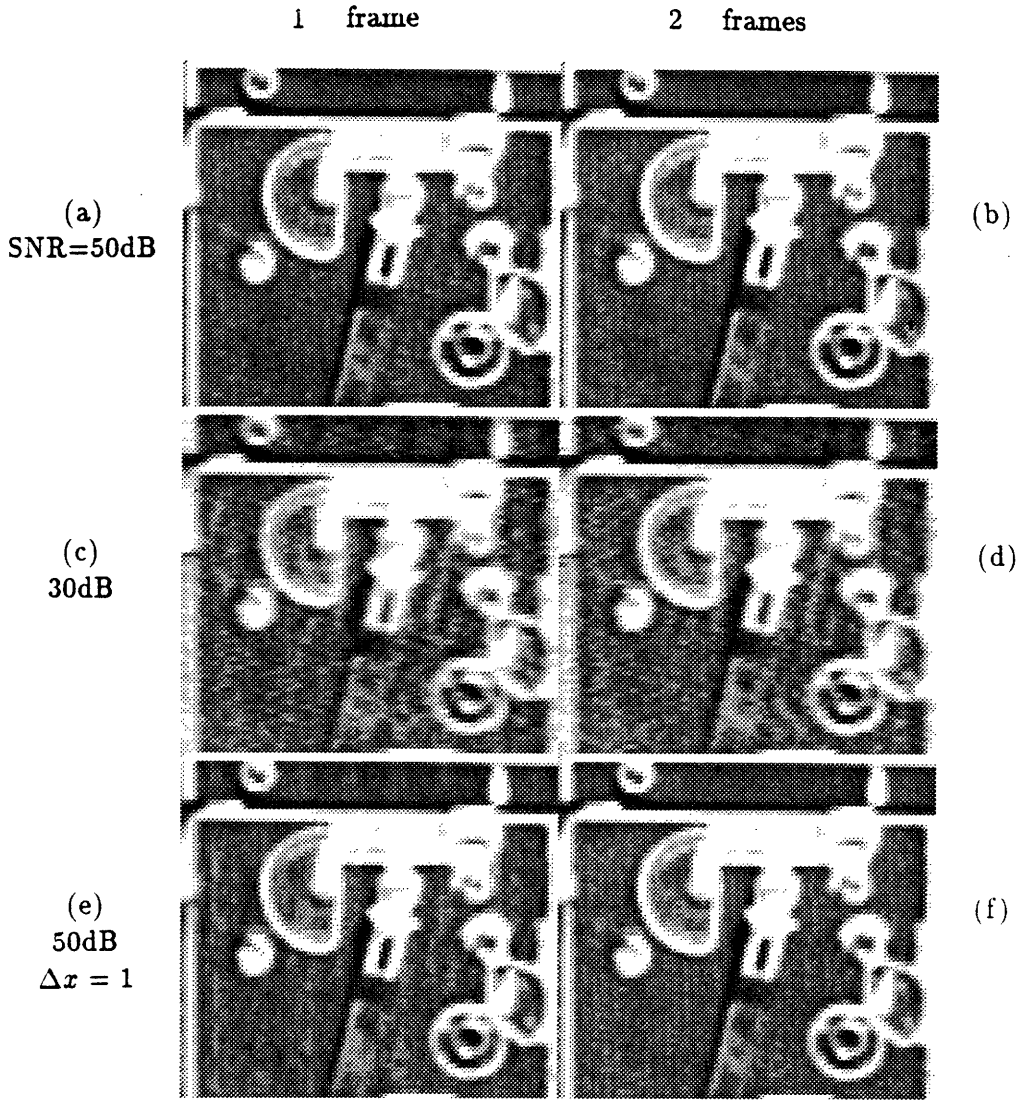

Figure 5.15: Reconstruction after transition zone compensation when $v_b/v_e < 1$.
$v_bT = 11$, $v_eT = -8$. (left) using one frame; (right) using two frames.
(a-d) continuous observation;
(e-f) discrete observation, $\Delta x = 1$.

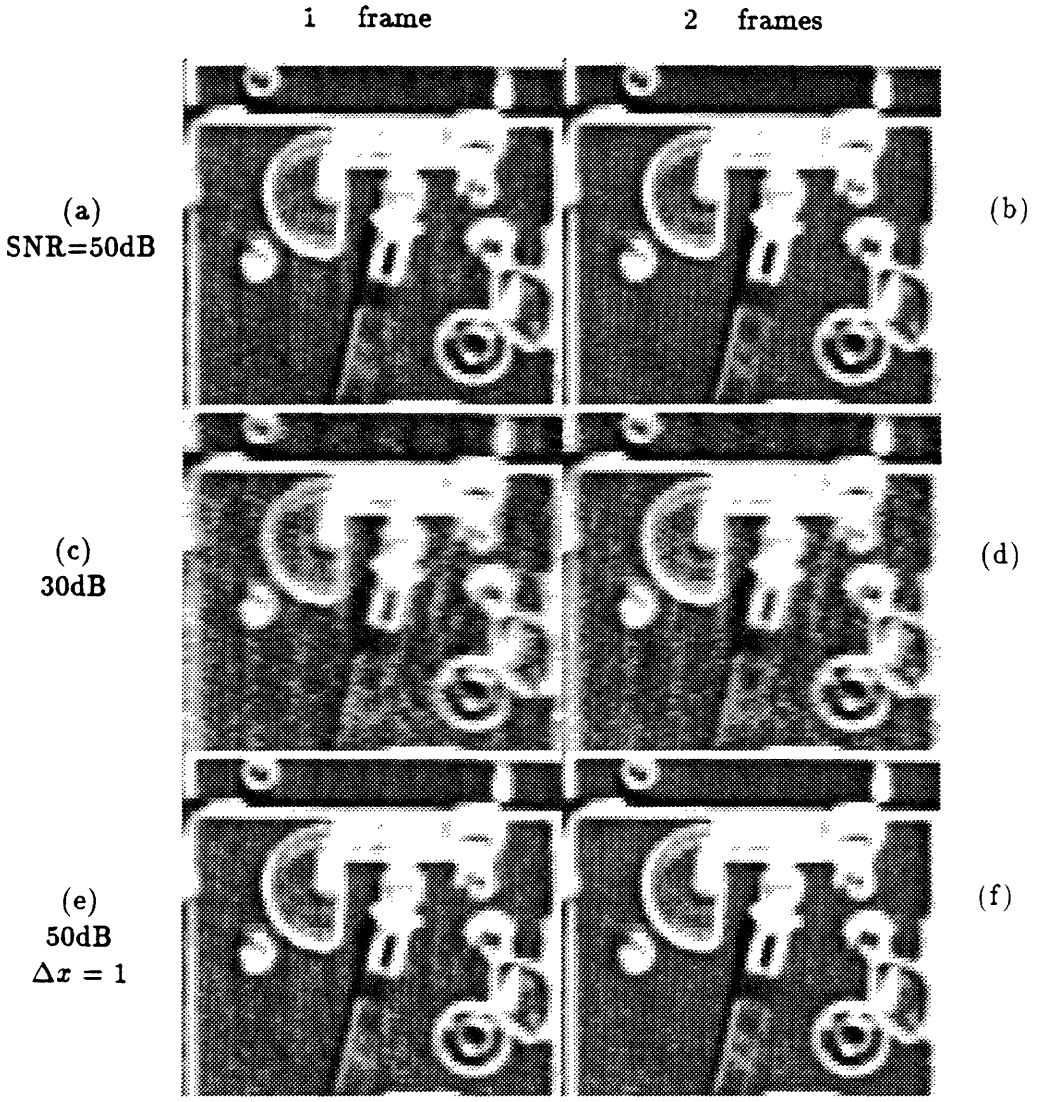

Figure 5.16: Reconstruction after transition zone compensation when $v_b/v_e > 1$
$v_bT = 11$, $v_eT = 8$. (left) using one frame; (right) using two frames.
(a-d) continuous observation;
(e-f) discrete observation, $\Delta x = 1$.

5.4.3.2 Interframe

A second frame generally reduces MSE by an additional 1–3 dB (Figure 5.13). In the velocity range $v_b/v_e > 1$ the improvement is greater because a family of unobservable modes is canceled. Figure 5.16b demonstrates the significance of this cancellation.

5.4.4 Interregion

5.4.4.1 Two frames

Ignoring peaks in MSE due to $\Pi_0(\gcd(v_bT, v_eT))$, the performance of interregion reconstruction using two frames lies between one- and two-frame transition zone compensation (Figure 5.17). As long as transition zones can be observed in two successive frames, knowledge of the foreground surface in order to subtract out its contribution may not be all that valuable.

Test pictures of interregion reconstruction look approximately the same as those of transition zone compensation when v_b/v_e is not close to a ratio of small integers. Compare Figure 5.18 and Figure 5.19 with Figure 5.15 and Figure 5.16.

Unfortunately, the velocity ratio is not under the observer's control and so the peaks cannot be avoided by choice in a practical problem. For example, when $v_b/v_e = 2/3$ the greatest common divisor wavelength is unobservable, and artifacts remain (Figure 5.20). Therefore, the disadvantage of interregion processing, compared to transition zone compensation, is variable performance. The fluctuations may be smaller than those of two-frame intraregion reconstruction, but the overall performance is worse.

The leftmost portion of the background surface happens to be relatively devoid of detail, with little difference among rows. Since only this portion interacts with the foreground, the experimental results might seem unrepresentative. Actually, the reconstruction artifacts, or lack thereof, are not fundamentally affected by this blank area because all parts of the surface contribute with equal weight to the periodic unobservable component.

5.4.4.2 Three frames

The situation is similar to transition zone compensation with two frames. MSE is reduced 1–3 dB by the third frame, except for greater improvement when $v_b/v_e > 1$.

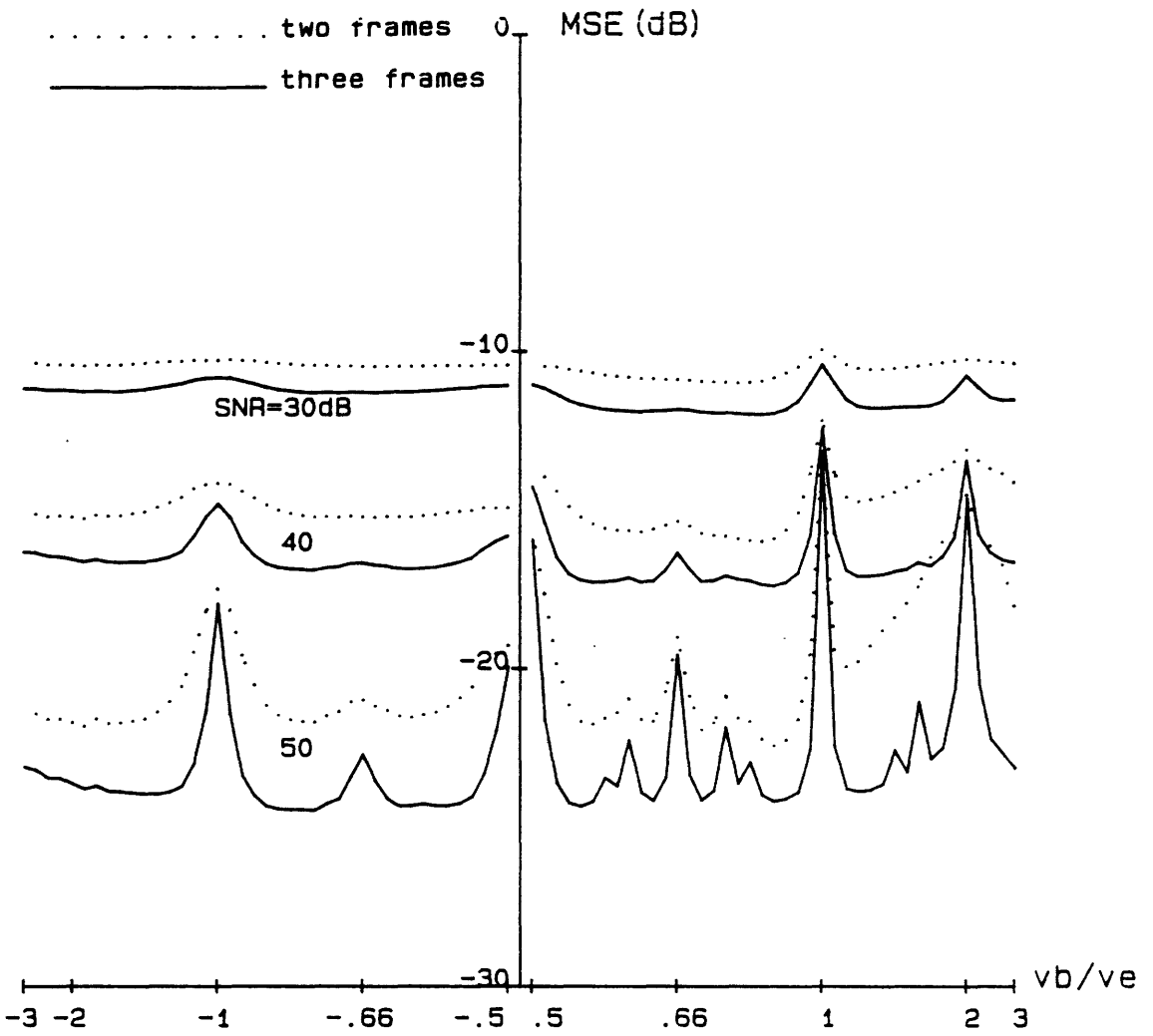

Figure 5.17: MSE of interregion reconstruction vs. v_b/v_e and SNR. $v_bT = 11$ is fixed. $L = 88$, $\rho = 0.74$.
(dotted) interregion reconstruction in two frames;
(solid) in three frames.

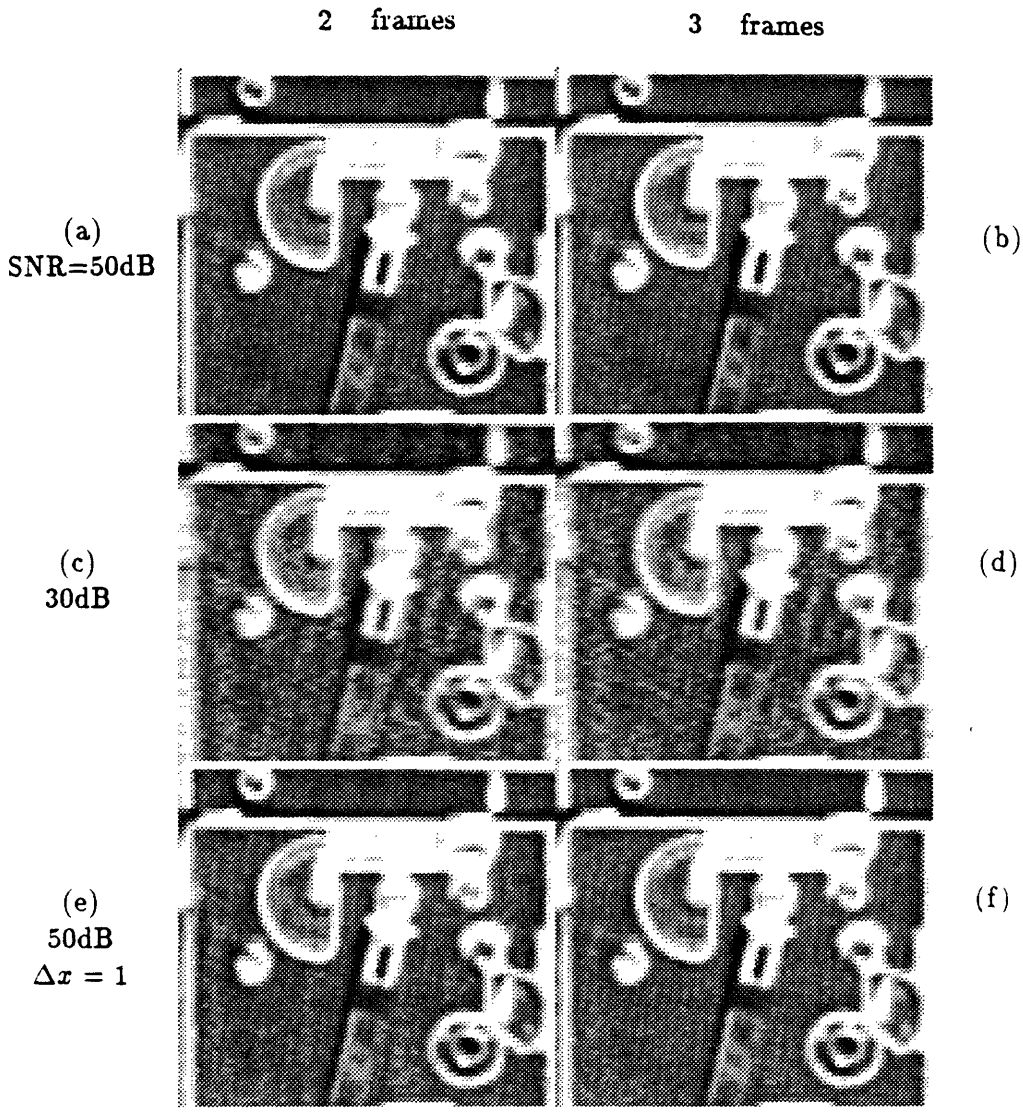

Figure 5.18: Interregion reconstruction of background surface when $v_b/v_e < 1$. $v_bT = 11$, $v_eT = -8$. (left) using two frames; (right) using three frames.
(a-d) continuous observation;
(e-f) discrete observation, $\Delta x = 1$.

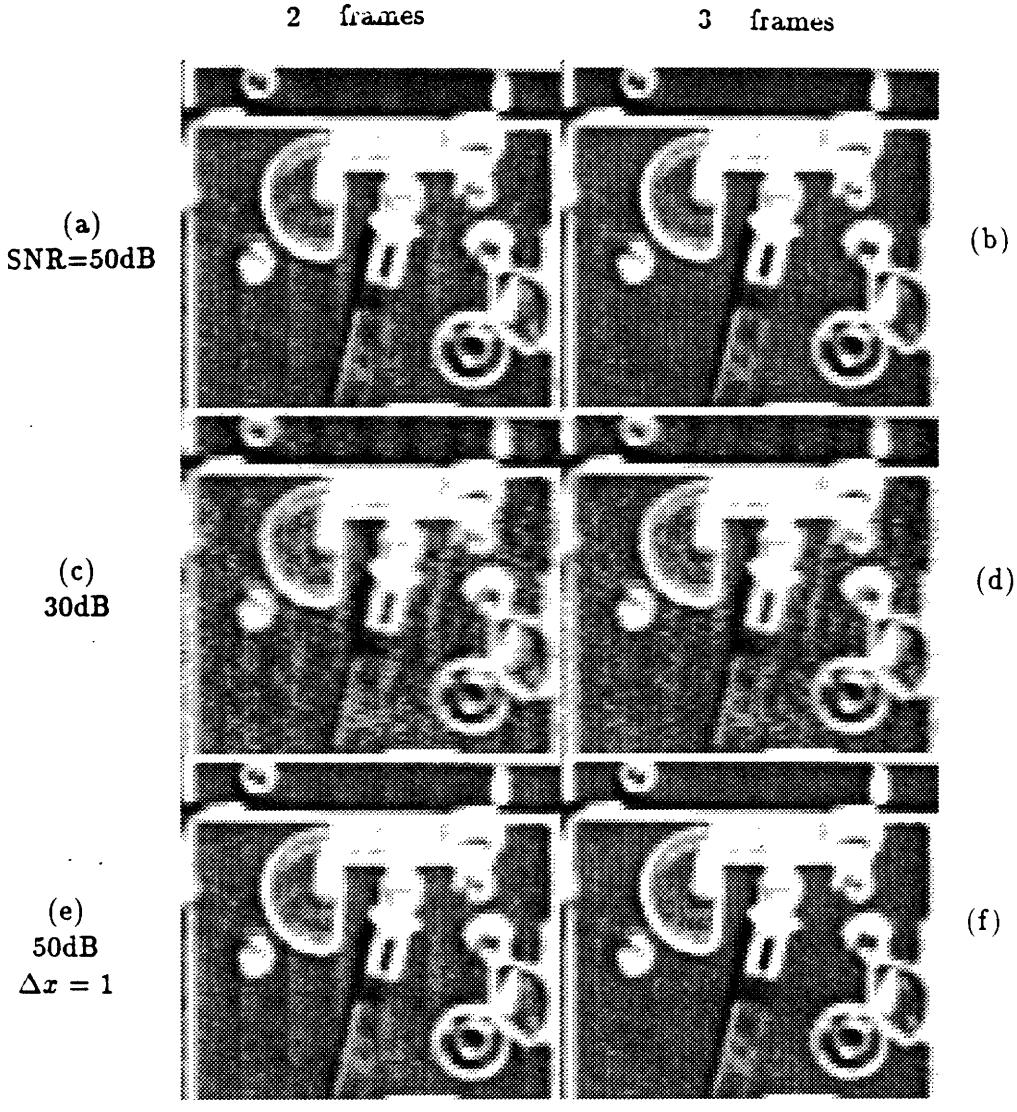

Figure 5.19: Interregion reconstruction of background surface when $v_b/v_e > 1$. $v_bT = 11$, $v_eT = 8$. (left) using two frames; (right) using three frames.
(a-d) continuous observation;
(e-f) discrete observation, $\Delta x = 1$.

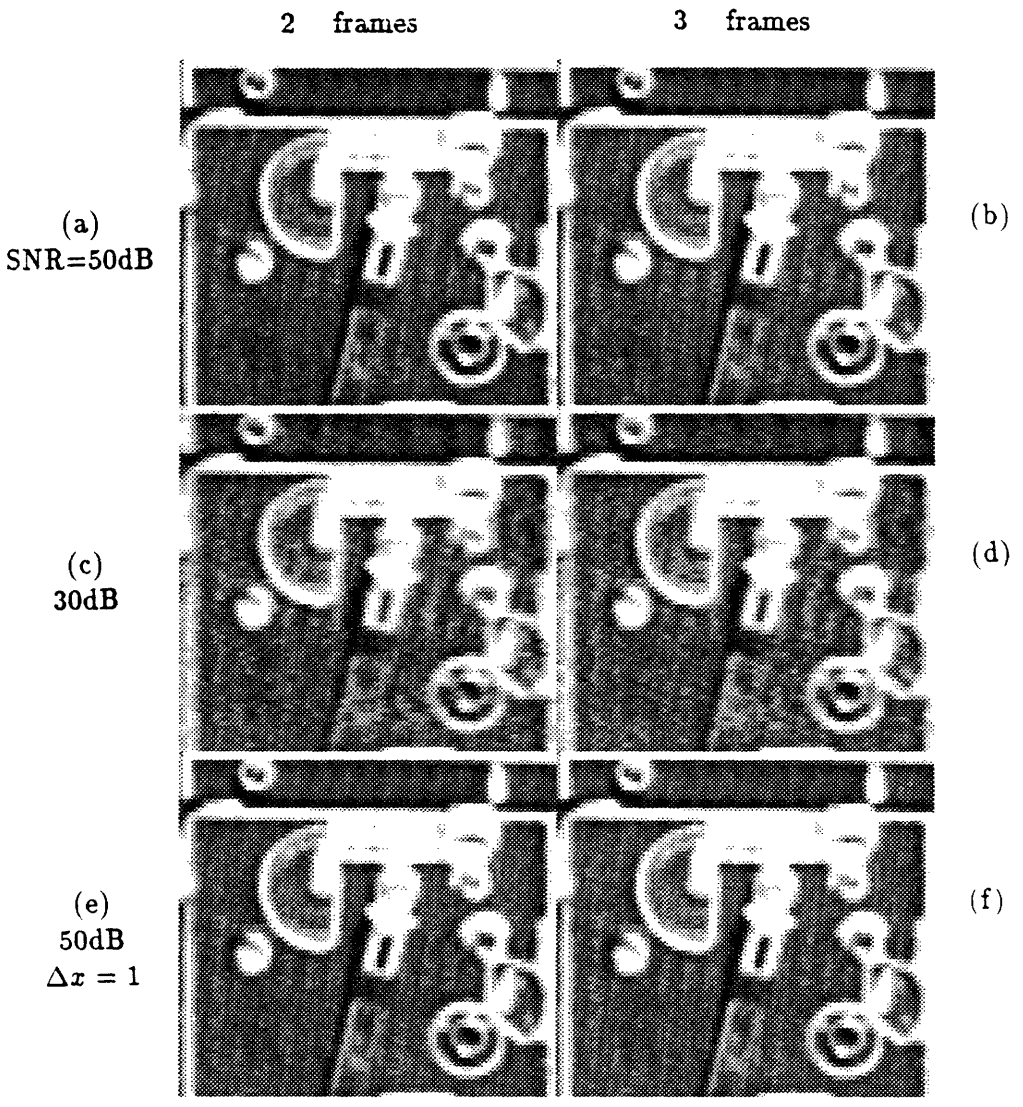

Figure 5.20: Interregion reconstruction of background surface when v_b/v_e is a ratio of small integers. $v_bT = 11$, $v_eT = 16.5$. (left) using two frames; (right) using three frames.
(a-d) continuous observation;
(e-f) discrete observation, $\Delta x = 1$.

5.4.5 Review

- The performance characteristics of Wiener estimation are fairly insensitive to the prior signal spectrum but highly dependent on the SNR of the observation.
- For any fixed SNR level and number of frames, intraregion reconstruction using frames with different blurs offers the best potential MSE reduction, but results could vary greatly with v_2/v_1.
- High SNR is required to take advantage of constraints between overlapping regions; otherwise, there is no worthwhile improvement over simple intraframe, intraregion reconstruction.
- Specifically, transition zone compensation may be the most reliable way, in theory, to avoid unobservable modes; in practice, however, it is not a panacea for underdeterminacy since noise reduces the quality of the new constraints.
- Interregion processing is potentially comparable to transition zone compensation but the performance also depends on v_b/v_e.

5.5 Discrete Observations

The nullspace theory developed in Chapter 2 and the Wiener filter performance evaluations in the last section both assume that the blurred, noisy frames are recorded as infinite bandwidth, spatially continuous signals. It is of practical importance to determine how much the results change when the observations are discretized. Since the linear system **H** is not shift-invariant, a bandlimited input image does not necessarily produce an equally bandlimited output image. Therefore, it might not be sufficient to spatially sample the frames at the Nyquist rate of the *input*. The following experiments show, however, that it is sufficient in many cases.

Let the sample spacing be Δx. For this discussion, we assume that the presampling filter is a rectangular impulse response of width Δx; in other words, samples $g_c(i\Delta x, t)$, $i = 0, 1, 2, \ldots$, are obtained by averaging non-overlapping cells in the continuous signal $g_c(x, t)$. Because this filter permits aliasing, it is not optimum for subsequent Wiener estimation [Malvar86], but it is convenient and mimics the response of a solid-state imaging array device.

The optimum MSE will be computed as a function of Δx for each of the three classes of reconstruction problems, on a representative set of velocity ratios. Other parameters are unchanged from the previous series of experiments. In particular, the signal spectrum cuts off at π, so that $\Delta x = 1$ corresponds to the Nyquist rate. We continue to define SNR in terms of the noise prior to filtering and sampling.

5.5.1 Intraregion

Performance curves for intraregion reconstruction using one frame blurred by $v_1 T = 11$ and two frames blurred by $v_1 T = 11$ and $v_2 T = 9.6$ are shown in Figure 5.21. If the MSE is relatively poor even when the observation is continuous, discretization has almost no effect. When SNR is at least 40 dB, the performance of the Wiener estimator degrades by 1–2 dB as Δx increases from 0 to 1. As one might expect, the MSE rises sharply when the sample spacing is increased even further; examination of the error variance in the cosine transform domain reveals that the MSE comes to be dominated by inability to estimate high frequencies (Figure 5.22).

A comparison of Figure 5.10e,f with Figure 5.10a,b verifies that sampling at the Nyquist

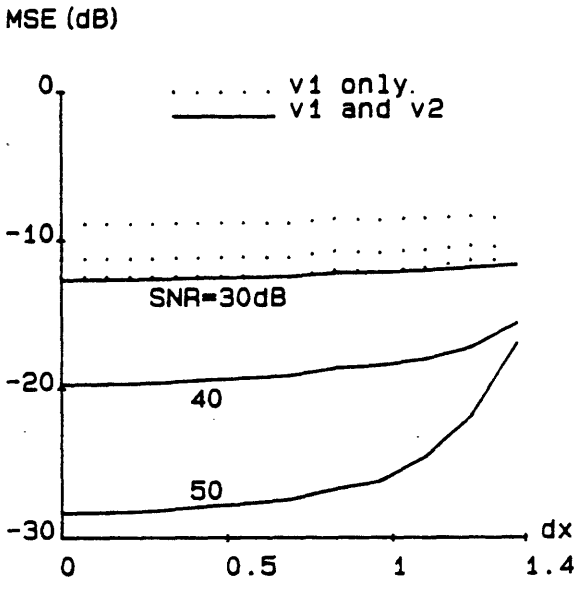

Figure 5.21: MSE of intraregion reconstruction vs. SNR and sample spacing Δx: $L = 88$, $\rho = 0.74$. The Nyquist rate for the input signal is attained at $\Delta x = 1$. $v_1 T = 11$, $v_2 T = 9.6$ are fixed. From top to bottom: SNR=30, 40, 50 dB.
(dotted) reconstruction using single frame of blur $v_1 T$;
(solid) reconstruction using both frames.

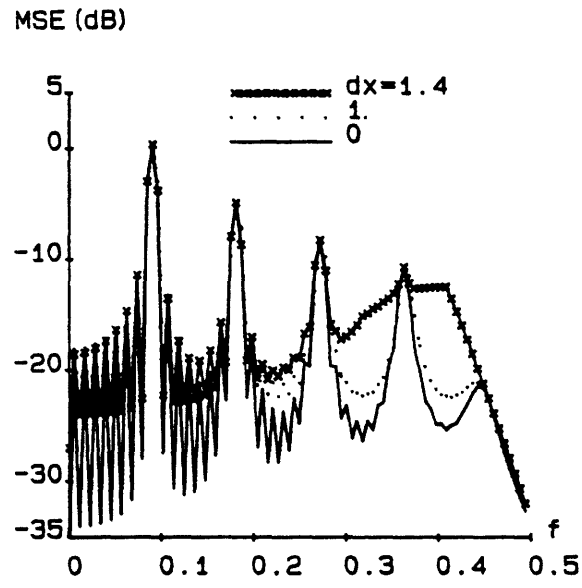

Figure 5.22: Error spectra of intraframe, intraregion reconstruction vs. Δx. $\rho = 0.74$, SNR=50 dB, $vT = 11$, $L = 88$.

rate does not hamper intraregion reconstruction in practice.

5.5.2 Transition Zone Compensation

The velocity of the surface to be restored is fixed at $v_bT = 11$. Three boundary velocities are selected, one from each distinct range of velocity ratios: $v_b/v_e < 0$, $0 < v_b/v_e \leq 1$, and $v_b/v_e > 1$ (Figure 5.23). The previous comments regarding large MSE at $\Delta x = 0$ apply equally well to transition zone compensation.

An exclusive feature of the $v_b/v_e < 0$ case is that performance seems to start degrading well before the Nyquist limit is exceeded, whereas for $v_b/v_e > 0$ the MSE is almost flat up to $\Delta x = 1$. For small values of Δx, most of the error energy resides in signals near $\Pi_0(v_bT)$; the corresponding peaks in the error spectrum seem to increase with Δx in the $v_b/v_e < 0$ case, but not otherwise.

A likely explanation for the preceding behavior is (5.7). Since $\mathbf{H}_{\backslash}$ for $v_b/v_e < 0$ expands the bandwidth of its input, the Nyquist limit on Δx is not longer 1 but some smaller value. An alternative explanation in the signal domain appeals to linear algebra. Theoretically,

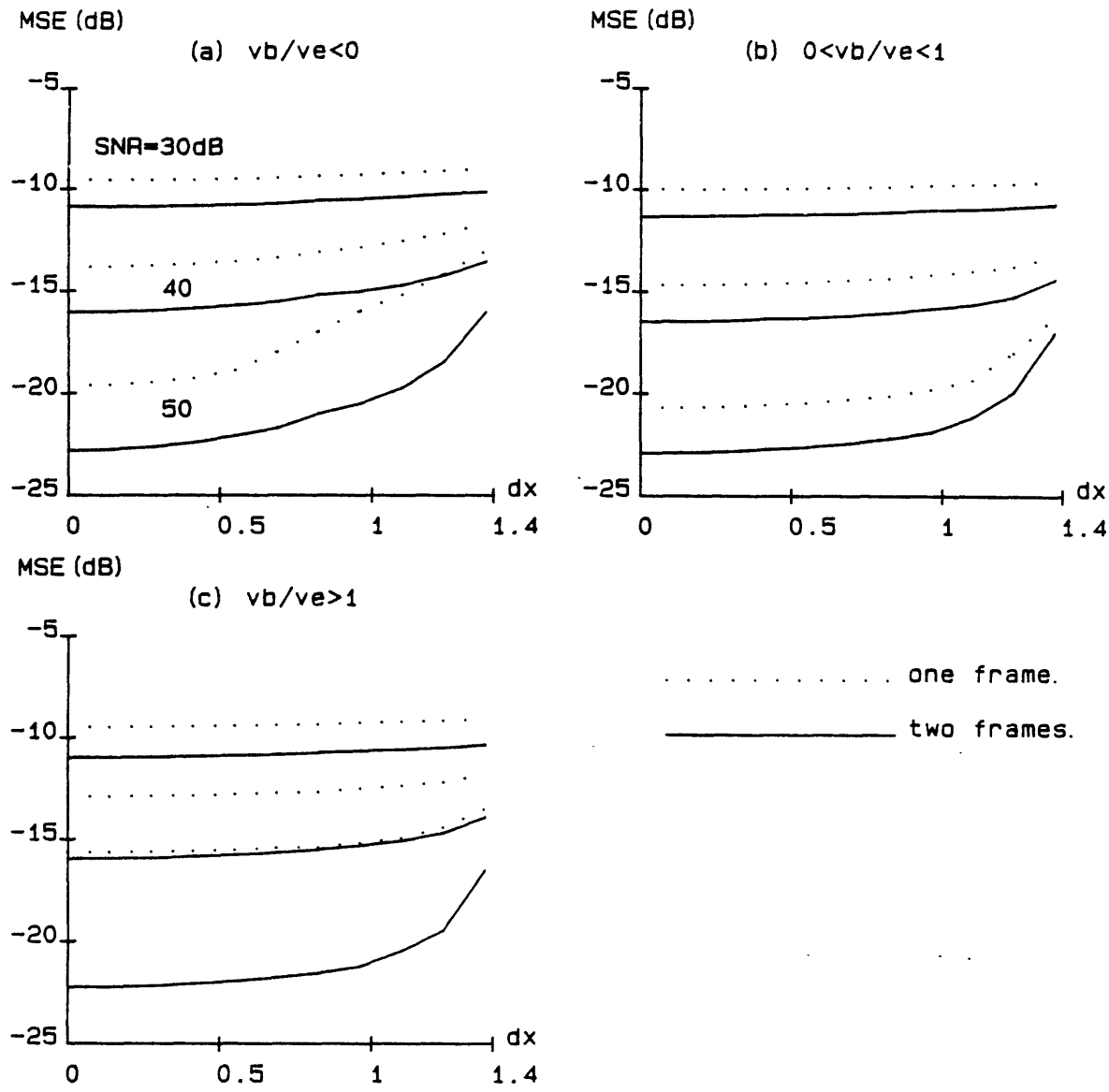

Figure 5.23: MSE of transition zone compensation vs. SNR and sample spacing Δx: $L = 88$, $\rho = 0.74$. The Nyquist rate for the input signal is attained at $\Delta x = 1$. $v_b T = 11$ is fixed; (a) $v_e T = -9.6$; (b) $v_e T = 12.4$; (c) $v_e T = 6.9$; From top to bottom: SNR=30, 40, 50 dB.
(dotted) reconstruction after transition zone compensation in one frame;
(solid) reconstruction after transition zone compensation in two frames.
Note: performance curves for interregion reconstruction using two or three frames are virtually identical, except for 1–2 dB improvement.

$\mathbf{H}_{\backslash}$ has no nullvectors, but (2.8) indicates that its input interval I is larger than its output interval $[0, |v_e T|]$ when $v_b/v_e < 0$. This suggests that the output interval must be sampled at least $1 - v_b/v_e$ more densely than the input interval in order to avoid the underdetermined condition of more unknowns than constraints. Therefore, the MSE ought to begin rising around $1/(1 - v_b/v_e) \approx 0.5$. Finally, this effect is not present when $0 < v_b/v_e < 1$, since I is smaller than the output interval, or when $v_b/v_e > 1$, since $\mathbf{H}_{\angle}$ possesses nullvectors even without discretization.

These performance predictions are borne out in experiments with picture data. Figure 5.16e,f, in which $v_b/v_e > 1$ and observations are sampled at the input signal's Nyquist rate, does not look any better or worse than Figure 5.16a,b, in which the sampling rate is infinite. On the other hand, for $v_b/v_e < 0$, a comparison of Figure 5.15e with Figure 5.15a reveals that discretization has impaired the ability of intraframe transition zone compensation to suppress unobservable modes.

5.5.3 Interregion

Since the qualitative behavior of the optimum MSE with respect to sample spacing is about the same for transition zone compensation and interregion reconstruction, it is unnecessary to show the performance curves. The MSE for interregion reconstruction using 2 (or 3) frames is consistently 1–2 dB better than reconstruction after transition zone compensation in 1 (or 2) frames, reaffirming that prior knowledge of the foreground surface may not be overwhelmingly important. Of course, the velocity combinations selected in these examples do not allow $\Pi_0(\text{gcd}(v_b T, v_e T))$ to be a factor.

The preceding remarks concerning the pictures of transition zone compensation apply as well to interregion reconstruction (Figures 5.18,5.19,5.20e,f). Discretization seems to impair interregion reconstruction in two frames if $v_b/v_e < 1$ and is far from a ratio of small integers, but not otherwise.

5.6 Summary

A standard procedure for estimating a signal from a noisy linear observation is the Wiener filter. This chapter used Wiener estimation to verify the predicted structure of the unobservable subspace, to calculate mean-square-error performance given a random process input, and to evaluate subjective quality for restorations of an actual picture. Experiments were performed for all three prototype reconstruction problems with varying numbers of frames.

Initially it is assumed that blurred frames are recorded as spatially continuous signals. It is found that the variation of MSE as a function of velocity ratio and number of frames can be completely explained by changes in the dimension of the theoretical nullspace, modified for finite bandwidth and nonzero noise. However, the elegance of the theoretical results is not matched by the success of the methods in practice. The value of transition zone information, compensated or not, is rapidly diminished by observation noise. Thus, neither transition zone compensation nor interregion reconstruction has the potential to reduce mean-squared reconstruction error as much as the simpler method of interframe, intraregion reconstruction. At the same time, both intraregion and interregion reconstruction methods deteriorate for unfavorable velocity ratios. In short, constraints obtained by utilizing multiple frames and overlapping surfaces cannot be guaranteed to overcome the basic underdeterminacy of the conventional intraframe, intraregion approach.

Additional experiments show that the performance of Wiener reconstruction from continuous observations is not materially degraded by imposing spatial sampling of the data, as long as the Nyquist rate for the spectrum of the *output* signal is heeded.

Chapter 6

Model Sensitivity and Identification

It has been shown that interframe and interregion constraints can greatly reduce the underdeterminacy of motion-blur restoration, provided that unfavorable velocity ratios do not exist. To some extent, noisy and discretized data do not change the basic behavior of reconstruction. However, a prerequisite for the application of any restoration technique is identification of the image formation system. The linear operator $\mathbf{H}$ encapsulates all scene configuration information and camera properties, including positions and velocities of surfaces and their boundaries, the arrangement of surfaces in depth, and camera integration duration DT. Clearly, many difficult and unsolved problems of scene analysis underlie the automatic identification of $\mathbf{H}$ from an arbitrary image sequence.

This chapter shall focus on boundary position estimation, which is a kind of segmentation problem, and blur estimation, which is related to the motion estimation problem. First, the sensitivity of reconstruction to errors in $\mathbf{H}$ is examined. Then, some approaches for boundary and blur estimation are presented. As usual, only one-dimensional problems are discussed.

The method of linear least squares estimation is carried over from the preceding chapter. The observation is still defined by $\mathbf{g} = \mathbf{H}\mathbf{f} + \mathbf{n}$, but the reconstruction is performed by

$$\hat{\mathbf{f}}(\mathbf{g}) = \left(\hat{\mathbf{H}}^{\mathrm{T}}\mathbf{\Lambda}_n^{-1}\hat{\mathbf{H}} + \mathbf{\Lambda}_f^{-1}\right)^{-1}\hat{\mathbf{H}}^{\mathrm{T}}\mathbf{\Lambda}_n^{-1}\mathbf{g},$$

where $\hat{\mathbf{H}}$ is the estimated system.

The covariance of the estimation error $\hat{\mathbf{f}} - \mathbf{f}$ can be shown to equal

$$\mathbf{P}_1 = \mathbf{P} + \mathbf{AP} + \mathbf{PA}^{\mathrm{T}} + \mathbf{A}\Lambda_f A^{\mathrm{T}},$$

where

$$\begin{aligned} \mathbf{A} &= \mathbf{P}\hat{\mathbf{H}}^{\mathrm{T}}\Lambda_n^{-1}(\hat{\mathbf{H}} - \mathbf{H}) \\ \mathbf{P} &= \left(\hat{\mathbf{H}}^{\mathrm{T}}\Lambda_n^{-1}\hat{\mathbf{H}} + \Lambda_f^{-1}\right)^{-1}. \end{aligned}$$

Note that $\mathbf{P}$ would be the error covariance if the system were actually $\hat{\mathbf{H}}$.

In this chapter, however, computing the MSE as a performance criterion makes less sense than before. For example, if a surface is reconstructed perfectly except for a uniform shift, a large objective error is measured but the subjective quality is unaffected. Furthermore, since errors in $\mathbf{H}$ can produce many qualitatively different reconstruction artifacts, MSE is less likely to correlate well with subjective quality than when the sole source of artifacts is unrecovered nullvectors. Thus, sensitivity analysis is limited to trials with a test picture.

6.1 Effect of Errors in Boundary Position

This section studies the distortions in transition zone compensation and interregion reconstruction when an error is made in estimating the position of the boundary—more precisely, the exact position within the original scene and not just some approximate position somewhere around the transition zone in one of the blurred frames. It is assumed that surface and boundary velocities are known exactly.

An error in boundary position estimation has a far greater effect on the resulting reconstruction than the mere loss or gain of a few samples near the boundary, which by itself might not be too visible. Because the role of the transition zone, compensated or not, is to provide boundary conditions to recover a signal in $\Pi_0(vT)$, reconstruction errors in the zone will be periodically replicated into the rest of the surface. Except for common periodicity, however, the artifacts due to boundary offset are completely different in character from those due to a missing nullvector. It is found that a fractional-sample boundary offset could produce distortions worse than just discarding $\Pi_0(vT)$.

6.1.1 Transition Zone Compensation Artifacts

In the following examples, the boundary is presumed to be rigidly attached to the foreground surface, i.e., $v_e = v_f$, even though this condition is not needed per se to perform transition zone compensation. Once again, the "background" surface is the immediate goal of reconstruction, and the "foreground" is an adjacent surface. A boundary offset leads to distortions in two ways. First, either too much or too little of the foreground surface contribution is subtracted out of the transition zone. Second, $\widehat{\mathbf{H}}$ will be a shifted version of $\mathbf{H}$, but because $\mathbf{H}$ is usually not shift-invariant within the transition zone, the inverse filter designed for $\widehat{\mathbf{H}}$ will not properly deconvolve a signal blurred by $\mathbf{H}$.

Figure 6.1a,c exhibits these effects clearly for offsets of $\epsilon = \pm 0.5$ and velocities $v_b T = 11$, $v_e T = -8$. Ideal boundary estimation permits unique reconstruction via intraframe transition zone compensation, and $N(\mathbf{H})$ is not of concern. The sign of ϵ affects only the polarity of all artifacts but not the apparent magnitude. The residual foreground signal leads to vertical stripes because the mean foreground and background levels are unequal. The vertically periodic component within the stripes comes from the foreground's periodic structure, which is shown in Figure 5.7. Some features of the background surface are

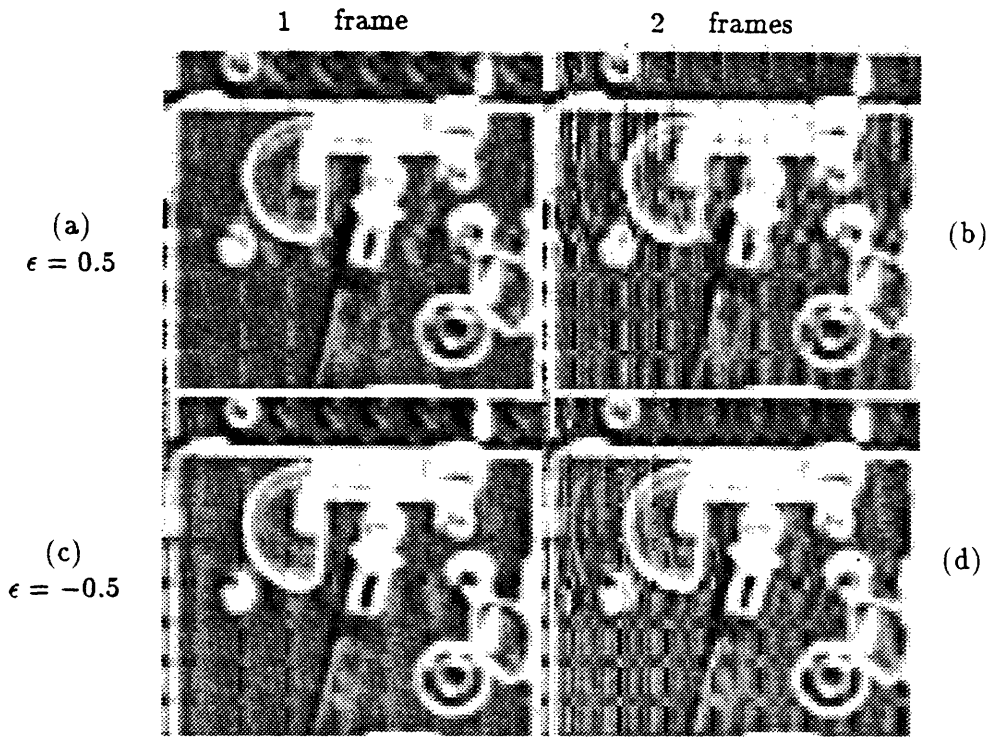

Figure 6.1: Transition zone compensation with segmentation error ϵ when $v_b/v_e < 0$. $v_bT = 11$, $v_eT = -8$. (left) using one frame; (right) using two frames. SNR=50 dB, discrete observation with $\Delta x = 0.25$.
(a,b) boundary skewed toward this surface, $\epsilon = 0.5$;
(c,d) boundary skewed away from this surface, $\epsilon = -0.5$.

periodically replicated, including the small round objects in the upper left and center left, but not the round object in the lower right. Only those details that enter the transition zone by being covered or uncovered during the exposure time can possibly contribute to the artifact. This property is unlike a signal in $\Pi_0(vT)$, which tends to collect details from the entire surface.

Except for possible improved noise suppression, it is unnecessary to perform transition zone compensation with two frames when $v_b/v_e < 0$. In fact, use of the additional frame of information increases reconstruction error in the presence of boundary offset (Figure 6.1b,d). Although the background-induced artifacts originally seen in intraframe transition zone compensation diminish in amplitude, this improvement is more than offset by two effects. First, the area of the background that undergoes occlusion increases, so that more surface details can contribute to the artifact. For example, outlines of the backwards-"D" shaped object are periodically replicated when two frames are used. Another effect is that the same residual foreground signal is added in twice.

The preceding remarks cannot be generalized to all scene configurations. Transition zone compensation with $v_bT = 11$, $v_eT = 8$ behaves quite differently, and not just because signals in $N(\mathbf{H}_\angle) \cap \Pi_0(v_bT)$ are not recovered. For the same boundary offsets as in the previous example, the distortions are qualitatively different and are visibly stronger (Figure 6.2a,c). Leakage from the foreground, plus large amplitude vertical bands induced by the bright vertical stripe on the left edge of the background, are now the dominant distortions. Other background features that enter the transition zone do not appear in the periodic artifact.

Reconstructions using two frames now show improvement over intraframe processing (Figure 6.2b,d). The large reduction in background-induced vertical bands offsets the increase in other distortion components.

Other combinations of velocity ratios have been tested, and the behavior of reconstruction with boundary offset exhibits even more variation than shown by the foregoing examples. A systematic explanation of all artifacts does not exist at this time.

6.1.2 Interregion Reconstruction Artifacts

As long as v_b/v_e is not close to a ratio of small integers, interregion reconstruction using $n+1$ frames has been shown to be comparable to transition zone compensation using n frames. In the presence of boundary offset, in fact, the interregion approach is better. Implicit to

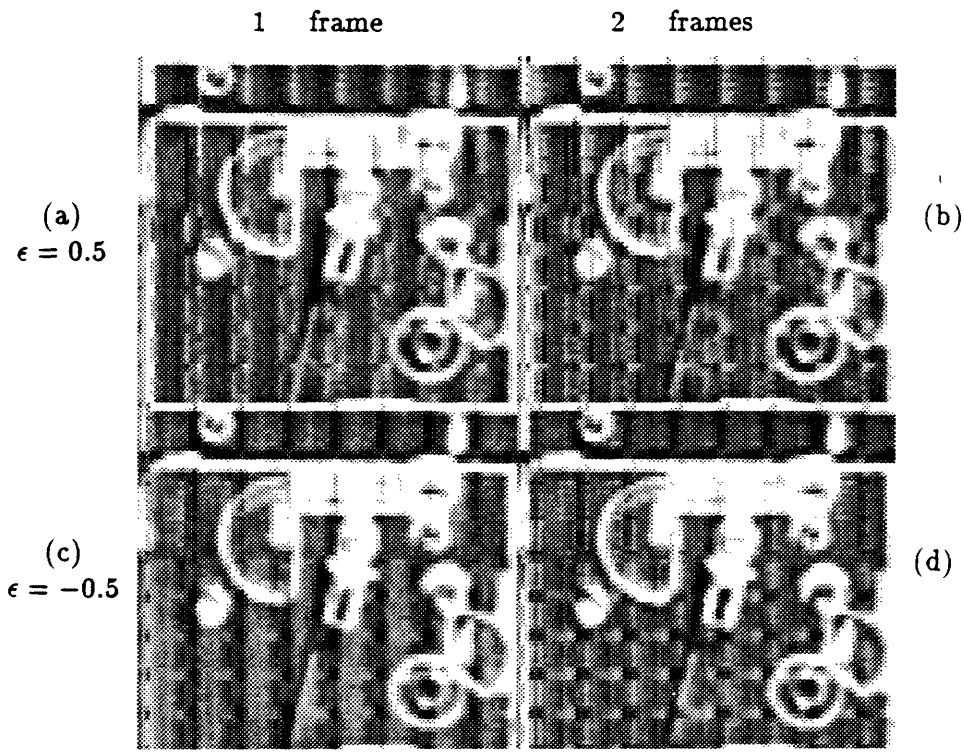

Figure 6.2: Transition zone compensation with segmentation error ϵ when $v_b/v_e > 1$. $v_bT = 11$, $v_eT = 8$. (left) using one frame; (right) using two frames. SNR=50 dB, discrete observation with $\Delta x = 0.25$.
(a,b) boundary skewed toward this surface, $\epsilon = 0.5$;
(c,d) boundary skewed away from this surface, $\epsilon = -0.5$.

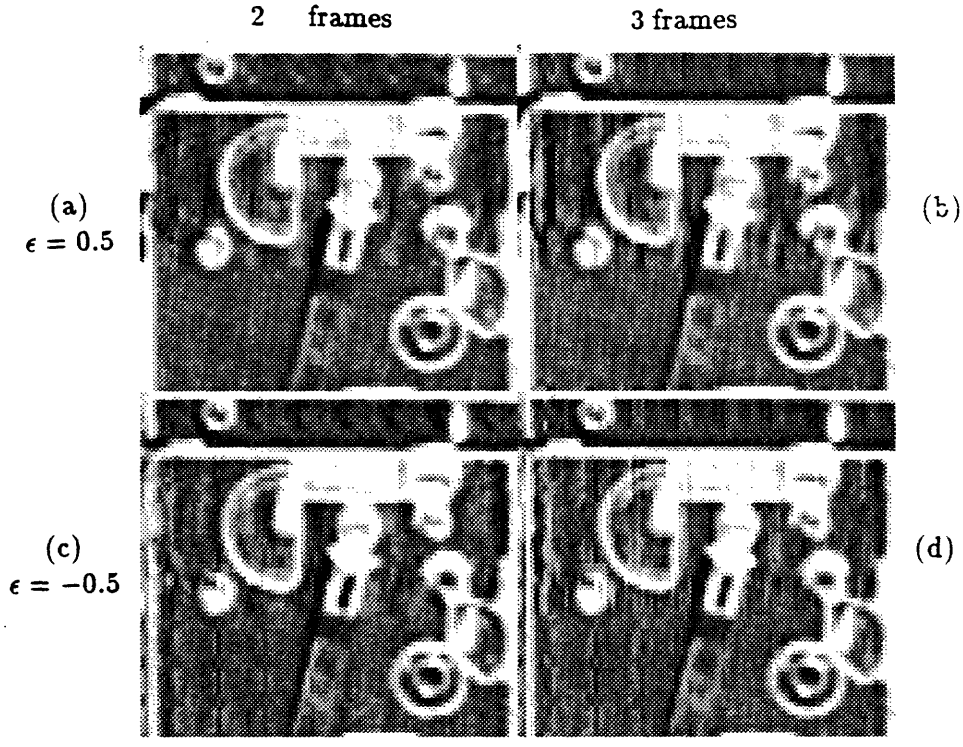

Figure 6.3: Interregion reconstruction with segmentation error ϵ when $v_b/v_e < 0$. $v_bT = 11$, $v_eT = -8$. (left) using two frames; (right) using three frames. SNR=50 dB, discrete observation with $\Delta x = 0.25$.
(a,b) boundary skewed toward this surface, $\epsilon = 0.5$;
(c,d) boundary skewed away from this surface, $\epsilon = -0.5$.

the process of interregion reconstruction is cancellation of the foreground contribution by subtracting displaced frames, which works without regard to the position of the boundary. Therefore, the telltale vertically periodic structure of the foreground is totally absent in the reconstruction when $\epsilon > 0$ (Figure 6.3a,b, Figure 6.4a,b), and is muted when $\epsilon < 0$ (Figure 6.3c,d, Figure 6.4c,d). The primary source of distortion is improper deconvolution, creating replicas of background surface features.

6.1.3 Sensitivity

So far the consequences of boundary offset have been discussed qualitatively for a fixed value of ϵ and SNR. To give some idea of the sensitivity at 50 dB SNR, ϵ is varied over the range ± 1 for interregion reconstruction using two frames. The background velocity is $v_bT = 11$.

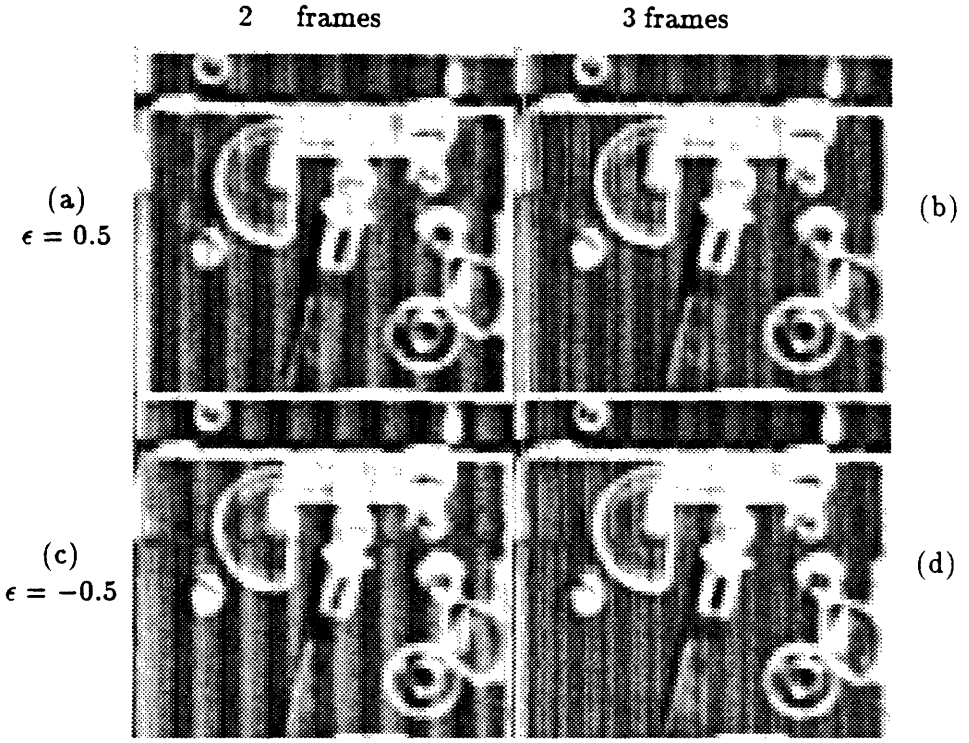

Figure 6.4: Interregion reconstruction with segmentation error ϵ when $v_b/v_e > 1$. $v_bT = 11$, $v_eT = 8$. (left) using two frames; (right) using three frames. SNR=50 dB, discrete observation with $\Delta x = 0.25$.
(a,b) boundary skewed toward this surface, $\epsilon = 0.5$;
(c,d) boundary skewed away from this surface, $\epsilon = -0.5$.

For $v_eT = -8$, an offset of ± 0.5 yields a reconstruction subjectively comparable to that of intraframe, intraregion processing (Figure 6.5). For $v_eT = 8$, an offset of just ± 0.25 suffices for the same level of impairment (Figure 6.6). At 30 dB SNR the sensitivity is lower, for several reasons (Figure 6.7, Figure 6.8). The amplified observation noise and residual unobservable modes tend to mask artifacts due to boundary offset. More importantly, the reconstruction procedure does not attempt to produce the sharpest possible picture and is therefore less sensitive.

The exact tolerance for boundary offset depends on SNR, surface velocities, and picture content, but an error of never more than one Nyquist sample spacing is permissible. Otherwise, it will be counterproductive to utilize boundary conditions from the transition zone.

Since the artifacts described in this section were computed by a Wiener reconstruction procedure, a relevant question is whether they are intrinsic effects of boundary offset or products of the specific reconstruction procedure. Like the pseudoinverse, the Wiener estimator does not effectively recover any signal in $N(\hat{\mathbf{H}})$, so the artifacts must lie in $N(\hat{\mathbf{H}})^{\perp}$. On the other hand, any low-bias estimator relying more on transition zone constraints than on a priori signal information should compute nearly the same signal in $N(\hat{\mathbf{H}})^{\perp}$, though its estimate of the signal in $N(\hat{\mathbf{H}})$ could well be different. Adding a signal in $N(\hat{\mathbf{H}})$ might create new distortions but cannot cancel out distortions in $N(\hat{\mathbf{H}})^{\perp}$. This argument suggests that the high sensitivity to boundary position offset is intrinsic to reconstructions via transition zone compensation or interregion processing.

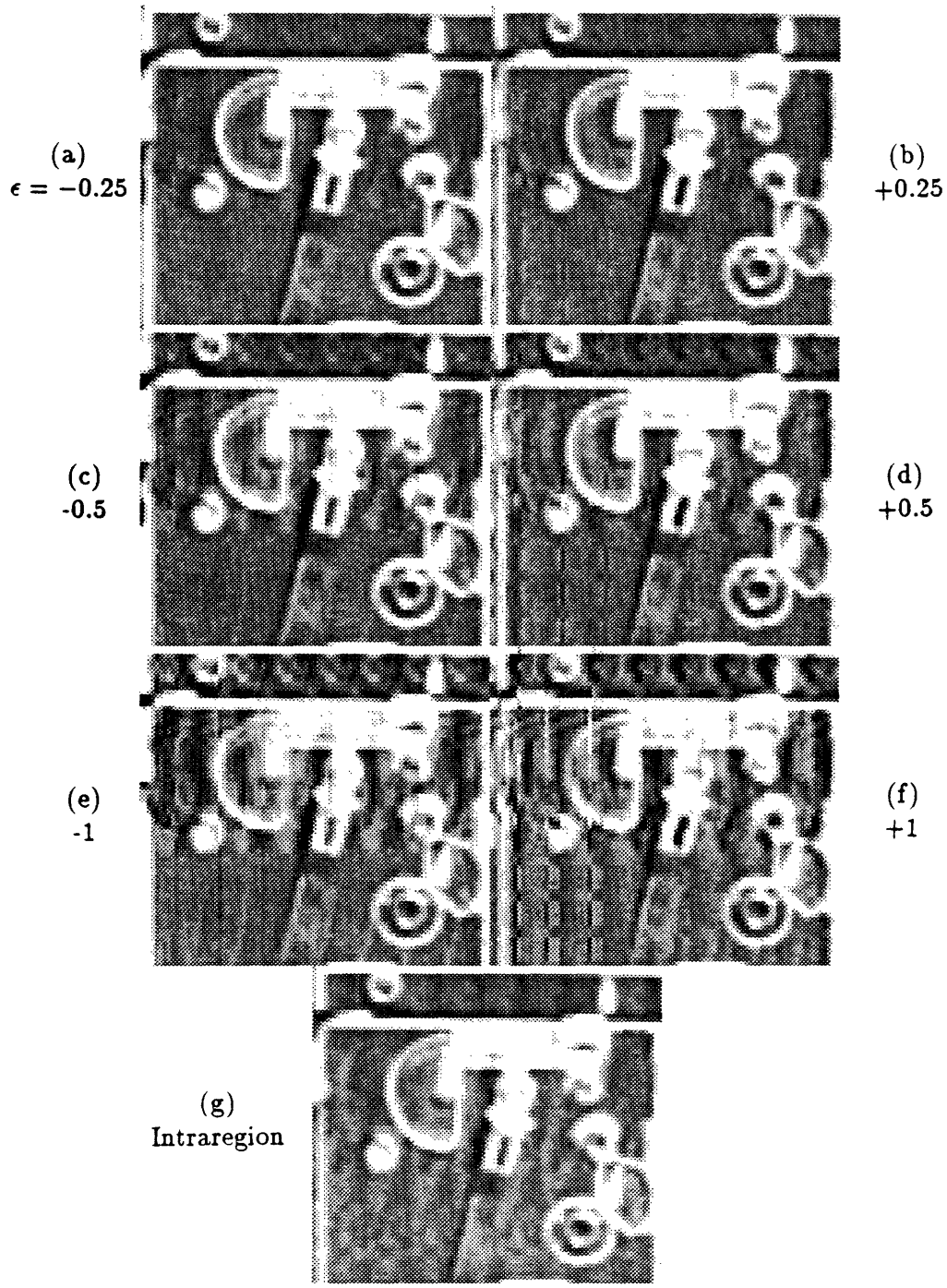

Figure 6.5: Artifacts of interregion reconstruction vs. ϵ when $v_b/v_e < 0$. Two frames, $v_bT = 11$, $v_eT = -8$, SNR=50 dB, discrete observation with $\Delta x = 0.25$. (a-f) Interregion reconstructions; (g) Intraframe, intraregion reconstruction for comparison.

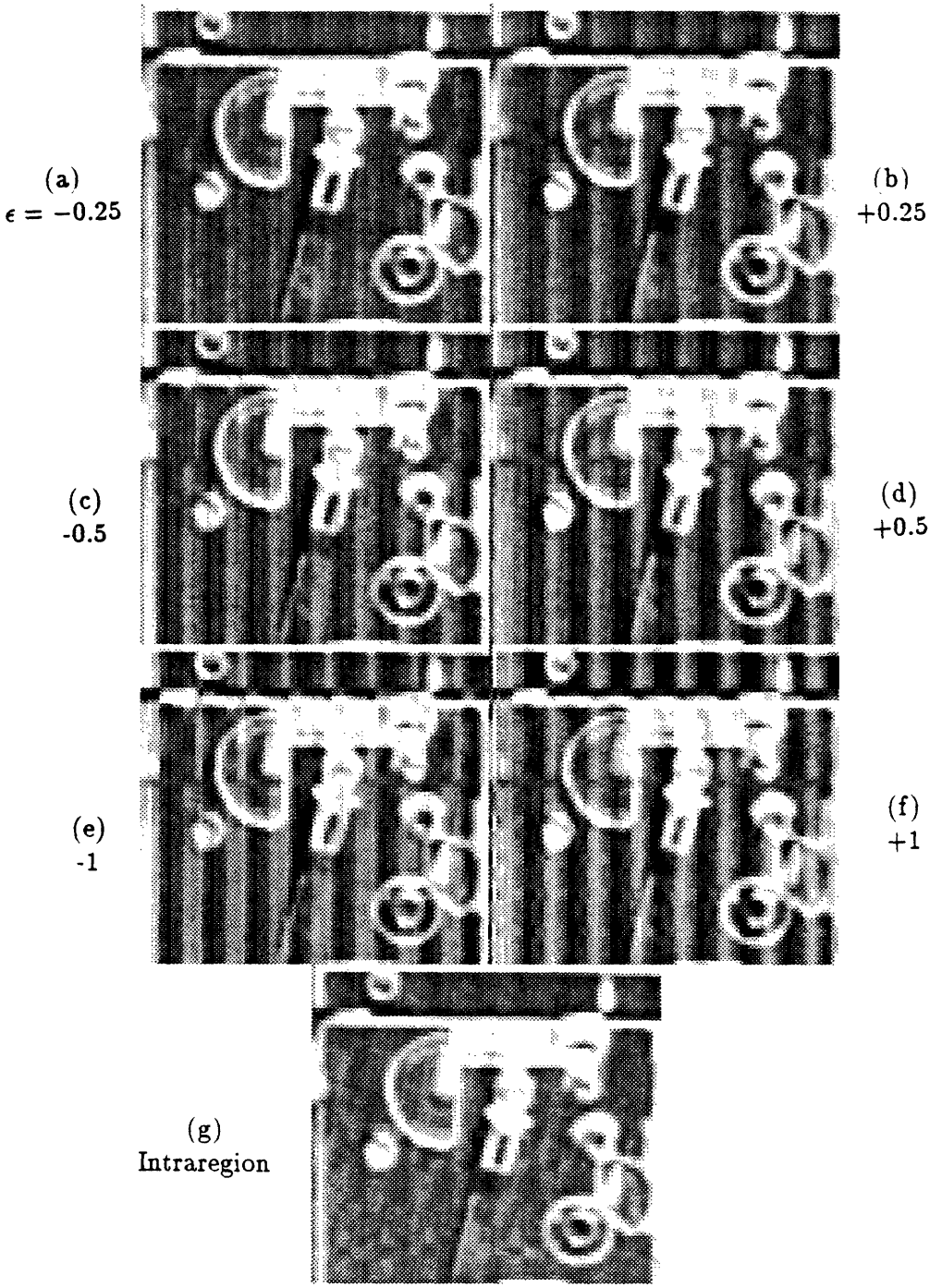

Figure 6.6: Artifacts of interregion reconstruction vs. ϵ when $v_b/v_e > 1$. Two frames, $v_bT = 11$, $v_eT = 8$, SNR=50 dB, discrete observation with $\Delta x = 0.25$. (a-f) Interregion reconstructions; (g) Intraframe, intraregion reconstruction for comparison.

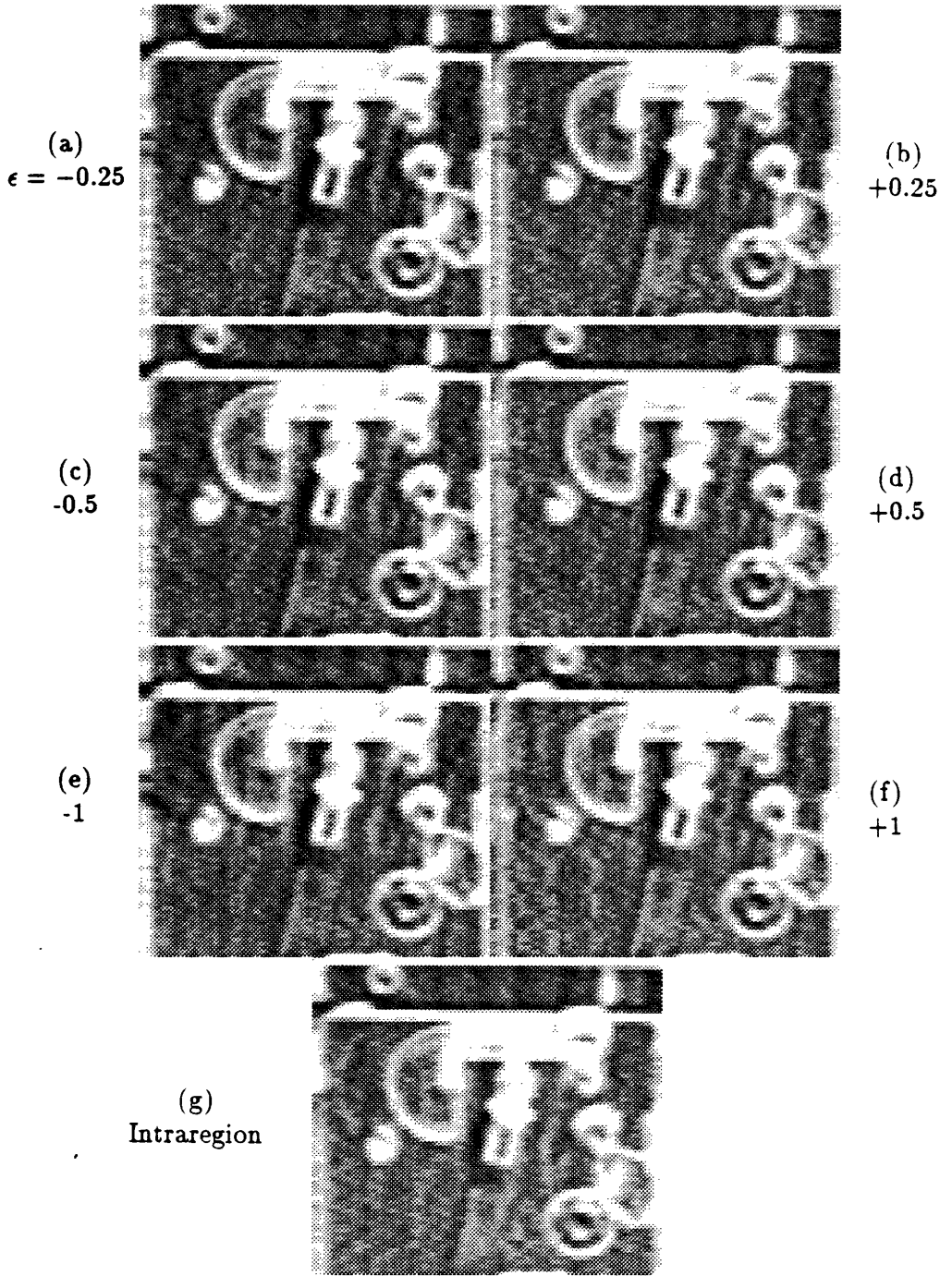

Figure 6.7: Artifacts of interregion reconstruction vs. ϵ when $v_b/v_e < 0$, moderate noise. Two frames, $v_bT = 11$, $v_eT = -8$, SNR=30 dB. discrete observation with $\Delta x = 0.25$. (a-f) Interregion reconstructions; (g) Intraframe, intraregion reconstruction for comparison.

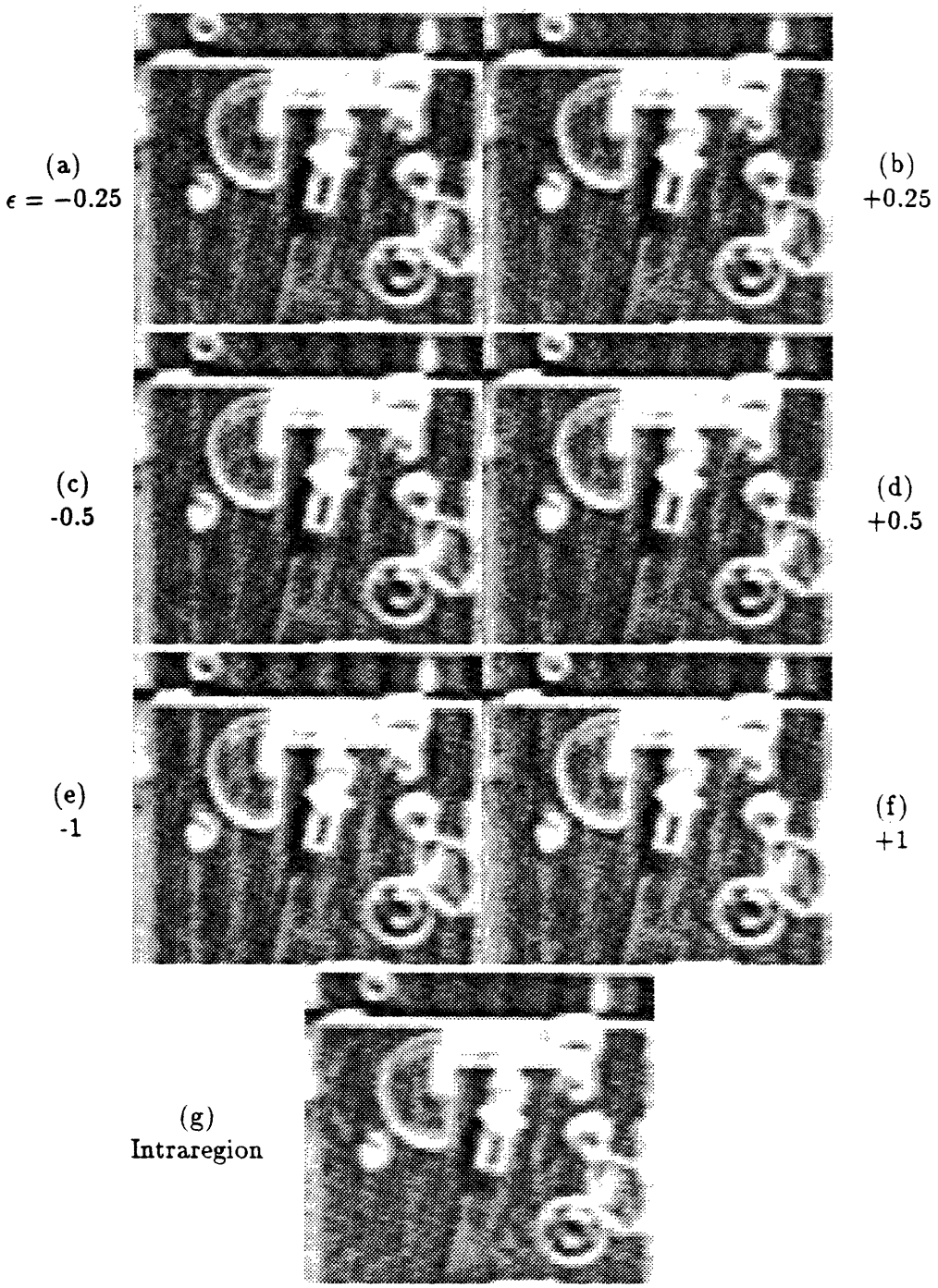

Figure 6.8: Artifacts of interregion reconstruction vs. ϵ when $v_b/v_e > 1$, moderate noise. Two frames, $v_bT = 11$, $v_eT = 8$, SNR=30 dB. discrete observation with $\Delta x = 0.25$. (a-f) Interregion reconstructions; (g) Intraframe, intraregion reconstruction for comparison.

6.2 Effect of Errors in Blur Impulse Response

This section briefly examines the distortions in intraregion reconstruction when an error is made in estimating the amount of motion blur. An investigation of corresponding distortions during transition zone compensation and interregion processing has not been carried out. It is speculated that boundary conditions cannot mitigate problems of mis-deconvolution since they mainly serve to fill in the unobservable subspace. Also, wrong information about the foreground surface blur could cause incomplete removal of the foreground contribution from the transition zone. These are subjects for further study.

A blur estimate is not tantamount to a displacement estimate. Both are functions of the trajectory of surface points over time, but blur is the distance moved during the exposure of one frame, and displacement, in conventional parlance, is the distance moved between frames. During constant acceleration, for example, the blur of one frame is approximately the average of the displacements to the previous and next frames. In addition, blur is proportionally reduced when camera integration is less than 100% duty cycle. Both estimates are needed to construct $\hat{\mathbf{H}}$, since blur gives the magnitude and extent of the impulse response, while displacement establishes registration between images of one surface among a set of frames.

In the Fourier transform domain it is easy to predict the basic structure of the distortion caused by incorrect blur estimates. If the actual and estimated blurs, vT and $\hat{v}T$, are unequal then the zeros of $\hat{H}(\omega)$ are not aligned with those of $H(\omega)$. The reconstruction system will give excessively high amplification to frequencies near $\omega = \frac{2\pi}{\hat{v}T}, \frac{4\pi}{\hat{v}T}, \ldots$; consequently, unnatural components of period $\hat{v}T$ will appear in the restored image [Wetta80].

Figure 6.9a,c,e illustrates the growth of this artifact for fixed $vT = 11$ as $\hat{v}/v$ is increased from unity in intraframe reconstruction. As seen previously, the only artifact in the $\hat{v}/v$ restoration is due to absence of $\Pi_0(vT)$. When blur is overestimated, the periodic artifact not only becomes larger in amplitude but also changes to a different repeating pattern.

These distortions are reduced by combining multiple frames of relatively prime velocities, because the reconstruction filter is able to fully restore signals near $\omega = \frac{2\pi}{\hat{v}T}, \frac{4\pi}{\hat{v}T}, \ldots$ using less amplification [Ghiglia84]. Figure 6.9b,d,f shows the significant improvement using two frames, provided that registration is perfect.

Perfect registration in the presence of skewed blur estimates implies that blur and dis-

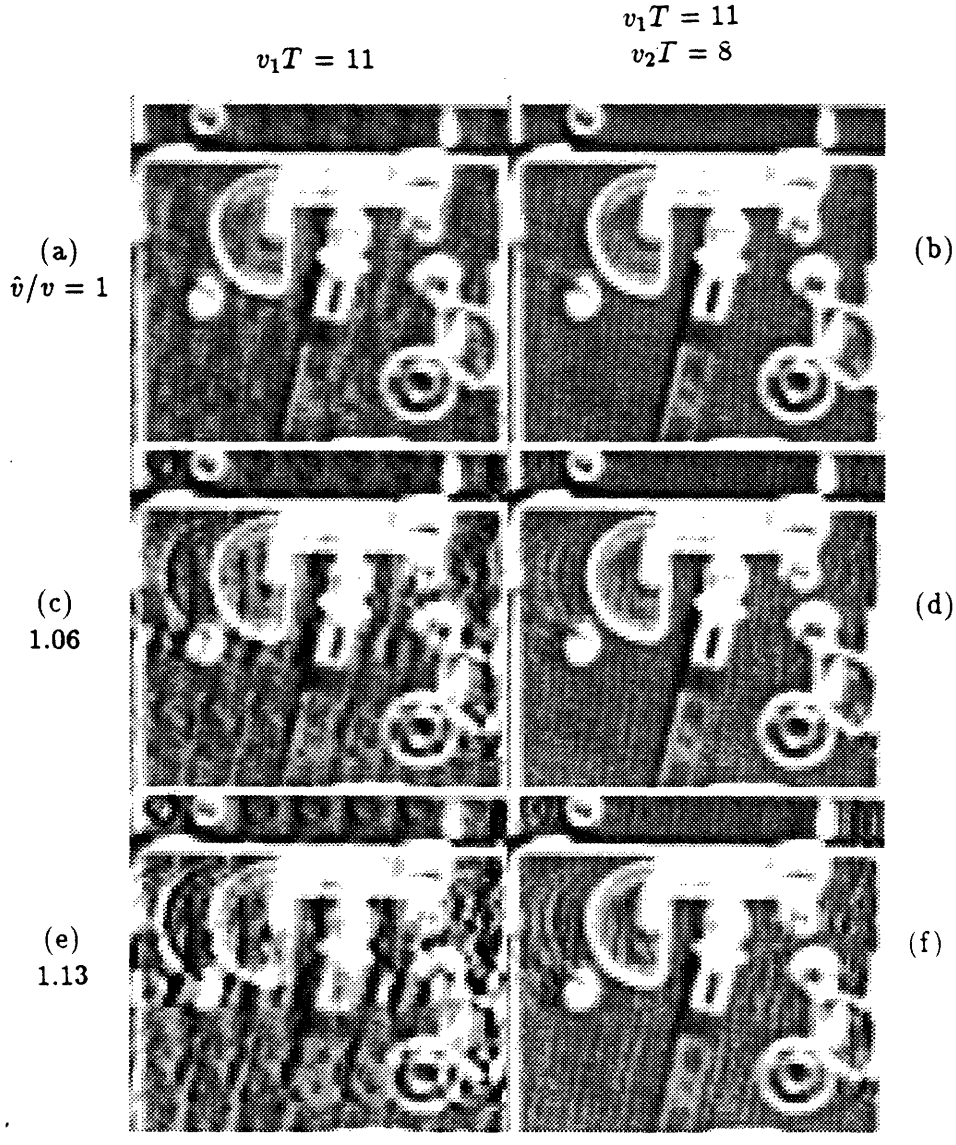

Figure 6.9: Artifacts of intraregion reconstruction with blur estimation error and ideal registration. SNR=50 dB, continuous observation. (left) using one frame, $v_1T = 11$; (right) using two frames, $v_1T = 11$, $v_2T = 8$.

placement estimation are performed independently. Logically, however, both quantities should be derived from a common estimate of the complete motion flow. When blur and displacement estimates are multiplied by the same error factor, the reconstruction deteriorates (Figure 6.10). Fortunately, an experiment using the same amount of misregistration along with ideal blur estimates suggests that the effects of blur and displacement errors combine linearly without much interaction. Thus, the two effects may be studied separately, if desired. There is no intention to present a full account of misregistration effects here, but one important fact should be recognized: the problem with a shifted frame is not loss of sharpness—the usual effect—but, rather, novel distortions.

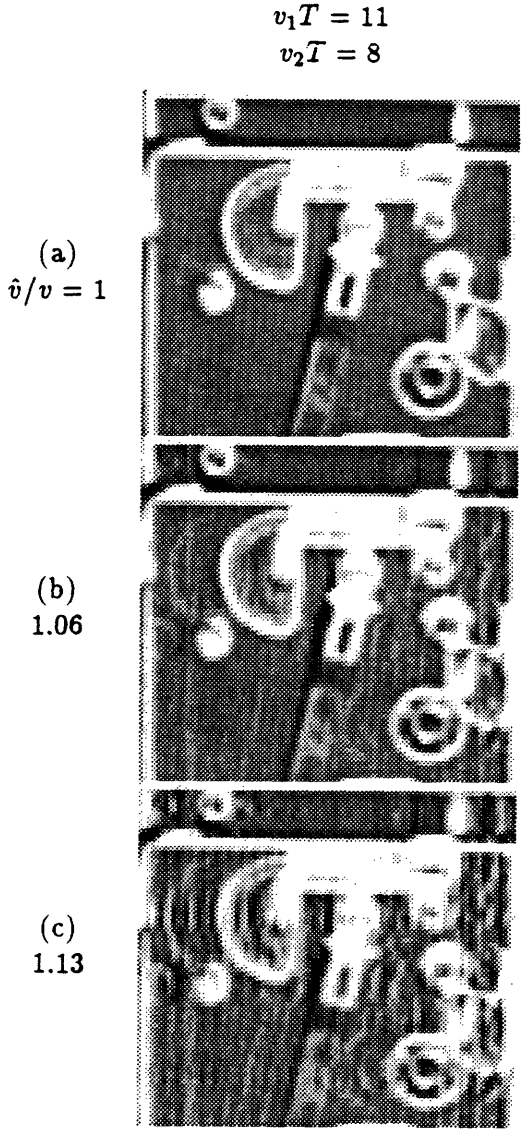

Figure 6.10: Artifacts of intraregion reconstruction with both blur estimation and registration errors. SNR=50 dB, continuous observation. Two frames, $v_1T = 11$, $v_2T = 8$.

6.3 Model-based Boundary Estimation

It is unlikely that the exact boundary position within the original scene can be determined to sufficient accuracy by conventional motion-based segmentation techniques, which are not specifically designed to handle blurred transition zones. This section examines general model-based system identification procedures which may be suitable for either boundary or blur estimation. If uncertainty in the system is limited to a few unknown parameters, they can be determined by minimizing a suitable cost function. When this approach is applied to boundary estimation, the result is more than accurate enough to achieve artifact-free image reconstruction.

6.3.1 General Approach

The blurred image sequence is a linear function of the unknown input signal $\mathbf{f}$ and a non-linear function of the unknown scene configuration parameters θ, plus additive noise:

$$\mathbf{g} = \mathbf{H}_\theta \mathbf{f} + \mathbf{n}.$$

$\mathbf{f}$ and θ might be jointly estimated from the data by minimizing a cost function of the form

$$J_\Sigma(\mathbf{f}, \theta | \mathbf{g}) = J(\mathbf{f}) + \mathcal{D}(\mathbf{g}, \mathbf{H}_\theta \mathbf{f}).$$

The "badness" of $\mathbf{f}$ is measured by $J(\mathbf{f})$, examples of which were presented in §1.2 as criteria for resolving underdeterminacy. $\mathcal{D}(\mathbf{g}, \mathbf{H}_\theta \mathbf{f})$ measures the discrepancy between actual data and the predicted data. Another term $J(\theta)$ could be added, but there is usually no a priori basis to favor one scene configuration over another. Joint minimization with respect to $\mathbf{f}$ and θ is equivalent to

$$\min_\theta J_\Sigma(\hat{\mathbf{f}}(\mathbf{g}|\theta), \theta | \mathbf{g}), \quad \hat{\mathbf{f}}(\mathbf{g}|\theta) = \arg\min_{\mathbf{f}} J_\Sigma(\mathbf{f}, \theta | \mathbf{g}). \tag{6.1}$$

The best cost function for signal reconstruction, on the other hand, might not be the best criterion for boundary estimation. An alternative approach could be the hybrid rule

$$\min_\theta J_\Sigma(\hat{\mathbf{f}}(\mathbf{g}|\theta), \theta | \mathbf{g}), \quad \hat{\mathbf{f}}(\mathbf{g}|\theta) = \arg\min_{\mathbf{f}} J'_\Sigma(\mathbf{f}, \theta | \mathbf{g}), \tag{6.2}$$

where J_Σ and J'_Σ are not necessarily related. For example, subjective image quality is maximized if $J_\Sigma = J_{\text{human}}$. A human experimenter with access to a fixed signal reconstruction algorithm based on J'_Σ could find a good reconstruction by manually adjusting θ to maximize $J_{\text{human}}(\hat{\mathbf{f}})$, producing $\hat{\theta}$ as a by-product.

To apply method (6.1) or (6.2), a straightforward procedure is to compute $\hat{\mathbf{f}}(\mathbf{g}|\theta)$ for many values of θ and then keep the one with minimum cost as the best signal estimate. Search strategies for multidimensional θ include minimization with respect to one variable at a time and gradient methods. One-dimensional techniques include variations of Newton's method and Golden section search. A different and potentially useful approach is joint optimization of $J_\Sigma(\mathbf{f}, \theta|\mathbf{g})$ by alternately minimizing with respect to the linear signal $\mathbf{f}$ and with respect to the nonlinear parameters θ. Implementation issues, however, have been de-emphasized in this research and will not be discussed further.

A natural candidate for J_Σ is the linear least squares cost function

$$J_\Sigma(\mathbf{f}, \theta|\mathbf{g}) = \mathbf{f}^{\mathrm{T}}\mathbf{\Lambda}_f^{-1}\mathbf{f} + \|\mathbf{g} - \mathbf{H}_\theta\mathbf{f}\|^2. \tag{6.3}$$

This is just (5.4) with the dependency of $\mathbf{H}$ on θ made explicit. (In this section it is understood that norms and orthogonality of signals in the observation space are defined with inner product $\mathbf{x}^{\mathrm{T}}\mathbf{\Lambda}_n^{-1}\mathbf{y}$.) By substituting the Wiener solution (5.2) for $\hat{\mathbf{f}}(\mathbf{g}|\theta)$ into (6.3), it is found that

$$\min_{\theta,\mathbf{f}} J_\Sigma(\mathbf{f}, \theta|\mathbf{g}) = \min_\theta \mathbf{g}^{\mathrm{T}}\mathbf{\Lambda}_n^{-1}(\mathbf{g} - \mathbf{H}_\theta\hat{\mathbf{f}}(\mathbf{g}|\theta)) \tag{6.4}$$

$$= \min_\theta \mathbf{g}^{\mathrm{T}}\left(\mathbf{H}_\theta\mathbf{\Lambda}_f\mathbf{H}_\theta{}^{\mathrm{T}} + \mathbf{\Lambda}_n\right)^{-1}\mathbf{g}. \tag{6.5}$$

As $\mathbf{\Lambda}_f^{-1} \to 0$, that is, the a priori uncertainty in $\mathbf{f}$ approaches infinity, the cost function (6.3) depends predominantly on the norm of the residual $\mathbf{g} - \mathbf{H}_\theta\hat{\mathbf{f}}$. The minimum cost with respect to $\mathbf{f}$ is achieved by the pseudoinverse estimate, and the resulting residual is the projection of $\mathbf{g}$ onto $R(\mathbf{H}_\theta)^\perp$, the orthogonal complement of the range space of $\mathbf{H}_\theta$. Therefore, (6.4) becomes

$$\min_{\theta,\mathbf{f}} J_\Sigma(\mathbf{f}, \theta|\mathbf{g}) = \min_\theta \left\|\mathbf{g}/R(\mathbf{H}_\theta)^\perp\right\|^2, \tag{6.6}$$

where / denotes projection onto a subspace. Ignoring noise for the moment, this estimation criterion makes sense because $\mathbf{g}/R(\mathbf{H}_\theta)^\perp$ is guaranteed to be zero, irrespective of $\mathbf{f}$, when θ is set to the correct parameter value and is typically nonzero when θ is set incorrectly. From (6.6) it appears that the scene configuration is estimated first, and afterwards the signal $\mathbf{f}$ is reconstructed once using the best $\hat{\theta}$. However, $\mathbf{g}/R(\mathbf{H}_\theta)^\perp$ is usually no easier to compute than the Wiener estimate, so this simpler looking method is not more efficient.

If a Bayesian viewpoint is desired, the foregoing cost functions can be related to likelihood functions. When $\mathbf{f}$ and $\mathbf{n}$ are independent zero-mean Gaussian random vectors and θ is a nonrandom parameter, the rule for joint MAP/ML estimation of $\mathbf{f}$ and θ is

$$\max_{\theta,\mathbf{f}} p(\mathbf{g}|\mathbf{f},\theta)p(\mathbf{f}),$$

which leads directly to (6.3) and (6.4). ML estimation of θ alone is given by

$$\begin{aligned} & \max_{\theta} p(\mathbf{g}|\theta) \\ \Leftrightarrow \quad & \min_{\theta} \mathbf{g}^{\mathrm{T}} \mathbf{\Lambda}_{\mathbf{g}|\theta}^{-1} \mathbf{g} + \log\det \mathbf{\Lambda}_{\mathbf{g}|\theta}, \quad \mathbf{\Lambda}_{\mathbf{g}|\theta} = \mathbf{H}_\theta \mathbf{\Lambda}_f \mathbf{H}_\theta{}^{\mathrm{T}} + \mathbf{\Lambda}_n. \end{aligned}$$

This is just (6.5) plus a bias term depending only on θ. Finally, if both $\mathbf{f}$ and θ are considered to be nonrandom, the joint ML estimate of $\mathbf{f}$ and θ is given by

$$\max_{\theta,\mathbf{f}} p(\mathbf{g}|\mathbf{f},\theta),$$

which leads directly to (6.6). As in Chapter 5, of course, it is not necessary to believe in the Gaussian assumption in order to make use of these cost functions.

There are many alternatives to $J(\mathbf{f}) = \mathbf{f}^{\mathrm{T}} \mathbf{\Lambda}_f^{-1} \mathbf{f}$ for the signal model component of cost function J_Σ. But minimization of $J(\mathbf{f}) + \|\mathbf{g} - \mathbf{H}_\theta \mathbf{f}\|^2$ with respect to $\mathbf{f}$ is not straightforward unless $J(\mathbf{f})$ is quadratic in $\mathbf{f}$. Therefore, a suggested hybrid method is to choose any desired $J_\Sigma(\hat{\mathbf{f}})$ in (6.2), but to retain Wiener estimation for $\hat{\mathbf{f}}(\mathbf{g}|\theta)$. There is no theoretical justification for this approach, and only experimentation can assess its merits.

6.3.2 Experiments

The performance of boundary estimation by a wide assortment of cost functions is tested on the scene configuration of interregion reconstruction in two frames. Assuming known surface and boundary velocities, the only unknown aspect of $\mathbf{H}_\theta$ is the position of the boundary; moreover, if the approximate position is already known via a conventional segmentation method, only local accuracy of the cost function is important. Independent cost minimizations are performed on each row of a test image, but using both frames simultaneously. Then, the RMS boundary offset (combining bias and variance) averaged over all lines is taken as a figure of merit.

The following eleven cost functions for boundary estimation were tested, fixing $\hat{\mathbf{f}}(\mathbf{g}|\theta)$ as the Wiener reconstruction for known θ.

- $J_1 = \mathbf{g}^{\mathrm{T}} \mathbf{\Lambda}_n^{-1} (\mathbf{g} - \mathbf{H}_\theta \hat{\mathbf{f}})$, the linear least squares criterion (6.4).

- $J_2 = \left\| \mathbf{g} - \mathbf{H}_\theta \hat{\mathbf{f}} \right\|^2$, the residual component of (6.3).

- $J_3 = \left\| \mathbf{g} / R(\mathbf{H}_\theta)^\perp \right\|^2$. This is (6.6), which doesn't depend on $\hat{\mathbf{f}}$ (neither do J_4 or J_5).

- $J_4 = \left\| \mathbf{g} / \mathcal{G}_\theta{}^\perp \right\|^2$, where $\mathcal{G}_\theta$ is the space of signals constant along motion trajectories under scene configuration θ. If both $g(x + vT, t + T)$ and $g(x, t)$ are interior points of a region moving with velocity v then their difference is ideally zero. This projection measures how much $\mathbf{g}$ deviates from the constant brightness assumption outside of the hypothesized transition zone. In the absence of boundary offset, J_4 contains only noise, but when θ is incorrectly estimated, some transition zone samples will be mistaken for interior points and J_4 should increase.

- $J_5 = \left\| \mathbf{g} / R(\mathbf{H}_\theta)^\perp \right\|^2 - \left\| \mathbf{g} / \mathcal{G}_\theta{}^\perp \right\|^2$. A substantial fraction of $R(\mathbf{H}_\theta)^\perp$ is occupied by $\mathcal{G}_\theta{}^\perp$, so this quantity measures the norm of the projection onto the rest of $R(\mathbf{H}_\theta)^\perp$.

The remaining six cost functions depend only on $\hat{\mathbf{f}}$, and are integrated over only the background surface during the experiments.

- $J_6 = \left\| \hat{\mathbf{f}} \right\|^2$, unweighted signal energy (1.5).

- $J_7 = \hat{\mathbf{f}}^{\mathrm{T}} \mathbf{\Lambda}_f^{-1} \hat{\mathbf{f}}$, spectrum-weighted energy (1.3), which is also a component of (6.3).

- $J_8 = \int \left\| \frac{d\hat{f}}{dx} \right\|^2 dx$, L_2-smoothness (1.4).

- $J_9 = \int \left| \frac{d\hat{f}}{dx} \right| dx$, L_1-smoothness (1.6).

- $J_{10} = \left\| \hat{\mathbf{f}} / \Pi_0(v_b T) \right\|^2$, energy of the DC-free signal component of period $v_b T$. This is motivated by the fact that artifacts caused by boundary offset are periodically replicated.

- $J_{11} = \int [\hat{f}(x)]_0^{255} dx$, where $[s]_A^B$ is defined by (1.2). Artifacts are often of such large amplitude that they exceed the normal dynamic range of the image. This cost function was inspired by the method of blur estimation based on a positivity criterion [Wetta80].

The test image is Figure 5.7a blurred by displacements $v_b T = 11$, $v_e T = \pm 8$. The observation $\mathbf{g}$ contains noise at 30 or 50 dB SNR and is discretized with $\Delta x = 0.25$, four times the input signal Nyquist rate. The actual experimental procedure is to compute $J_i(\hat{\mathbf{f}}(\mathbf{g}|\theta))$ on each line while the boundary is perturbed in both directions from the true position by $|\epsilon| = 0, \frac{1}{16}, \frac{1}{8}, \frac{3}{16}, \frac{1}{4}, \frac{1}{2}, 1$, taking the minimizing ϵ as the estimation error. The RMS error is shown in Figure 6.11. Because the step size becomes coarser at large ϵ, the larger values of RMS error are less accurate. Values of RMS error much smaller than the smallest nonzero ϵ would also be suspect, but this potential problem did not present itself. Many values are smaller than Δx, showing the possibility of boundary estimation with sub-pixel accuracy. In this experiment J_4 cannot provide sub-pixel accuracy because $\mathbf{g}$ is discretized and $\mathbf{g}/\mathcal{G}_\theta{}^\perp$ changes only when θ moves more than Δx.

The performance of boundary estimation by the last six cost functions is noticeably better when $v_e T = 8$ than when $v_e T = -8$, especially at the higher SNR. Since J_6 through J_{11} are indirect attempts to measure the amount of reconstruction artifact, they become better boundary estimators when, for the same ϵ, artifacts are more severe. All boundary estimators perform much better at 50 dB SNR, again when artifacts are more serious. In general, lower tolerance to boundary offset is nicely matched by enhanced ability to do boundary estimation.

Although some are more accurate than others, most of the cost functions work well enough as boundary estimation criteria as far as image reconstruction is concerned. Excluding J_4, J_6, J_{10},and J_{11}, the subsequent interregion reconstructions of the test image contained virtually no visible distortions beyond the inevitable effects of noise and unobservable modes. After all is said and done, though, the most reliable method is to use J_1—in other words, jointly minimize the linear least squares cost function with respect to θ and $\mathbf{f}$.

This entire discussion has concerned only local accuracy, and the problem of coarse boundary estimation still remains. Likelihood functions in nonlinear estimation problems—FM detection, time-of-arrival estimation, boundary estimation, etc.—may possess multiple local extrema or, worse, a global extremum far from the correct estimate. Thus an estimator must be judged not only on local accuracy but also on probability of anomaly [VanTrees68]. Any cost function can be fooled by unfavorable combinations of foreground and background signals, with or without noise, and such difficulties are not easily resolved when boundary estimation is performed as a series of independent one-dimensional procedures. Consider-

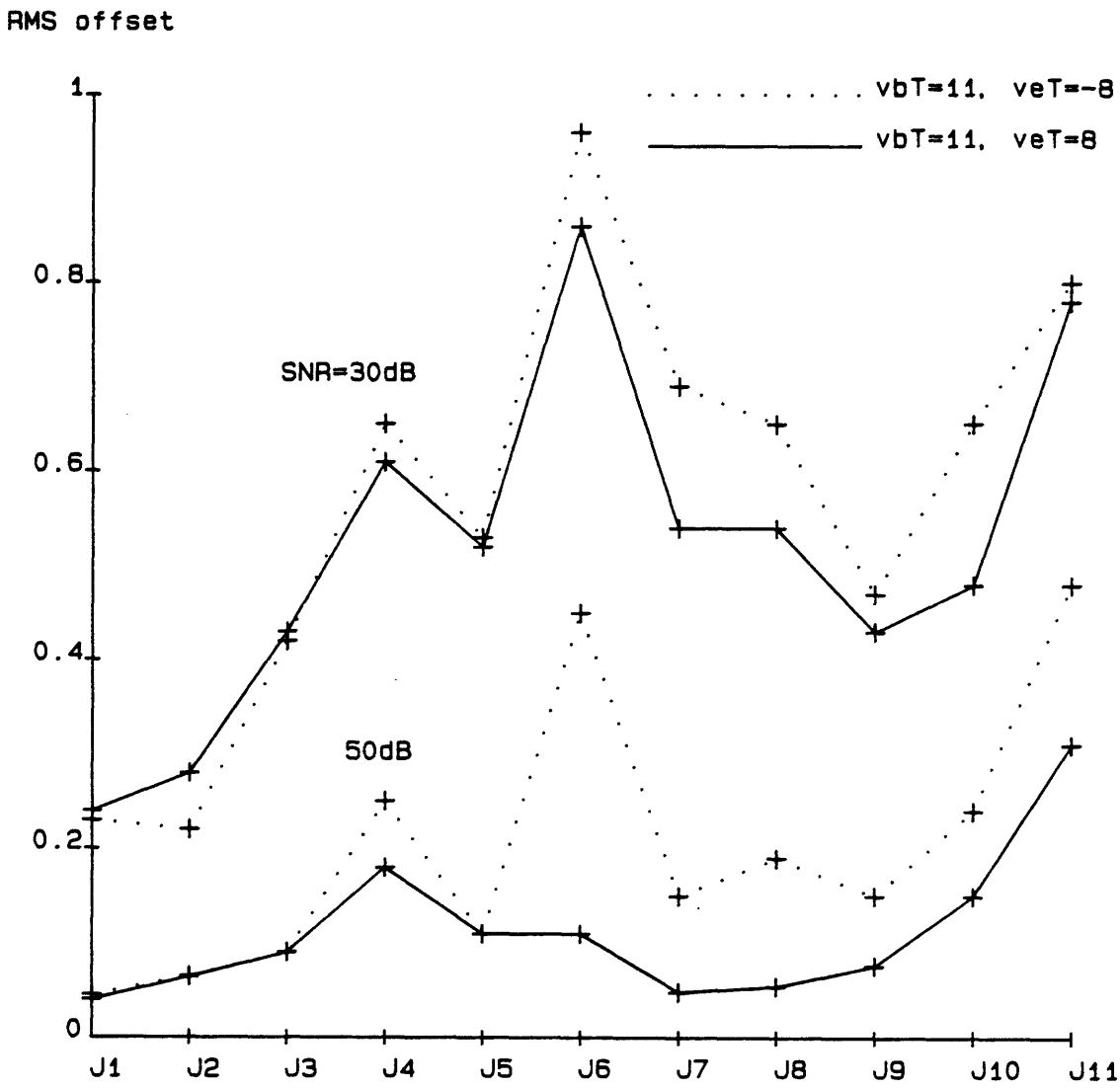

Figure 6.11: RMS errors of boundary position estimators for interregion reconstruction using two frames

ations like continuity of boundaries in two spatial dimensions and in time are essential to robust segmentation of dynamic scenes but are beyond the scope of this research.

6.4 Blur and Displacement Estimation

No experiments with blur or displacement estimation algorithms were conducted in the course of this research, but it is interesting to comment upon the proper linkage between two dissimilar but ultimately related problems. Blur estimation has been studied for the purpose of blind restoration of individual frames, disregarding interframe motion. On the other hand, all known displacement estimation techniques try to match together parts of adjacent frames without regard to the blur present inside each frame. Since both blur and displacement arise from the same continuous flow of motion, a joint approach to these previous separate estimation problems should exist.

A few blur estimation techniques have been reported. If a blurred signal is generated by passing an autoregressive input signal through an FIR blur, then blur estimation can be viewed as a problem of ARMA model identification [Tekalp86]. This approach is more general than necessary since the impulse response of uniform motion blur has a known form, namely, a boxcar. Fourier-domain methods exploit the periodic zero crossings of $H(\omega)$, which give rise to a negative impulse in the cepstrum. The tendency of the input signal and noise to obscure this impulse can be reduced by averaging the cepstra of many image blocks [Cannon76], as long as the moving region is large enough. Fourier-domain methods can be extended directly to two-dimensional problems, where linear motion is characterized by speed and direction. Alternatively, when the image is projected horizontally and vertically into two one-dimensional signals, independent one-dimensional blur estimates will give the corresponding projections of the blur [Wetta80].

Most of the cost functions described in the preceding section are candidates for an optimization approach to intraframe blur estimation. J_3–J_5 are ruled out, though, since $R(\mathbf{H}_\theta)^\perp$ and $\mathcal{G}_\theta{}^\perp$ are empty for an intraframe, intraregion observation. The linear least squares cost function, J_1, should be the first experiment to try.

Displacement estimation algorithms have been categorized as matching methods and differential methods [Huang81], although the distinction is not absolute. Matching methods compute the displacement between corresponding entities in a pair of frames. Feature matching relies on distinctive patterns like edges, contours, or brightness corners. Gray-level matching divides a frame into blocks and shifts each one around to get the best alignment with another frame, as measured by a cost function combining all displaced frame differences

DFD $= g(x + vT, t + T) - g(x, t)$ in the block. Differential methods estimate velocity by attempting to satisfy $\frac{\partial g}{\partial x} v + \frac{\partial g}{\partial t} = 0$, which is just the Taylor expansion of DFD around $v = 0$; in two dimensions additional constraints must be imposed to resolve ambiguity. While matching methods prefer sharp images and differential methods prefer low-passed ones, none of these algorithms cares that $g(x, t)$ is specifically a motion-blurred image of some surface.

The joint approach to blur, displacement, and signal estimation is almost too obvious to state. If the continuous motion flow field in some spatio-temporal neighborhood is characterized by a model with a small set of parameters θ (e.g., velocity and acceleration), then the unknown signal and the motion should be jointly chosen to minimize a suitable cost function. The linear transformation $\mathbf{H}$ depends only on θ and the camera integration time DT, presumably known. Parametric motion models have been advocated as a basis for motion estimation in blur-free signals [Martinez86], and motion blur adds a new dimension for further investigation.

6.5 Summary

The crux of most signal reconstruction problems is identification of the distorting system. In the restoration of motion-blurred image sequences, the system is linear once the scene configuration is known through dynamic scene analysis, including boundary and blur estimation.

A sub-pixel discrepancy between the actual and presumed positions of the boundary can lead to highly visible distortions during transition zone compensation and interregion reconstruction, in the form of periodic replications of foreground and background surface features. A straightforward but sufficiently accurate model-based boundary estimation technique has been established, with the proviso that surface velocities, boundary velocity, and an approximate segmentation are all known. It is based on minimizing the same cost function previously used for Wiener signal estimation for a fixed linear system.

A cursory examination of blur estimation issues—the consequences of incorrect blur and techniques of joint blur and displacement estimation—was presented.

In closing, the existence of blind image restoration methods that do not require explicit system identification should be mentioned. They are better suited for uncertainties in blur rather than boundary position. The power spectrum method of image restoration can be carried out using $S_g(\omega)$, which is estimated from the observation, and $S_f(\omega)$, which is known or estimated from unblurred prototype signals of the same genre as the unknown image [Pratt78]. Another idea is to model uncertainties in $\mathbf{H}$ statistically and apply the Wiener estimator for $\mathbf{f}$, which will involve only first and second moments of $\mathbf{H}$. This approach tends to reduce the sensitivity of reconstruction to perturbations in $\mathbf{H}$ by sacrificing a little sharpness, and could even be employed for protection against errors after an estimate of $\mathbf{H}$ is developed through scene analysis.

Chapter 7

Conclusions

This thesis has investigated the problem of reconstructing the surface brightness patterns in a scene of overlapping moving objects from a sequence of frames blurred by temporal integration in the camera. The main contribution of this work is a systematic analysis and simulation of reconstruction using interframe and interregion constraints. A summary of the principal results follows, and problems for further study are indicated as well.

7.1 One-dimensional, 100% Duty Cycle Reconstruction

Three prototype reconstruction problems—intraregion, transition zone compensation, and interregion—have been studied mathematically and experimentally for one-dimensional signals blurred by 100% camera integration.

The conventional formulation of motion blur deconvolution is an intraframe, intraregion reconstruction problem—intraregion because information from transition zones is disregarded for lack of a suitable model of image formation. The component of the input signal that is periodic with wavelength vT, minus a constant DC level, is completely nulled out by the blurring system and thus cannot be recovered. When vT is more than a minor fraction of the finite observation interval, loss of the unobservable component leaves a visible periodic disturbance in the deblurred image.

Intraregion reconstruction can be improved by using multiple frames in which the amount of motion blur is unequal. In theory, the period of the unobservable component drops to the largest wavelength evenly dividing the respective blurs of each frame. Perfect reconstruction should occur if and only if the velocity ratio v_i/v_j is irrational for some pair

of frames. In practice, the finite bandwidth of most input signals means that v_i/v_j may be regarded as "irrational" as long as it is not close to a ratio of small integers. Observation noise also modifies the theoretical predictions, not only by precluding perfect reconstruction for any combination of velocities but also by ensuring smooth changes in reconstruction behavior under continuous changes in velocity. Simulations show that interframe, intraregion reconstruction yields the best results of all three prototype problems for a fixed number of frames, provided that unfavorable velocity combinations are avoided. A further advantage is that boundary position estimation is not required.

Transition zone compensation assumes constant boundary and surface velocities, with prior knowledge of the contribution of one side to a transition zone so that it can be removed at the outset. Suppose the unknown side is deemed the background surface. The theory predicts that the compensated transition zone furnishes enough constraints for complete recovery of the background if $v_b/v_e \leq 1$ (the background velocity does not surpass the edge velocity) or if $v_b/v_e \neq 2$ and two frames are observed; in short, this method almost always succeeds. In practice, however, a high SNR in the camera is required to take advantage of the constraints. Knowledge of the boundary position with sub-pixel accuracy is also mandatory to avoid additional reconstruction artifacts.

Interregion reconstruction takes transition zone compensation one step further, replacing prior knowledge of one side with the assumption of equal foreground and boundary velocities. By forming displaced-frame-difference images with respect to the boundary velocity, interregion reconstruction using M frames can be related to transition zone compensation using $M-1$ frames. A periodic signal component whose wavelength evenly divides both the background and foreground blurs is always unobservable. As long as three frames are observed and $v_b/v_e \neq 2$, all other components can be completely recovered in principle. Experiments show that interregion reconstruction does indeed perform about as well as transition zone compensation with one fewer frame, provided that unfavorable velocity ratios are avoided. High SNR is required to take advantage of interregion constraints. Although the reconstruction artifacts due to boundary offset are less severe than in the case of transition zone compensation, good boundary estimation is still needed.

In conclusion, the strategy of exploiting interframe and interregion constraints can produce deblurred images of better quality than the conventional intraframe, intraregion approach. However, the constraints fail to achieve complete reconstruction when certain

velocity ratios are unfavorable. Furthermore, observation noise and boundary offset may degrade transition zone compensation or interregion reconstruction to the extent that the image quality is no better than, or worse than, the conventional restoration. Therefore, signal modeling approaches to recovering the unobservable component should not be abandoned after all; instead, they should be employed in conjunction with constraints from multiple frames and overlapping surfaces.

7.2 Generalizations

Admittedly, the simplified image formation model used to obtain the foregoing results bears little resemblance to the complexities of real-world scenes. Two efforts to generalize the theoretical analysis were pursued with partial success—extensions to arbitrary duty cycle and to certain motions in two dimensions.

Many results for duty cycle $D < 1$ are obvious generalizations of the results for $D = 1$, where the only change involves scaling certain wavelengths by D. On the other hand, there is a significant gap in the theory affecting interframe transition zone compensation and interregion reconstruction. For certain values of D the equations constraining the unobservable component also characterize the dynamics of a piecewise linear oscillator whose behavior is not fully known. The study of this and other nonlinear dynamic systems is an open area of research. The most direct resolution of this problem, however, would be to repeat the experiments of Chapter 5 to calculate the MSE of Wiener filtering and to reconstruct actual pictures while varying both v_b/v_e and D.

Extensions to two dimensions were limited to straight-line translation and straight boundaries, in order to preserve mathematical tractability. Many results are obvious generalizations of the one-dimensional results, where the only change involves replacing scalar quantities by vector ones. One major difference is fundamental to the increased dimensionality: while a pair of incommensurate velocities achieves complete reconstruction in one dimension, a pair of velocity vectors does not suffice in two dimensions because two-dimensional signals can naturally support biperiodicity. Since no two-dimensional reconstruction problems were simulated in the course of this research, the theory remains to be verified. Restoration of more general two-dimensional scenes, including rotation and curved boundaries, is difficult to analyze but could also be studied experimentally.

Even with the realm of one-dimensional, 100% duty cycle problems, there are many degrees of freedom that have not been explored. For instance, constant boundary and surface velocities were assumed in transition zone compensation and interregion reconstruction because the non-constant velocity case could not be analyzed. As a second example, in the analysis of interframe, intraregion reconstruction the surface velocity was assumed to be constant during each exposure yet different across frames: this behavior is unlike the motion of a smoothly accelerating surface. The point spread function of motion blur under acceleration is no longer a rectangular boxcar. These and other perturbations on the idealized scene configuration most certainly will change the theory of unique reconstruction and could affect performance in practice.

7.3 Scene Analysis

A requirement shared by conventional image restoration and the methods proposed in this thesis is knowledge of the amount of blur within each region and frame. Interframe methods also need to measure interframe displacements in order to align surfaces observed across frames. This suggests that joint blur and displacement estimation could be a fruitful subject for further study.

A special requirement of reconstruction techniques that utilize the transition zone is knowledge of the boundary position and velocity. An experimental comparison of some boundary position estimation techniques shows that minimization of the linear least squares cost function with respect to both the unknown signal and unknown boundary position yields reconstructions free of artifacts associated with boundary offset. However, this approach is just a one-dimensional local boundary estimator that needs to start from a valid coarse estimate. Motion-based scene segmentation is a general problem that must be solved before the results of this research can be applied to automatic image sequence deblurring.

It is fitting to end on this note, for it was the utility of scene analysis concepts in image sequence coding, interpolation, and noise reduction that originally prompted this entire investigation. Motivations work in reverse, too, and perhaps the prospect of performing reconstruction from motion-blurred image sequences will spur new developments in dynamic scene analysis.

Appendix A

Derivations

A.1 Intersection of $\Pi(z_i; S)$

Lemma A.1. For real numbers $z_1, \ldots, z_M$ let S be an interval whose length is at least $\min_i |z_i| + \max_i |z_i|$.

a) $\bigcap_{i=1}^{M} \Pi(z_i; S) = \Pi(\gcd(z_1, \ldots, z_M); S)$

b) $\Pi_0(z_1; S) \cap \left(\bigcap_{i=2}^{M} \Pi(z_i; S)\right) = \Pi_0(\gcd(z_1, \ldots, z_M); S)$

N.B. While these identities are almost self-evident when $S = (-\infty, \infty)$, e.g. see [Kuczma68] for $M = 2$, their validity within a finite interval is not obvious. The stated length of S is sufficient, but not necessary.

Proof. Let $\lambda = \gcd(z_1, \ldots, z_M)$. It is trivial to check that $f \in \Pi(\lambda; S)$ or $f \in \Pi_0(\lambda; S)$ implies that f belongs to the left hand sides of (a) or (b), respectively, regardless of the length of S.

To show the converse, let $z = \min_i |z_i|$ and suppose $f(x) \in \bigcap_{i=1}^{M} \Pi(z_i; S)$, where $S = [0, L]$, $L \geq z + \max_i |z_i|$. For every i,

$$\begin{aligned} f(x) \in \Pi(z_i; S) \quad &\Longrightarrow \quad f(x) = f(x + z_i), \quad \forall x \in [0, L - |z_i|] \\ &\Longrightarrow \quad \sum_{k=-\infty}^{\infty} a_k (e^{j2\pi k z_i / z} - 1) e^{j2\pi k x / z} = 0, \end{aligned}$$

where $f(x)$ has been represented by $\sum a_k e^{j2\pi k x / z}$. Since $\left\{e^{j2\pi k x / z}\right\}$ are orthogonal over $[0, z]$, which always lies within $[0, L - |z_i|]$, it follows that

$$a_k (e^{j2\pi k z_i / z} - 1) = 0 \qquad \Longrightarrow \qquad a_k = 0 \text{ or } k z_i / z = \text{integer}, \quad \forall i, k.$$

When $\lambda = 0$, kz_i/z cannot equal an integer for all i unless $k = 0$; in this case only a_0 is nonzero and thus $f(x) = a_0 \in \Pi(0)$.

On the other hand, if $\lambda > 0$ let $m_i = z_i/\lambda$, $m = z/\lambda$. Since the m_i's are relatively prime, $kz_i/z = km_i/m$ will equal an integer for all i if and only if k is a multiple of m. Therefore,

$$f(x) = \sum_l a_{lm} e^{j2\pi lx/\lambda} \in \Pi(\lambda; S),$$

proving assertion (a).

Finally, if the condition $f \in \Pi(z_1; S)$ is replaced by $f \in \Pi_0(z_1; S)$ then

$$\begin{cases} \int_0^\lambda f(x)\,dx = \dfrac{1}{m_1}\int_0^{z_1} f(x)\,dx = 0 \Longrightarrow f \in \Pi_0(\lambda; S) & \text{if } \lambda > 0; \\ a_0 z_1 = \int_0^{z_1} f(x)\,dx = 0 \Longrightarrow a_0 = 0 \Longrightarrow f \in \Pi_0(0; S) & \text{if } \lambda = 0, \end{cases}$$

thereby proving (b). ∎

A.2 Construction of Solution to (2.19)

In connection with interregion reconstruction from two frames when $v_b/v_e > 1$, it is desired to find functions satisfying

$$\begin{aligned} \Delta f_b(x) &\in N(\mathbf{H}_\angle) \\ f_b(x) &\in \Pi_0(v_b T) \end{aligned}$$

without having $\Delta f_b(x)$ identically zero. It is known how to generate all possible solutions when v_b/v_e is rational, but the irrational case is unsolved.

If v_b/v_e is rational, let $(v_b/v_e)^{-1} = m/n$ in lowest terms. Choose any nonzero function

$$\phi(x) = \sum_l b_l e^{j\frac{2\pi l}{v_e T}x}, \quad x \in [0, v_e T]$$

for which $b_{rm} = b_{r(m-n)}$, $\forall r$. Extend the domain of this function via the antisymmetry relationship

$$\phi(x) = (1 - v_b/v_e)^{-1}\phi((1 - v_b/v_e)^{-1}x), \quad x \in [(v_e - v_b)T, 0]$$

to produce an element of $N(\mathbf{H}_\angle)$. Now let the Fourier expansion of $\phi(x)$ on $[(v_e - v_b)T, v_e T]$ be

$$\sum_k c_k e^{j\frac{2\pi k}{v_b T}x}. \tag{A.1}$$

It can be verified that the foregoing constraints force $c_{rn} = 0, \quad \forall r$.

The formal series

$$f_b(x) = \sum_k \frac{c_k}{e^{-j2\pi k(1-m/n)} - 1} e^{j\frac{2\pi k}{v_b T}x}$$

satisfies $f_b(x) \in \Pi_0(v_b T)$ as well as $\Delta f_b(x) = \phi(x) \in N(\mathbf{H}_\angle)$. Since $|e^{-j2\pi k(1-m/n)} - 1|$ is bounded between 2 and $|e^{-j2\pi/n} - 1|$ as long as $k \neq rn$, the convergence of $f_b(x)$ is equivalent to the convergence of (A.1). Therefore, this series gives a valid nontrivial solution to the problem.

On the other hand, if v_b/v_e is irrational, the foregoing scheme breaks down. The denominator $|e^{-j2\pi k(1-v_e/v_b)} - 1|$ can become arbitrarily small, and it is not known how to choose $\phi(x) \in N(\mathbf{H}_\angle)$ to guarantee convergence of $f_b(x)$. This inability doesn't imply that convergence is impossible, though.

A.3 Solution of Equations (2.13)

General references for the mathematical concepts needed in this section are [Devaney86, Hockett87, Kuczma68]. Although more notation will be introduced here than absolutely necessary to solve this particular problem, this material is background for the generalization to arbitrary duty cycle in §A.4.

Defining $F(x) = \int_0^{v_b T x} f_b(u + (v_e - v_b)T)\, du$, a problem equivalent to (2.13) is the set of simultaneous functional equations

$$\begin{aligned} F(\alpha z + 1 - \alpha) &= F((\alpha - 1)z + 1 - \alpha), & z \in [0,1] \\ F(\alpha z) &= F((\alpha - 1)z), & z \in [0,1] \\ F(x) &= F(x+1), & \forall x \\ F(0) &= 0, \end{aligned} \tag{A.2}$$

where $\alpha = (v_b/v_e)^{-1} \in (0,1)$. By periodicity, it suffices to solve for $F(x), \quad x \in [0,1]$.

Necessary conditions on F can be found by considering the iteration structure of a certain invertible point mapping $Y : [0,1] \to [0,1]$, designed so that $F(x) = F(Yx)$. Call the sequence $\{\ldots, Y^{-2}x, Y^{-1}x, x, Yx, Y^2x, \ldots\}$ the *orbit* of x under Y, and let $O(x)$ be the orbit's *closure*, namely, the orbit together with its limit points. If $O(x) \cap O(x') \neq \emptyset$ and F is assumed to be continuous at some point in the intersection, it follows that $F(x) = F(x')$. For example, in Lemma 2.3.2, Y was defined as $Yx = (B/A)x$; since every orbit converged

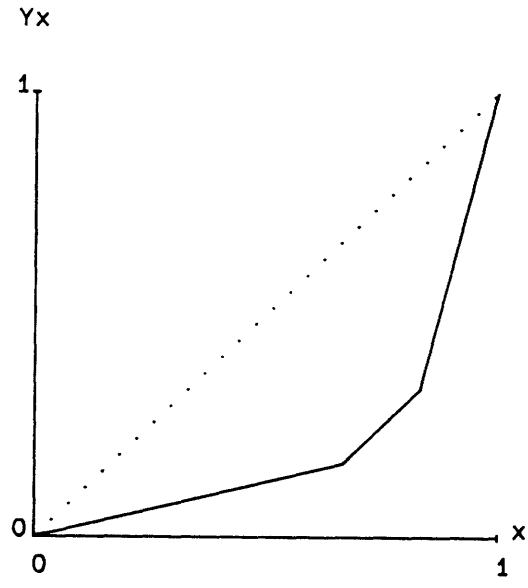

Figure A.1: The circle map Y for $\alpha = 1/3$

to 0, $F(x) = F(0)$ for all x. In the problem being discussed here, one way to satisfy $F(x) = F(Yx)$ is to let

$$Y = G_\alpha R_{1-\alpha} G_\alpha R_{-(1-\alpha)},$$

where

$$R_z x = x + z \pmod 1 \tag{A.3}$$

$$G_\alpha x = \begin{cases} 1 - \frac{1-\alpha}{\alpha} x, & \text{if } x \le \alpha; \\ \frac{\alpha}{1-\alpha}(1-x), & \text{if } x \ge \alpha. \end{cases} \tag{A.4}$$

This is because the first equation in (A.2) is the same as $F(x) = F(R_{1-\alpha} G_\alpha R_{-(1-\alpha)} x)$ and the second equation is the same as $F(x) = F(G_\alpha x)$.

Sketched in Figure A.1, this Y is a nonlinear circular shift of $[0, 1]$, i.e., an orientation-preserving map (homeomorphism) of the unit circle. Its orbits can be completely described (proofs omitted):

1. If $\alpha = 1/2$, Y is just the identity mapping and every x is a fixed point. In short, the second equation in (A.2) is redundant and the problem degenerates into intraframe

transition zone compensation. According to the example in §2.3.2, nullvectors in $N(\mathbf{H}_\angle) \cap \Pi_0(v_b T)$ possess odd symmetry within each period.

2. If $\alpha \neq 1/2$, the graph of Y is tangent to the identity mapping at a single saddle-node fixed point, located at 0. Since all orbits converge to this fixed point, regardless of initial condition, $F(x) = F(0)$ for all x. Therefore, $N(\mathbf{H}) = \mathbf{0}$.

A.4 Solution of Equations (3.1)

A.4.1 Provable Results

Refer to §A.3 for preliminary notions necessary to follow this section. Defining $F(x) = \int_0^{v_b DTx} f_b(u + (v_e - v_b)T)\, du$, a problem equivalent to (3.1) is the following generalization of (A.2):

$$\begin{aligned} F(\alpha z + \delta) &= F((\alpha - 1)z + \delta), \quad z \in [0,1] \\ F(\alpha z) &= F((\alpha - 1)z), \quad z \in [0,1] \\ F(x) &= F(x+1), \quad \forall x \\ F(0) &= 0, \end{aligned} \tag{A.5}$$

where $\alpha = (v_b/v_e)^{-1} \in (0,1)$ and $\delta = (1-\alpha)/D \pmod 1$.

In order to satisfy $F(x) = F(Yx)$, define $Y : [0,1] \to [0,1]$ by

$$Y = G_\alpha R_\delta G_\alpha R_{-\delta},$$

where R_z and G_α were defined in (A.3) and (A.4). For example, a typical Y is shown in Figure A.2.

The orbits of Y can be described easily for some values of (α, δ):

1. If $\delta = 0$, Y is just the identity mapping and every x is a fixed point.

2. If $\alpha = 1/2$, Y is just the rigid rotation $R_{-2\delta}$. When δ is irrational, Y has no periodic points and each orbit is dense in $[0,1]$; hence, $F(x) = 0$ for all x. Otherwise, $2\delta = n/m$ for some integers m, n. Every x is a fixed point of Y^m and each orbit under Y touches points spaced $1/m$ apart; hence, $F(x) \in \Pi(1/m)$.

3. If $\alpha \neq 1/2$ and $\delta \in [\alpha, 1-\alpha]$, Y has two fixed points, a source-sink pair (indistinct if δ is an endpoint of the interval), and all orbits converge to them; hence $F(x) = 0$ for all x.

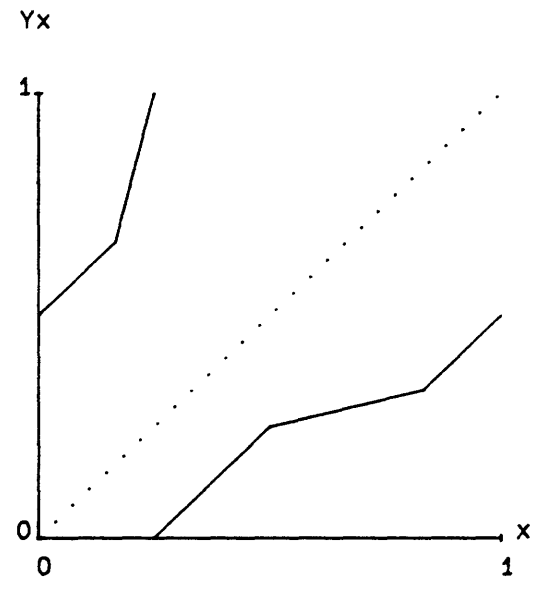

Figure A.2: The circle map Y for $\alpha = 1/3$, $\delta = 1/6$

These findings determine the nullvectors of interframe transition zone compensation. First, $\delta = 0$ means that the second equation in (A.5) is redundant; i.e., the problem degenerates into intraframe reconstruction, for which the nullspace is $N(\mathbf{H}_\angle) \cap \Pi_0(v_b DT)$. This condition is attained when $1 - (v_b/v_e)^{-1}$ happens to be an integer multiple of D. Second, when $\alpha = 1/2$ the usual pathology of $v_b/v_e = 2$ appears: if $D = m/n$ then the nullspace has odd-symmetric signals in $\Pi_0(v_b T/n)$, but if D is irrational then $N(\mathbf{H}) = \{\mathbf{0}\}$. Third, the only nullvector is again $\mathbf{0}$ when the condition $\alpha \neq 1/2$, $\delta \in [\alpha, 1-\alpha]$ is attained. There are many ways this can happen: for example, if $v_b/v_e < 2$ and $D \geq v_b/v_e - 1$, or if $v_b/v_e > 2$ and $D = 1$. Some of these statements were summarized in Theorem 3.1.

A.4.2 Conjectures

What about other combinations of (α, δ)? To begin to answer this question, consider the *rotation number* of a circle map, which measures the average amount of circular shift per iteration as the number of iterations tends to infinity. A fundamental theorem is that an order-preserving circle map possesses fixed points if, and only if, its rotation number is rational [Devaney86].

The general relationship between (α, δ) and the rotation number of Y is presently unknown. Some experiments have been performed, however, leading to the conjecture that for every rational $p/q \in [0, 1)$ with odd q there is exactly one region in the (α, δ) plane on which Y has rotation number p/q. For example, the region for rotation number $2k/(2k+1)$ is

$$\left\{(\alpha, \delta) \,\middle|\, \delta \in \left[\frac{\alpha(1-\alpha)}{k+1-\alpha}, \frac{\alpha(1-\alpha)}{k+\alpha}\right]\right\};$$

taking $k = 0$ yields the result in item (3), above. In such regions Y^q has q source-sink pairs of fixed points (pairs merge at the region boundary), and all orbits converge to them; hence $F(x) = 0$ for all x. Consequently, it appears that $N(\mathbf{H})$ might be $\{\mathbf{0}\}$ for a substantial subset of the plane. The bifurcation diagrams in Figure A.3 show just a few of these regions.

Motivated by the known properties of the "canonical two-parameter family" of circle maps $Ux = x + a + b \sin 2\pi x$, one can speculate on some additional properties of Y. The regions for valid p/q are non-empty and bounded by continuous curves. Taken together, they densely fill the plane, yet they leave Cantor-like gaps whose total area is nonzero in the Lebesgue measure [Arnold65, Herman77]. Despite the small area of the gaps, they should not be ignored (for reasons cited in §5.3.4). The set of points for any fixed irrational rotation number should be a continuous arc, positioned inside a gap. If Y only had continuous second derivatives (as U does), it would follow that every irrational orbit is dense on $[0, 1]$, implying $F(x) = 0$ for all x [Boyland87]. However, Y is piecewise linear and no such general property is known: it's conceivable that $O(x) \cap O(x') = \emptyset$ for two initial conditions.

It would be nice to prove that $F(x) = 0$ is the only solution for all values of (α, δ) not covered in §A.4.1, for then the complete solution to (A.5) could be stated very simply. The proof of the preceding conjectures and characterization of irrational orbits is beyond the means of this author and could be a basic open question in nonlinear dynamical systems. Of course, perhaps there is an entirely independent approach to solving (A.5). Any such result could have implications for Y and similar piecewise linear oscillators.

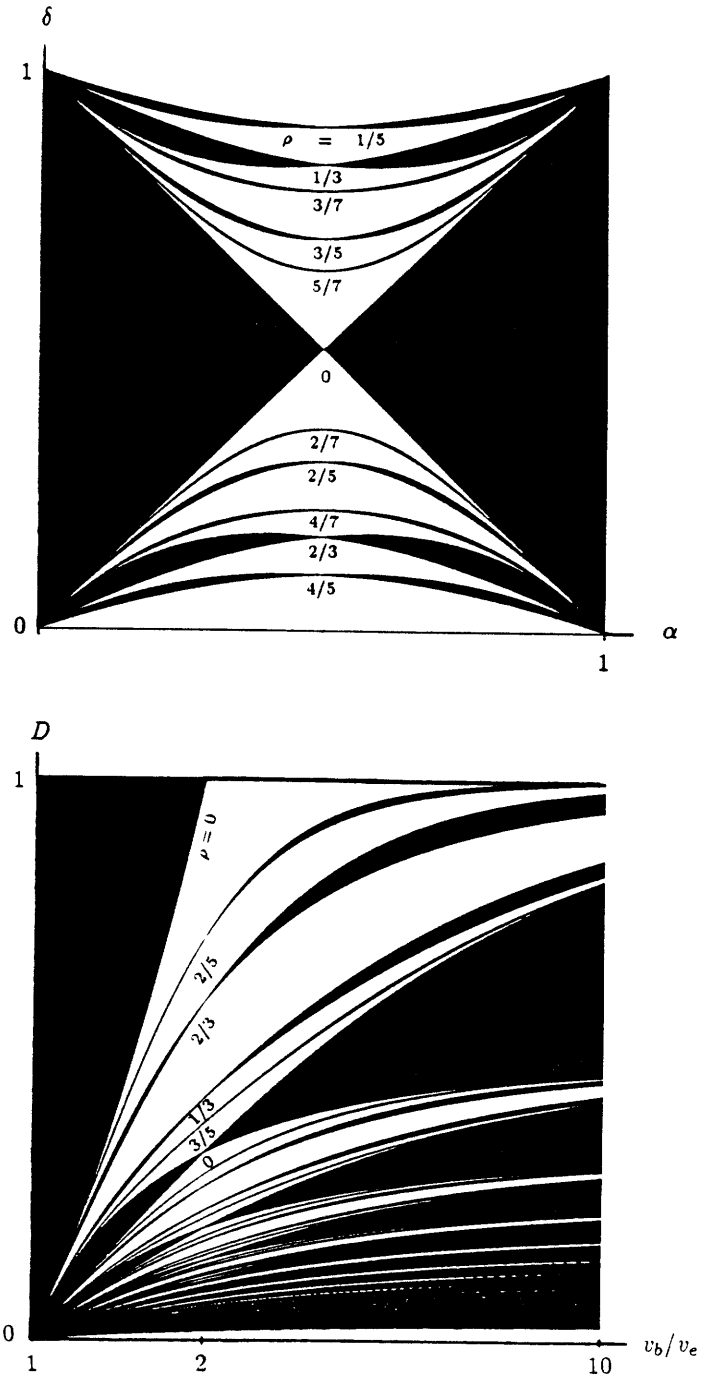

Figure A.3: Bifurcation structure of the circle map Y: (top) in the (α, δ) plane; (bottom) in the $(v_b/v_e, D)$ plane. The coordinates are related by $\alpha = (v_b/v_e)^{-1}$, $\delta = (1 - (v_b/v_e)^{-1})/D \pmod 1$. The rotation number ρ is rational in each shaded region. An infinite nesting of smaller regions resides in each gap but is omitted for clarity.

Bibliography

[Abramatic82] J. Abramatic and L.M. Silverman. Nonlinear restoration of noisy images. *IEEE Trans. Pattern Anal. & Mach. Intell.*, 4(2):141–149, Mar. 1982.

[Anderson76] G.L. Anderson and A. Netravali. Image restoration based on a subjective criterion. *IEEE Trans. Syst. Man & Cybern.*, 6(12):845–853, Dec. 1976.

[Arnold65] V.I. Arnol'd. Small denominators I. Mappings of the circumference onto itself. *Amer. Math. Soc. Translations, 2nd Ser.*, 46:213–284, 1965.

[Bovik85] A.C. Bovik, T.S. Huang, and D.C. Munson. Edge-sensitive image restoration using order-constrained least squares methods. *IEEE Trans. Acoust. Speech & Signal Process.*, 33(4):1253–1263, Oct. 1985.

[Boyland87] P. Boyland. Bifurcations of circle maps, Arnold tongues, bistability and rotation intervals. *Commun. Math. Phys.*, 106:353–381, 1987.

[Cannon76] M. Cannon. Blind deconvolution of spatially invariant image blurs with phase. *IEEE Trans. Acoust. Speech & Signal Proc.*, 24(1):58–63, Feb. 1976.

[Clarke81] R.J. Clarke. Relation between the Karhunen Loeve and cosine transforms. *IEE Proc. Part F*, 128(6):359–360, Nov. 1981.

[Devaney86] R.L. Devaney. *An Introduction to Chaotic Dynamical Systems.* Benjamin Cummings, 1986.

[Devles85] L.M. Devles and J.L. Mohamed. *Computational Methods for Integral Equations.* Cambridge Univ. Press, 1985.

[Dudgeon84] D.E. Dudgeon and R.M. Mersereau. *Multi-Dimensional Digital Signal Processing.* Prentice-Hall, 1984.

[Frieden80] B.R. Frieden. Statistical models for the image restoration problem. *Comput. Graphics Image Process.*, 12, 1980.

[Gallager68] R.G. Gallager. *Information Theory and Reliable Communication.* Wiley, New York, 1968.

[Ghiglia84] D.C. Ghiglia. Space-invariant deblurring given N independently blurred images of a common object. *J. Opt. Soc. Am. A*, 1(4):398–402, Apr. 1984.

[Herman77] M.R. Herman. Mesure de Lebesgue et nombre de rotation. In *Geometry and Topology*, volume 597, pages 271–293. 1977. Springer Lecture Notes in Math.

[Hockett87] K. Hockett and P. Holmes. Nonlinear oscillators, iterated maps, symbolic dynamics, and knotted orbits. *Proc. IEEE*, 75(8):1071–1080, Aug. 1987.

[Hou87] H.S. Hou. A fast recursive algorithm for computing the discrete cosine transform. *IEEE Trans. Acoust. Speech Signal Process.*, 35(10):1455–1461, Oct. 1987.

[Huang81] T.S. Huang. *Image Sequence Analysis.* Springer-Verlag, 1981.

[Hunt73] B.R. Hunt. The application of constrained least squares estimation to image restoration by digital computer. *IEEE Trans. Comput.*, 22(9):805–812, Sept. 1973.

[Knuttson83] H.E. Knuttson, R. Wilson, and G.H. Granlund. Anisotropic nonstationary image restoration and its applications: Part I – restoration of noisy images. *IEEE Trans. Commun.*, 31(3):388–397, Mar. 1983.

[Ku86] F.N. Ku and J.M. Hu. A new approach to the restoration of an image blurred by a linear uniform motion. *Comput. Vision Graphics Image Process.*, 34:20–34, 1986.

[Kuczma68] M. Kuczma. *Functional Equations in a Single Variable.* Polish Scientific Publ., Warsaw, 1968.

[Malvar86] H.S. Malvar. *Optimal Pre- and Post-Filtering in Noisy Sampled-Data Systems.* PhD thesis, MIT Dept. of Electr. Eng., Aug. 1986.

[Martinez86] D.M. Martinez. *Model-Based Motion Estimation and its Application to Restoration and Interpolation of Motion Pictures.* PhD thesis, MIT Dept. of Electr. Eng., Sept. 1986.

[Powell82] P.G. Powell and B.E. Bayer. A method for the digital enhancement of unsharp, grainy photographic images. In *Int'l. Conf. Electronic Image Processing*, pages 179–183. 1982.

[Pratt78] W.K. Pratt. *Digital Image Processing.* Wiley-Interscience, 1978.

[Root87] W.L. Root. Remarks, mostly historical, on signal detection and signal parameter estimation. *Proc. IEEE*, 75(11):1446–1457, Nov. 1987.

[Sahasrabudhe79] S.C. Sahasrabudhe and A.D. Kulkarni. Shift variant image degradation and restoration using SVD. *Comput. Graphics Image Process.*, 9(3):203–212, Mar. 1979.

[Slepian67] D.A. Slepian. Restoration of photographs blurred by image motion. *Bell Syst. Tech. J.*, 46:2353–2362, Dec. 1967.

[Tekalp86] A.M. Tekalp, H. Kaufman, and J.W. Woods. Identification of image and blur parameters for the restoration of non-causal blurs. *IEEE Trans. Acoust. Speech & Signal Proc.*, 34(4):963–972, Aug. 1986.

[Tricomi85] F.G. Tricomi. *Integral Equations.* Dover, 1985.

[VanTrees68] H.L. Van Trees. *Detection, Estimation, and Modulation Theory, Part I.* Wiley, New York, 1968.

[Wetta80] P. Wetta, R. Goutte, and M. Amiel. Digital deconvolution of degraded images by a space-invariant motion blur. *Signal Process.*, 2(4):323–338, Oct. 1980.

[Woods85] J.W. Woods, J. Biemond, and A.M. Tekalp. Boundary Value Problem in Image Restoration. In *Proc. IEEE Int'l. Conf. Acoust. Speech Signal Process.*, volume 2, pages 692–695. 1985.

Biography

Stephen Hsu was born in New York in 1960. He received the B.S. degree in electrical engineering from the California Institute of Technology, Pasadena, CA, in 1982, and the M.S. and Ph.D. degrees in electrical engineering from the Massachusetts Institute of Technology, Cambridge, MA, in 1985 and 1988, respectively.

Between 1980 and 1982 he was employed at the GM Research Laboratories in Warren, MI, at the California Institute of Technology, and at the IBM Thomas J. Watson Laboratories in Yorktown Heights, NY. From 1982 to 1988 he was a graduate student at the Massachusetts Institute of Technology, where he was successively a National Science Foundation Graduate Fellow, a teaching assistant, a research assistant, and an AT&T Bell Laboratories Ph.D. Scholar. His research interests include vision and psychophysics, television picture processing, software tools for signal processing, and image reconstruction and enhancement. He is a member of Tau Beta Pi and IEEE.